UNIVERSITY OF CALIFORNIA, SAN DIEGO

Inhibitory Circuits in the Olfactory Cortex

A dissertation submitted in partial satisfaction of the
requirements for the degree Doctor of Philosophy

in

Neurosciences

by

Caleb C. A. Stokes

Committee in charge:

Professor Jeffry S. Isaacson, Chair
Professor Edward M. Callaway
Professor Takaki Komiyama
Professor Roberto Malinow
Professor Massimo Scanziani

2011

The Dissertation of Caleb C. A. Stokes is approved, and it is acceptable in quality and form for publication on microfilm and electronically:

_____

_____

_____

_____

_____

Chair

University of California, San Diego

2011

Dedication

This work is dedicated to the memory of Louis Nguyen:

awesome surfer, fierce scientist, peerless DJ, and incredible BFF. Oots.

Table of Contents

List of Figures

Chapter 1.

Chapter 2.

Chapter 3.

Chapter 4.

Acknowledgments

My deepest gratitude goes to:

Jeff Isaacson for being a dear friend as well as a mentor, for being supportive and caring at the darkest and at the brightest times, and for being a patient and thorough teacher always.

Massimo Scanziani, to whom this work owes a great intellectual and scientific debt, for being an engaged and dedicated mentor.

Cindy Poo, who either carried me or kicked me through my Ph.D., for being a reliable and professional lab-mate, and a science idol.

Kyla Drushka, for more support than I even knew was possible, and for challenging me too when I need it.

All the members of the Isaacson and Scanziani labs, for incredible discussion, food, and general good times.

Chapters 1 and 2 are a reprint, with some rearrangement to create separate chapters, of the material in Stokes C.C and Isaacson J.S. From dendrite to soma: dynamic routing of inhibition by complementary interneuron microcircuits in olfactory cortex. Neuron (2010) vol. 67 (3) pp. 452-65. Some figures from the original paper are reproduced in Chapter 3. The dissertation author was the primary author of this material.

Vita

2011 Ph.D. in Neurosciences, **University of California, San Diego** La Jolla, CA
Medical Scientist (M.D.-Ph.D.) Training Program

2002 B.S. in Biology, **Stanford University**, Stanford, CA, USA

Research

PhD thesis: Dr. Jeffry S. Isaacson. University of California, San Diego, La Jolla, CA
Project: Inhibitory microcircuits that shape the processing of olfactory information in primary olfactory cortex

Advisor: Dr. Ben A. Barres. Stanford University, Stanford, CA
Project: The role of glia in the initiation and refinement of synaptic connections

Publications

Stokes, CC & Isaacson, JS (2010). From dendrite to soma: dynamic routing of inhibition by complementary interneuron microcircuits in olfactory cortex. Neuron 67(3):452-65.

Bjartmar L, Huberman AD, Ullian EM, Rentería RC, Liu X, Xu W, Prezioso J, Susman MW, Stellwagen D, **Stokes CC**, Cho R, Worley P, Malenka RC, Ball S, Peachey NS, Copenhagen D, Chapman B, Nakamoto M, Barres BA, Perin MS (2006). Neuronal pentraxins mediate synaptic refinement in the developing visual system. J Neurosci. 26(23):6269-81

Bliss TM, Kelly S, Shah AK, Foo WC, Kohli P, **Stokes C**, Sun GH, Ma M, Masel J, Kleppner SR, Schallert T, Palmer T, Steinberg GK (2006). Transplantation of hNT neurons into the ischemic cortex: cell survival and effect on sensorimotor behavior. J Neurosci Res. 83(6):1004–1014

Christopherson KS, Ullian EM, **Stokes CC**, Mullowney CE, Hell JW, Agah A, Lawler J, Mosher DF, Bornstein P, Barres BA (2005). Thrombospondins are astrocyte-secreted proteins that promote CNS synaptogenesis. Cell 120(3):421-33.

ABSTRACT OF THE DISSERTATION

Inhibitory circuits in the Olfactory Cortex

by

Caleb C. A. Stokes

Doctor of Philosophy in Neurosciences

University of California, San Diego, 2011

Professor Jeffry S. Isaacson, Chair

In sensory areas of cortex, inhibitory neurons play a critical role in regulating the activity of principal cells in space and time. The diversity of intrinsic electrical properties and connectivity patterns among inhibitory cells suggests that different cell types contribute specific functions to the processing of sensory information by cortical circuits. In pyramidal cells of primary olfactory (piriform) cortex, odors evoke widespread and broadly-tuned inhibition, but the cells producing this inhibition are not known. Here, using acute slices of piriform cortex, we identify three inhibitory circuits that are recruited by activation of sensory afferents and act over distinct spatial and temporal domains. We find that physiologically realistic burst stimulation of mitral and tufted (M/T) cell axons results in early but transient dendritic inhibition progressing to somatic feedback inhibition in pyramidal cells of piriform cortex. Interneurons in layer 1a (L1a) receive highly convergent M/T cell input and govern feedforward inhibition onto the dendrites, but short-term synaptic depression decreases their influence as the burst progresses. Dendritic inhibition from L1a interneurons is branch-specific and

locally blocks the calcium transients associated with back-propagating action potentials. The late-onset feedback inhibitory circuit is composed of layer 3 (L3) fast-spiking and low threshold-spiking cells that target pyramidal cell bodies and basal dendrites. L3 interneurons are highly interconnected with local pyramidal cells and we demonstrate that activation of pyramidal cells leads to recurrent inhibition that dominates excitation. Our results reveal the diversity of inhibitory circuits in olfactory cortex and suggest that separate classes of interneurons may have distinct functional roles regulating spike timing, odor tuning, and plasticity.

This work defines a basic set of features by which inhibitory circuits can be identified in piriform cortex and demonstrates a diversity of functional roles played by distinct interneuron cell types. Our findings offer testable hypotheses regarding the influence of specific inhibitory circuits in olfactory information processing and odor representations in the piriform cortex.

Introduction

The sense of smell plays a fundamental role in our experience of the world, from enhancing the enjoyment of a delicious meal to triggering the recall of distant memories. Many animals make use of olfactory cues for finding food, navigating the world, even for communication, and the neural circuits that convey odor information from the periphery to the brain have been remarkably conserved throughout evolution (Neville and Haberly, 2004). However, while significant advances have been made in our understanding of odor coding at the initial stages of olfactory processing (Shepherd et al., 2004), less is known about how the cortex decodes this information and generates a representation of the olfactory world. The broad aim of my graduate work has been to elucidate the neural circuits governing odor processing in the primary olfactory (piriform) cortex. In particular, the experiments described here seek to define the role that inhibitory cells play in the integration of odor-evoked synaptic activity and the generation of spike output in principal cells of piriform cortex. We describe three independent circuits of inhibitory interneurons recruited during the processing of olfactory sensory input and demonstrate that they play independent but complementary roles in shaping the flow of information through piriform cortex.

Initial representation of odors: a spatial code

Odor detection in mammals begins at the olfactory epithelium in the nose, where odorant molecules bind to and activate receptors expressed on the surface of

olfactory sensory neurons (OSNs). Olfactory receptor proteins are encoded by a large gene family (more than 1000 functional genes in rodents; (Buck and Axel, 1991; Zhang and Firestein, 2002)). However, individual OSNs express receptors from one allele of a single receptor gene (for review see (Serizawa et al., 2004)), restricting their olfactory receptive field to molecules activating this receptor (Malnic et al., 1999; Zhao et al., 1998). The axons of OSNs coalesce into the olfactory nerve and project centrally to the ipsilateral olfactory bulb, where they defasciculate and form synapses within spherical regions of neuropil known as glomeruli. All of the sensory axons entering a single glomerulus originate from OSNs expressing a single receptor gene (Mombaerts et al., 1996; Treloar et al., 2002), thus individual glomeruli are tuned to particular molecular features of odorant molecules (Rubin and Katz, 1999). Odorants are therefore represented at the level of glomeruli as unique spatial patterns of activity around the olfactory bulb (Rubin and Katz, 1999; Uchida et al., 2000; Wachowiak and Cohen, 2001).

Output from the olfactory bulb: a temporal code

The output cells of the olfactory bulb are the mitral and tufted (M/T) cells, which receive direct sensory input via an apical dendrite that projects to a single "cognate" glomerulus (Shepherd et al., 2004). M/T cells fire action potentials (APs) spontaneously at a low rate in the absence of odor, but when activated by synaptic excitation in their cognate glomerulus they increase their spiking (Pager, 1985; Rinberg et al., 2006a). A fundamental feature of spiking activity from M/T cells, and within the

olfactory bulb in general, is that it is highly periodic. One dominant rhythm governing M/T cell firing is respiration (Bathellier et al., 2008; Margrie and Schaefer, 2003; Rinberg et al., 2006a; Spors and Grinvald, 2002): during each sniff cycle activated M/T cells fire bursts of APs, with longer bursts reflecting stronger synaptic excitation (Cang and Isaacson, 2003; Margrie and Schaefer, 2003). This has led to the idea that a sniff represents a discrete unit of olfactory information (Kepecs et al., 2006), which has been supported by experiments demonstrating that rodents can reliably make odor discriminations within a single sniff (Rinberg et al., 2006b; Uchida and Mainen, 2003).

In the olfactory bulb therefore, odorants are initially represented as the spatial and temporal patterns of M/T cell activity in a number of glomeruli. How do cortical circuits decode the bursts of M/T cell spiking that occur within a sniff cycle in order to generate an accurate representation of odor?

Cortical representations of olfactory information

The axons of M/T cells project via the lateral olfactory tract (LOT) to a number of cortical areas, the largest of which is *piriform* cortex (Neville and Haberly, 2004). The piriform cortex is important for olfactory learning and memory (Wilson et al., 2006), and lesions to it produce deficits in odor recognition and to discrimination of complex odors (Staubli et al., 1987; Zhang et al., 1998). In humans, activity in the anterior piriform cortex is correlated with odor identification and in the posterior piriform cortex it is correlated with odor categorization, reflecting the multiple roles of this area in the processing of olfactory information (Gottfried et al., 2006).

Structurally, the circuits of piriform cortex resemble those in associational areas of cortex(Johnson et al., 2000), and a major function of piriform cortex is thought to be the synthesis of information from multiple glomerular "channels" into a unified odor percept (Haberly, 2001; Haberly et al., 1987). However, the local circuits that mediate this transformation of olfactory bulb input are not well understood.

In contrast to other primary sensory areas of cortex, piriform cortex receives sensory information that has not passed through a thalamic relay nucleus (Haberly and Price, 1978). Recent anatomical tracing studies have shown that, also unlike other sensory cortical areas, there is no topographical or stereotyped representation of odors in piriform cortex (Ghosh et al., 2011; Miyamichi et al., 2011; Sosulski et al., 2011). Studies of neuronal activity from single cells and populations (Illig and Haberly, 2003; Litaudon et al., 2003; Poo and Isaacson, 2009; Rennaker et al., 2007; Stettler and Axel, 2009) have also revealed that individual odorants recruit spiking in spatially distributed populations. The spike output of single cells is narrowly tuned to only a few odorants of many tested (Poo and Isaacson, 2009; Stettler and Axel, 2009; Zhan and Luo, 2010). In order to understand the transformation from M/T cell input to spike output by principal cells of piriform cortex, we must define the cell types and circuit properties that govern excitation and inhibition onto these cells. Whole-cell recordings of synaptic activity in piriform cortex *in vivo* have found that odor-evoked excitation onto pyramidal cells is narrowly tuned while odor-evoked inhibition is broadly tuned (Poo and Isaacson, 2009). However, the circuits that underlie this odor-evoked activity, and in particular the inhibitory circuits, are not well understood.

Circuits in the piriform cortex

The piriform cortex has a simple three-layered structure with functionally distinct inputs largely segregated to separate layers, which makes it an attractive model system for understanding how cortical circuits contribute to the processing of sensory-evoked activity (Neville and Haberly, 2004). Layer 1 (L1) contains mainly apical dendrites and axon afferents, as well as sparse cell bodies that are mostly GABAergic interneurons (Young and Sun, 2009). M/T cell axons traveling in the LOT send descending collaterals that make excitatory synaptic connections exclusively within the upper half of layer 1 (L1a, (Haberly, 1985; Haberly and Price, 1978)). The deeper half, L1b, contains axons from other principal cells making recurrent associational (ASSN) connections as well as axons from other brain regions (Haberly and Bower, 1984; Tseng and Haberly, 1989b). Layer 2/3 (L2/3) is tightly packed with cell bodies. The majority of these are principal cells that extend dendrites upward into L1 and receive direct M/T cell input (Tseng and Haberly, 1989a, b). The principal cells can be grossly divided into two subtypes: semilunar cells possess multiple apical dendrites but no basal dendrites and reside only in the superficial region of L2/3; pyramidal cells possess both apical and basal dendrites and are found throughout L2/3 (Neville and Haberly, 2004; Suzuki and Bekkers, 2006). Inhibitory interneurons comprise between ten and thirty percent of the cells in L2/3 and represent a diversity of cell types according to morphological, immunohistochemical, and electrophysiological analyses (Ekstrand et al., 2001; Suzuki and Bekkers, 2007, 2010a, b). Despite the relatively simple

architecture and distinct inhibitory cell types of piriform cortex, the specific recruitment, synaptic connectivity, and functional consequences of inhibition within the local circuit have not been well studied.

Inhibitory circuits in the cortex

Synaptic inhibition in the cortex is composed of a wide array of cell types and postsynaptic targets; however a few broad functional categories can be defined that encompass the central roles of inhibition in sensory information processing (Markram et al., 2004). First, inhibitory cells can be activated via direct synaptic connections from afferent fibers (for example, thalamocortical projections onto layer 4 inteneurons) and inhibit nearby cells that are activated by the same complement of afferent fibers, a situation known as "feedforward" inhibition. Feedforward inhibition can impose a narrow time window in which principal cells are able to integrate synaptic excitation, only allowing spiking in response to coincident excitatory input (Gabernet et al., 2005; Pouille and Scanziani, 2001). Inhibitory cells can also be activated via connections from the same population of cells that they inhibit (for example, other layer 4 neocortical cells), a situation known as "feedback" inhibition. One proposed role for feedback inhibition is producing and modulating the oscillations in neural activity that are strongly evoked by sensory stimuli (Atallah and Scanziani, 2009; Hasenstaub et al., 2005; Leung, 1982).

In addition to the mechanisms through which inhibitory cells are recruited, the site of inhibitory synapses on the postsynaptic cell determines the effect of inhibition on

local circuits. Perisomatic inhibition is thought to strongly regulate spike timing and output from the cell due to its proximity to the AP initiation zone (Andersen et al., 1963; Cobb et al., 1995). Dendritic inhibition can influence synaptic integration and excitability (Kim et al., 1995), affecting calcium signaling and plasticity (Kanter et al., 1996; Larkum et al., 1999a; Miles et al., 1996). These configurations—feedforward, feedback, somatic and dendritic inhibition—are all thought to be present in the piriform cortex, but their role in the processing and representation of olfactory information by L2/3 pyramidal cells has not been examined.

Inhibitory circuits in the piriform cortex

Activation of M/T cell axons via a stimulating electrode placed in the LOT results in a complex but reproducible pattern of excitatory and inhibitory postsynaptic currents in space and time (Biella and de Curtis, 1995; Haberly and Shepherd, 1973; Ketchum and Haberly, 1993), suggesting that there is a canonical flow of activity through the circuit in piriform cortex. In brief, synaptic excitation from M/T cell axons in L1a generates spiking in L2/3 principal cells, leading to recurrent excitation in L1b and L2/3 (reviewed in (Neville and Haberly, 2004). Activation of M/T cell axons also recruits inhibition onto multiple regions of L2/3 pyramidal cells (Biedenbach and Stevens, 1969), but the sources of odor-evoked inhibition have not been well characterized. Inhibitory postsynaptic currents in L2/3 pyramidal cells can be recruited both via direct excitation from M/T cell axons and by recurrent excitation from piriform principal cells (Biedenbach and Stevens, 1969; Haberly and Bower, 1984; Satou et al.,

1983; Tseng and Haberly, 1988). In addition, inhibitory connections onto pyramidal cells are made both in the dendrites and at the soma (Kanter et al., 1996; Kapur and Haberly, 1998; Tseng and Haberly, 1988). The cell types that govern these various forms of inhibitory input have not been well characterized.

Inhibition powerfully influences the integration and spiking of principal cells, but in order to understand its role in the processing of sensory information, we must know the relevant interneuron subtypes and the ways that they are integrated within the cortical circuit. Therefore, defining the cell types that govern inhibition in olfactory cortex and understanding how these diverse sources of inhibition shape integration and spike output in L2/3 pyramidal cells has been the central focus of my thesis work.

Experimental Procedures

In vitro electrophysiology

Experiments followed approved national and institutional guidelines for animal use. Rats (Sprague-Dawley, P14-P25) were anesthetized using a mixture of ketamine and xylazine (100 mg and 10 mg per kg, respectively) and decapitated. The cortices were quickly removed and placed into ice cold artificial CSF (aCSF) containing (in mM): 83 NaCl, 2.5 KCl_2, 0.5 $CaCl_2$, 3.3 $MgSO_4$, 1 NaH_2PO_4, 26.2 $NaHCO_3$, 22 glucose, and 72 sucrose, equilibrated with 95% O_2 and 5% CO_2. Parasagittal slices (350 μm) of anterior piriform cortex were cut using a vibrating slicer (Vibratome) and incubated at 34ºC for 30 min. For some experiments, we confirmed that coronal slices gave identical results. Slices were then maintained at room temperature until they were transferred to a recording chamber on an upright microscope equipped with infrared, differential interference contrast optics (DIC; BX50WI; Olympus Optical, Tokyo, Japan) and superfused with aCSF containing (in mM): 119 NaCl, 2.5 KCl, 2.5 $CaCl_2$, 1.3 $MgSO_4$, 1 NaH_2PO_4, 26.2 $NaHCO_3$ and 22 glucose. All experiments were conducted at 28-30ºC

Voltage and current clamp recordings were collected using a Multiclamp 700B amplifier (Axon Instruments), digitized at 10 kHz and analyzed with AxographX software. For voltage clamp recordings, patch pipettes (3-5 MΩ) typically contained a cesium-based internal solution (in mM: 130 D-Gluconic acid, 130 CsOH, 5 NaCl, 10 HEPES, 10 EGTA, 12 phosphocreatine, 3 Mg-ATP and 0.2 Na-GTP (pH 7.31; 280-290

mOsm). For all current clamp (and some voltage clamp recordings), pipettes were filled with a K^+-based internal (in mM: 150 potassium gluconate, 1.5 $MgCl_2$, 5 HEPES buffer, 0.1 EGTA 10 phosphocreatine and 2.0 Mg-ATP; pH 7.45; 280-290 mOsm; 0.2% biocytin added for interneuron recordings). For most pyramidal cell recordings, a fluorescent dye (Alexa 488, 20 μM, Invitrogen) was added to the internal solution to confirm the presence of intact apical dendrites. Voltages were corrected for a measured liquid junction potential of 15 mV. Series resistance was <20 MOhm and compensated by >80% and recordings were terminated if series resistance increased by >20%. Unless noted otherwise, synaptic responses were evoked at 0.1-0.2 Hz with a concentric bipolar stimulating electrode placed in the LOT. The stimulating electrode was always placed >300 μm lateral of the recorded cells to reduce monosynaptic activation of interneuron axons. Unless stated otherwise, individual traces show the average of 10-20 trials and values are expressed as mean ± SEM.

Paired recordings

L1a and L3 interneurons could be easily identified by position of their soma, morphology, and by their intrinsic properties (low input resistance, AP shape, spiking profile). Deep L2 pyramidal cells were identified by their position in the lower half of the most densely packed cell body layer, a triangular cell body with a prominent single apical dendrite, and intrinsic properties including a higher input resistance and bursting spike profile (Suzuki and Bekkers, 2006). For studying connections between L1a interneurons and pyramidal cells, we made recordings from 317 interneuron-pyramidal

cell pairs, of which 27 (8.8%) had unitary connections. However, the laminar distance between the cell bodies in these paired recordings could be >200 μm. To control for slices in which the interneuron axonal arbor may have been partially severed, we first identified a recorded interneuron that evoked an IPSC in a pyramidal cell. Then, while keeping the identified interneuron, we recorded sequentially from additional pyramidal cells. Thus, the probability of connections from interneurons to pyramidal cells was computed exclusively using the additional pairs—that is, it did not include the initial pair used to identify the intact interneuron. For L3 FS cells, all cell pairs (n=64) were used to determine the probability of connections, since connections were tested in cells with nearby somata (<150 μm). Biocytin-filled cells were revealed by a DAB reaction with nickel intensification. Slices were dehydrated in alcohols and xylenes and mounted in damar resin. Cells were then manually reconstructed and neurite length measured using a Neurolucida system.

Pharmacology

The $GABA_A$ receptor antagonist gabazine (SR 95531, Tocris Biosciences, Ellisville MO) was applied focally via a pipette (10 μm tip diameter) using pressure (10-20 p.s.i, 20 ms, Picospritzer). Pulses (2-4) were applied at the start of stimulus trials first close to the soma of the recorded cell and then after the pipette was translated parallel to the apical dendrite and positioned in L1a. In half the experiments, gabazine was first applied to the dendrites, and following recovery of the response, the antagonist was applied to the cell body. For current clamp experiments examining the role of

dendritic inhibition in synaptic integration, pyramidal cells were held depolarized by ~10 mV. This allowed us to study integration of bursts of weak LOT excitation in individual pyramidal cells without recruiting widespread recurrent inhibition from the cortical population. The selective antagonist CGP55845 (Tocris Biosciences, Ellisville MO) was used to block currents through the $GABA_B$ receptor. The glutamate receptor antagonists NBQX ((Tocris Biosciences, Ellisville MO) and D-APV (Tocris Biosciences, Ellisville MO) were used to block synaptic currents from AMPA and NMDA receptors, respectively.

Transgenic mouse lines

We identified a line of bacterial artificial chromosome (BAC) transgenic mice, Ntsr1-creGN209, from the GENSAT project that selectively express Cre recombinase in a fraction of L2/3 pyramidal cells of piriform cortex, but not in pyramidal cells of other cortical regions (Methods). Mice derived from crossing this Ntsr1-cre strain with a Rosa-yellow fluorescent protein (YFP) reporter line revealed YFP expression in deep layer 2 and layer 3 pyramidal cells of piriform cortex (Fig. 9A). Cells expressing YFP did not overlap with those immunolabeled for the interneuron marker GAD-67 (Fig. 9A) and all YFP-expressing cells targeted for recording had regular spike firing properties typical of pyramidal cells (7/7, not shown).

Ntsr1-cre animals (Tg(Ntsr1-cre)209Gsat) were obtained from the Gensat Project and the expression pattern of Cre-recombinase in this line can be viewed at http://www.gensat.org/creGeneView.jsp?founder_id=44880&gene_id=511. Ntsr1-cre

mice were crossed with the Rosa-YFP reporter line (*Gt(ROSA)26Sor*$^{tm1(Smo/(EYFP)Cos}$/J, strain 006148, The Jackson Laboratory, Bar Harbor, ME) to produce mice expressing YFP in pyramidal cells of piriform cortex. For immunohistochemistry of Ntsr1-cre/Rosa-YFP progeny, whole brains were fixed in 4% PFA and frozen in 20% sucrose/PBS before being cut into thin (50 μm) sections using a sliding microtome (Thermo Scientific, Waltham MA). GABAergic interneurons were revealed using anti-GAD-67 (clone 5406, Millipore, Billerica, MA) and goat-anti mouse conjugated with Alexa 594 (A-11032, Invitrogen, Carlsbad, CA). Slices were mounted in Vectashield mounting medium with DAPI (Vector Labs, Burlingame, CA).

GIN (GFP Inhibitory Neuron, (Oliva et al., 2000)) mice were obtained as a gift from Dr. Massimo Scanziani. Somatostatin-cre mice (*Sst*$^{tm2.1(cre)Zjh}$/J, stock# 013044) were obtained from Jackson Laboratories (Bar Harbor, ME).

Viral injections

High-titer ($1.2*10^{12}$) stock of channelrhodopsin-2 virus, AAV-FLEX-*rev*-ChR2-tdTomato, was produced from Addgene plasmid #18917 by the University of Pennsylvania Gene Therapy Program Vector Core. High-titer halorhodopsin-3.0 virus, pAAV-double floxed-eNpHR3-EYFP-WPRE-pA, was obtained as a kind gift of Dr. Karl Deisseroth. Mouse pups from pairings between Ntsr1-cre (or somatostatin-cre) heterozygotes and ICR WT mice were injected at p0-2 since the skull at this age is soft enough to be penetrated by an injection pipette. Pups were anesthetized by placing them on ice for 2 minutes and positioned in a custom-made mold, which stabilized the

head with the dorsolateral surface facing upward. Injections were targeted to the anterior piriform cortex based on empirically determined landmarks including the posterior border of the eye and the superficial temporal vein. Injection volume was set to 13 nl using a Nanoject II nanoliter injector (Drummond Scientific, Broomall, PA) fitted with a pulled glass beveled micropipette. Location and depth were controlled using a 3-axis micromanipulator (Luigs & Neuemann, Ratingen, Germany). In each animal, anterior piriform cortex was injected at a depth of (0.25-0.5 mm) and the pipette was kept at each site for 30 seconds to allow virus to spread locally. Experiments were performed from animals (p30-40) in which only one hemisphere expressed ChR2-tdTomato and only ipsilateral slices were used for recording. We confirmed that the major anatomical and functional properties of L3 FS and L1a interneurons were equivalent to those characterized in rats (not shown). For photostimulation, light emitted from a 480-nm or 590-nm wavelength LED (Thor Labs, Newton, NJ) was collimated and delivered via the 40X objective positioned over L 2/3.

Calcium imaging

Patch pipettes (4-5 MOhm) for imaging experiments were filled with potassium-based internal solution containing (in mM): 150 KGluc, 1 MgCl2, 5 HEPES, 0.1 EGTA, 10 Phosphocreatine and 2 MgATP, pH 7.45. For calcium imaging in pyramidal cells, Oregon Green BAPTA-1 (100μM, for pyramidal cells) or Alexa 594 (50 μM, for interneurons) was included in the internal solution. For cell fills, biocytin-HCl (2 mg/ml) was included in the internal solution, slices were fixed using

paraformaldehyde (4%) and processed using a diaminobenzidine (DAB) reaction. Cells were reconstructed using Neurolucida and analyzed using Neurolucida explorer. Stimulation was delivered to the LOT or to layer1 using a concentric bipolar electrode. EPSCs were recorded at a holding potential of -70 mV and IPSCs were recorded at a holding potential of -40 mV.

Fluorescent calcium signals were collected using a TILL epifluorescence system with an IMAGO CCD camera via a 40x objective or using FluoView software on a two-photon microscope via a 60x objective. Trials were interleaved to maintain consistence across conditions. Movies (TILL) or linescans (two-photon) were analyzed off-line using imageJ and Igor Pro software. Calcium transients were measured by initially subtracting background fluorescence (measured from a nearby region not containing dendrites) then calculating the change in fluorescence relative to an initial baseline period (deltaF/F). To quantify the degree of reduction in calcium signal, transients were first smoothed (original sampling rate of 50Hz for two-photon, Gaussian smoothing algorithm in Igor Pro software over 5-10 neighboring points) and fitted with an exponential. Peak calcium signals were extracted from the fits and for each condition 2-5 peak values were averaged together to compute a mean deltaF/F. Reduction in dF/F was quantified as the difference in peak dF/F with or without inhibition, expressed as a percent of the initial peak dF/F without inhibition.

All recordings were performed at 28-30deg C. All electrophysiology data were acquired using a Multiclamp 700B and AxoGraph software and analyzed off-line in AxoGraph or Igor Pro software.

Chapter 1. Dendritic feedforward inhibition by layer 1a interneurons

Abstract

Diverse inhibitory pathways shape cortical information processing; however the relevant interneurons recruited by sensory stimuli and how they impact principal cells are unclear. Here we show that two major interneuron circuits govern dynamic inhibition in space and time within the olfactory cortex. Dendritic-targeting layer 1 interneurons receive strong input from the olfactory bulb and govern early-onset feedforward inhibition. However, this circuit is only transiently engaged during bursts of olfactory bulb input. In contrast, somatic-targeting layer 3 interneurons, recruited exclusively by recurrent excitation from pyramidal cells, produce late-onset feedback inhibition. Our results reveal two complementary interneuron circuits enforcing widespread inhibition, which shifts from the apical dendrites to the soma of pyramidal cells during bursts of sensory input.

Introduction

Local inhibitory circuits shape the responses of cortical pyramidal cells to excitatory sensory input (Ferster and Jagadeesh, 1992; Gabernet et al., 2005; Poo and Isaacson, 2009; Wehr and Zador, 2003; Wilent and Contreras, 2005). Interneurons governing cortical inhibition are anatomically and functionally highly diverse and often specialized to target inhibition to different subcellular compartments of principal cells (Markram et al., 2004; Silberberg, 2008; Somogyi et al., 1998). Furthermore, the activation of distinct populations of interneurons is a dynamic process that varies with the strength and timing of excitation (Markram et al., 2004; Silberberg, 2008). For example, trains of excitatory stimuli can produce a progressive shift in inhibition from the soma to the dendrites of principal cells in hippocampus and somatosensory neocortex (Pouille and Scanziani, 2004; Silberberg and Markram, 2007; Tan et al., 2008). However, in many cortical regions the functional properties of interneuron circuits and how they shape the integration and transmission of sensory information remains unclear.

The primary olfactory (piriform) cortex is a three-layered cortical region that plays an important role in odor discrimination, recognition, and memory (Neville and Haberly, 2004; Wilson et al., 2006). In vivo studies have found that odor-evoked activity is sparse and distributed across the population of layer 2/3 principal cells in piriform cortex (Poo and Isaacson, 2009; Stettler and Axel, 2009). Odors evoke inhibition that is widespread and broadly tuned (Poo and Isaacson, 2009), in contrast to other primary sensory cortices where stimuli elicit balanced excitation and inhibition

(Anderson et al., 2000; Wehr and Zador, 2003; Wilent and Contreras, 2005). Local inhibitory pathways are likely to be critical for sparse odor representations by principal cells. However, the interneuron circuits governing sensory-evoked inhibition in piriform cortex are not well established.

Olfactory information is first encoded in the olfactory bulb, where mitral and tufted (M/T) cells belonging to unique glomeruli are activated by particular molecular features of individual odorants (Rubin and Katz, 1999; Uchida et al., 2000; Wachowiak and Cohen, 2001). A fundamental feature of M/T cell activity is that odor-evoked responses are tightly coupled to respiration (Bathellier et al., 2008; Margrie and Schaefer, 2003; Rinberg et al., 2006a; Soucy et al., 2009; Spors and Grinvald, 2002). During a single respiratory cycle, activated M/T cells typically fire short bursts of action potentials (APs) at a frequency of 10-50 Hz (Cang and Isaacson, 2003; Margrie and Schaefer, 2003) and the number of APs during each respiratory-coupled burst is correlated with the strength of input from olfactory receptor neurons. This sensory information is relayed via M/T cell axons within the lateral olfactory tract (LOT) directly to the piriform cortex. M/T cell axons in the LOT make collateral projections only within the most superficial layer of piriform cortex (layer 1a) and form excitatory synaptic contacts onto the distal apical dendrites of layer 2/3 principal cells (Neville and Haberly, 2004). Given the characteristic temporal structure of odor-evoked M/T cell activity, inhibitory circuits in olfactory cortex may have features that optimize the processing of bursting sensory input.

Here we show that bursts of M/T cell activity drive a progressive shift in

inhibition from the distal apical dendrite to soma of pyramidal cells in piriform cortex and we reveal two complementary interneuron circuits that govern the spatio-temporal dynamics of this inhibition. Dendritic-targeting interneurons in layer 1a (L1a) receive a higher convergence of M/T cell input than pyramidal cells and mediate short-latency, disynaptic inhibition. However, target-specific differences in the short-term dynamics of M/T cell synapses lead to the early but transient recruitment of L1a interneurons during bursts of input. In contrast, perisomatic-targeting layer 3 fast-spiking (FS) cells receive excitation exclusively from active principal cells and mediate late-onset "feedback" inhibition during bursts. Individual layer 3 FS cells inhibit many pyramidal cells but preferentially target those that excite them. Using an optogenetic approach, we show that recurrent excitation to layer 3 FS cells is much stronger than excitation onto pyramidal cells themselves, resulting in somatic feedback inhibition that dominates excitation in local pyramidal cells. Together, these results reveal how the functional properties of two complementary interneuron circuits direct the flow of inhibition in space and time.

Results

Bursts of LOT input elicit a shift in inhibition from dendrite to soma

We studied synaptic responses using parasagittal slices of rat anterior piriform cortex (Franks and Isaacson, 2005, 2006; Poo and Isaacson, 2007). We made whole-cell recordings from deep layer 2 pyramidal cells and evoked synaptic responses via a stimulating electrode placed in the LOT (Fig. 1.1A, Methods). Pyramidal cells were

voltage-clamped at the reversal potential for excitatory postsynaptic currents (EPSCs, V_m= 0 mV) to isolate inhibitory responses. We first examined the nature of inhibitory postsynaptic currents (IPSCs) evoked by bursts of LOT stimuli that approximate the respiratory-coupled activity of M/T cells in vivo (5 pulses at 20 Hz delivered every second). Under these conditions we could distinguish two distinct components of inhibition—the "early-transient" component was strongly recruited by the first (1-2) pulses in a burst then rapidly decreased in amplitude, and the "late onset" component was strongest on the later (3-5) pulses in a burst. Early-transient inhibition, consisting of short-latency IPSCs whose amplitude was greatest on the first pulse, was always evoked at lower stimulus intensities than late-onset inhibition (Fig. 1.1B). The amplitude of early-transient IPSCs grew in a graded fashion when stimulus strength was increased to recruit more LOT fibers. As stimulus strength was further increased, the late-onset component of inhibition was recruited, and with still higher stimulus intensities the amplitude of both early and late IPSCs continued to grow (Supplemental Fig. 1.1). Late-onset IPSCs could be readily distinguished from the transient early-onset IPSCs, since they occurred with a longer latency after each individual stimulus pulse and typically increased in amplitude on successive pulses (Fig. 1.1C). Both types of IPSCs were abolished in the presence of the glutamate receptor antagonists NBQX (10 μM) and D-APV (50 μM) (Fig. 1.1D), confirming that these LOT-evoked responses are not due to direct activation of local interneurons; rather they require excitatory transmission from M/T cell axons.

We also observed that early-onset IPSCs had significantly slower rise times (10-90%) than the late-onset, long latency events (c.f. Fig 1C, 2.2 ± 0.4 ms for IPSCs evoked by the first pulse vs. 0.6 ± 0.1 ms for IPSCs evoked by the fifth pulse, n=7, p=0.005). Given the somatic location of our recordings and the electrotonic filtering properties of dendrites, the slower rise times of early-transient IPSCs suggest they may occur at more distal locations along the somato-dendritic axis of pyramidal cells than late-onset IPSCs. To determine the location of the two components of LOT-evoked inhibition onto pyramidal cells, we used focal application of the $GABA_A$ receptor antagonist gabazine (40 μM) via puffer pipette. Stimulus intensity was set above the threshold for recruiting both early-transient and late-onset IPSCs (Fig. 1.1E, Supplemental Fig. 1.1A). When gabazine was focally applied to the distal apical dendritic region of the recorded pyramidal cell (250 μm from soma), the early-onset IPSCs were reversibly abolished while IPSCs late in the train remained essentially unchanged (Fig. 1.1 E,F). In contrast, when gabazine was applied near the soma of the pyramidal cell (40 μm away), the late-onset IPSCs were blocked while the early IPSCs were unaffected. Dendritic application of gabazine (245 ± 18 μm from soma, n=4) reduced the early-transient component of inhibition on average to 8 ± 4% ($p<0.01$) of control (measured as IPSC charge evoked by the first pulse) while late-onset inhibition (IPSC charge during the last three pulses) averaged 104 ± 13% of control (Figure 1G). During somatic gabazine application (34 ±5 μm from soma, n=5) late-onset inhibition was reduced to 10 ± 4% of control levels while early inhibition was not significantly affected (86 ± 15% of control, p=0.4, Figure 1G). These results indicate that during

bursts of sensory input inhibition shifts from the distal apical dendrite to the perisomatic compartment.

L1a interneurons mediate dendritic feedforward inhibition

What mechanisms underlie these spatio-temporally distinct sources of LOT-evoked inhibition in olfactory cortex? We first addressed the early, dendritic component of inhibition by studying responses to single, weak LOT stimuli. Under these conditions, the onset of LOT-evoked IPSCs (V_m = 0 mV) followed monosynaptic EPSCs (recorded at -90 mV, close to the reversal potential for inhibition, $[Cl^-]_{int}$=5 mM) with a very brief delay (1.95 ± 0.2 ms, *n* = 7; Fig. 1.2A). This short latency indicates that the dendritic IPSC is recruited through a disynaptic, feedforward mechanism by LOT input rather than a feedback mechanism requiring the activation of pyramidal cells (Cruikshank et al., 2007; Gabernet et al., 2005).

We hypothesized that interneurons located in L1a, close to the site of LOT collateral inputs, would be poised to govern feedforward inhibition. To test this idea, we monitored spiking in L1a interneurons when LOT stimulus strength was set at the threshold for recruiting feedforward inhibition. We could resolve clear successes and failures of IPSCs on 50% of trials in a voltage-clamped pyramidal cell, and in a simultaneous recording in cell-attached mode from a L1a interneuron, we observed successes and failures of individual APs that co-varied with the IPSCs evoked in the pyramidal cell (Fig. 1.2B). Subsequent whole-cell recording of the interneuron confirmed that it made a direct unitary connection onto the pyramidal cell with an

average IPSC amplitude identical to that of successful IPSCs evoked by LOT stimulation (Fig. 1.2C). This result indicates that L1a interneurons are a source of LOT-evoked feedforward inhibition in piriform cortex.

To determine whether the axons of L1a interneurons target the distal apical dendrites of pyramidal cells as suggested by our focal application of gabazine, we filled L1a interneurons with biocytin and reconstructed their morphology. Despite variability in their spike-firing patterns, all recorded L1a interneurons had dendritic and axonal arbors restricted to layer 1 (Fig. 1.2D-F, Supplemental Figure 1.2). On average, 92 ± 16% of the total axon length of L1a interneurons (n = 11) was distributed superficial to layer 2 (Fig. 1.2G). Although L1a interneurons have axons that spread laterally for hundreds of microns (Fig. 1.2D-F), they exclusively target the apical dendrites of principal cells. These anatomical data suggest that L1a interneurons represent a major circuit governing widespread, dendritic inhibition.

L1a interneurons receive strong LOT input

Do L1a interneurons sample from the same sensory afferents as neighboring pyramidal cells? To address this, we used simultaneous recordings from L1a interneurons and nearby pyramidal cells (within 300 μm) to compare the properties of M/T cell inputs onto these two cell types. LOT stimulation evoked short-latency, monosynaptic EPSCs in all voltage-clamped (V_m= -90 mV) L1a interneurons (Fig. 1.3), confirming that they can be activated in a feedforward manner. We first measured the amplitude of LOT-evoked EPSCs in response to bulk LOT stimulation at progressively

stronger intensities (Fig. 1.3B,C). In virtually all paired recordings (n=12/13), the LOT-evoked EPSC was larger in the interneuron than in the pyramidal cell over a range of stimulus intensities (Fig. 1.3D). On average, the compound EPSC was 6.1 ± 1.2 times larger in interneurons than pyramidal cells (Fig. 1.3E; at stimulus strengths that were 4-8 times threshold for recruiting single fiber inputs). This difference in LOT-evoked compound EPSC amplitude could be due either to stronger unitary connections between M/T cells and L1a interneurons or a higher convergence of M/T cell axons onto L1a interneurons than pyramidal cells.

To differentiate between these two possibilities, we determined the strength of single M/T axon connections in simultaneously recorded L1a interneurons and pyramidal cells using minimal LOT stimulation (Franks and Isaacson, 2006). In most cases this required adjusting the stimulus strength first to isolate a single fiber in one cell, then readjusting it to isolate a single fiber in the other cell. In one example, minimal LOT stimulation evoked successes and failures of transmission that were perfectly correlated in the two cells (Fig. 1.3F), indicating that the same M/T cell axon could contact both a pyramidal cell and interneuron. The strength of single fiber inputs varied over a large range in L1a interneurons (Fig. 1.3C), similar to previous observations for pyramidal cells (Franks and Isaacson, 2006). The distributions of single-fiber EPSC amplitude measured in cell pairs were virtually identical (mean 43.1 ± 12 pA and 38.6 ± 9.6 pA for interneurons and pyramidal cells, respectively; Kolmogorov-Smirnov (KS) test, $p = 0.2$, $n = 18$; Fig. 1.3C). Together, these data suggest that feedforward L1a interneurons and pyramidal cells sample sensory input

from the same complement of M/T cells. Since the amplitudes of single-fiber EPSCs were equivalent in both cell types, the simplest explanation of these findings is that there is a 6-fold greater convergence of LOT fibers onto L1a interneurons than onto pyramidal cells.

Synaptic properties underlying early-transient activation of L1a interneurons

We next used bursts of stimuli to compare the temporal dynamics of LOT-evoked EPSCs in simultaneously recorded pairs of L1a interneurons and pyramidal cells (5 pulses, 20 Hz; Fig. 1.3H). In striking contrast to the short-term facilitation of EPSC amplitude in pyramidal cells, we found across the population of L1a interneurons that LOT-evoked EPSCs depressed during stimulus trains (Fig. 1.3H,I). Although a minority of interneurons showed weak facilitation on the 2nd pulse, all cells had strongly depressed EPSCs by the last pulse in the train. On average, the EPSC amplitude of the 2nd pulse relative to the first (P2/P1) was 2.36 ± 0.43 for pyramidal cells and 0.97 ± 0.10 for interneurons (n=12 pairs), whereas the ratio P5/P1 was 1.53 ± 0.31 vs. 0.45 ± 0.06 for pyramidal cells and interneurons, respectively. This relationship held true for a range of stimulus frequencies (10 Hz: P5/P1 pyramidal=1.64 ± 0.22, interneuron=0.51 ± 0.04, n=7 pairs; 50 Hz: P5/P1 pyramidal=1.06 ± 0.27, interneuron=0.21 ± 0.03, n=9 pairs). These results indicate that there are target cell-specific differences in the short-term dynamics of synaptic inputs to pyramidal cells and L1a interneurons and suggest that L1a interneurons may preferentially fire early in response to bursts of LOT activity.

We therefore investigated synaptic integration and threshold firing of L1a interneurons in response to trains of LOT stimuli (5 pulses, 20 Hz). We determined AP threshold by making non-invasive cell-attached recordings and adjusting the strength of LOT stimulation such that APs were evoked on 50% of individual trials (Franks and Isaacson, 2006). We then ruptured the membrane patch and recorded the underlying EPSCs (V_m=-90 mV) at the same stimulus setting. L1a interneurons were most likely to fire APs only in response to the first or second pulse during the stimulus train (Fig. 1.4A, n=16). APs were precisely time-locked: they occurred within a very narrow time window (standard deviation of latencies for APs on the first pulse = 0.28 ± 0.03 ms, n=10) and their average latency from the onset of the underlying EPSC was brief (1.89 ± 0.31 ms). Furthermore, the amplitude of the EPSC producing threshold firing averaged 482 ± 53 pA (n=11) in interneurons, only moderately larger than the EPSC amplitude (~300 pA) found previously to bring pyramidal cells to spike threshold (Franks and Isaacson, 2006). Given the average single-fiber EPSC amplitude of ~40 pA, these experiments suggest that the coincident activation of only ~12 M/T cell inputs are sufficient to bring L1a interneurons to AP threshold. Together, these results indicate that while L1a interneurons can be precisely activated by relatively few M/T cells, depressing synaptic input favors their early-transient recruitment during bursts of activity.

Connectivity of L1a interneurons

The influence of L1a interneurons within the cortical circuit depends on their connectivity with cortical pyramidal cells. For connected pairs of L1a interneurons and pyramidal cells, single action potentials in the interneuron always evoked short-latency (0.6 ± 0.1 ms, n=10) unitary IPSCs (uIPSCs) in simultaneously recorded pyramidal cells (V_m=-40 mV, Fig. 1.4B). The mean unitary conductance was 0.6 ± 0.1 nS (n = 23) and uIPSCs were blocked by the $GABA_A$ antagonist bicuculline (50 μM, Fig. 1.4B). The rise time of uIPSCs (2.0 ± 0.3 ms, n = 10) was identical to the rise time of early-transient feedforward IPSCs evoked by LOT stimulation (2.2 ms), consistent with the idea that L1a interneurons are a source of feedforward inhibition. L1a interneurons inhibited 29% of local pyramidal cells (n = 46 pairs, Fig. 1.4B, Methods). Feedback projections (unitary excitatory connections from pyramidal cells back onto L1a interneurons) were only rarely observed (2%, n = 46). These results suggest that individual L1a interneurons provide widespread feedforward inhibition onto a large number of pyramidal cells but are unlikely to be a major source of "feedback" inhibition. Additionally, when interneurons were driven to fire bursts of spikes (5 APs, 20 Hz) uIPSC amplitude always depressed (P2/P1= 0.58 ± 0.02; P5/P1=0.39 ± 0.02, n = 23; Fig. 1.4C). Therefore, the short-term synaptic depression of both their excitatory input and inhibitory output ensures L1a interneurons produce only early-transient dendritic inhibition during bursts of M/T cell activity.

Dendritic inhibition enforces late temporal integration of bursting input

What role does early-transient dendritic feedforward inhibition play in regulating the integration and firing of pyramidal cells in response to M/T cell input? Given that the transformation of synaptic input to spike output relies on the relative balance of excitation and inhibition, we compared the amplitude of excitation and dendritic inhibition in pyramidal cells during trains of weak LOT stimuli. The ratio of the EPSC on the fifth pulse relative to the first (P5/P1) averaged 1.61 ± 0.4 (n=5) while for the IPSC this value fell to 0.16 ± 0.02 (Fig. 1.5A, B). This relationship was also observed at higher stimulus frequencies (50 Hz: P5/P1 EPSC=3.3±1, IPSC=0.25±0.04, n=5). To determine the relative magnitudes of excitation and inhibition, we measured the fraction of the total conductance contributed by the excitatory postsynaptic conductance (EPSG). While excitation and inhibition were perfectly balanced on the first pulse (fractional EPSG=0.49 ± 0.08, n=5), by the last pulse in the train, the total synaptic conductance was dominated by excitation (fractional EPSG=0.88 ± 0.03; Fig. 1.5C). Thus, bursts of sensory input cause a dramatic shift in the balance of feedforward inhibition and excitation received by pyramidal cell dendrites.

This relationship suggests that dendritic inhibition may act synergistically with excitation to enforce temporal summation and limit early spiking by pyramidal cells in response to trains of weak stimuli. We explored this possibility by recording pyramidal cells in current clamp to monitor spike output, under conditions in which they were just above threshold to fire a single AP in response to bursts of LOT stimuli (fraction of trials eliciting an AP=0.63 ± 0.07, n=9). Stimulus strength was sufficient to evoke

early-transient inhibition, but only minimal late-onset inhibition. In control conditions, AP latency was skewed toward EPSPs later in the train (Fig. 1.5D, E). Focal application of gabazine at the soma had little effect on the likelihood that a cell would reach AP threshold (0.61 ± 0.10 of trials) or on the timing of APs (Fig. 1.5E, F) during stimulus trains, indicating that somatic inhibition was not limiting integration of weak LOT input under these conditions (Methods). In contrast, focal dendritic application of the antagonist increased the probability that APs were evoked (0.94 ± 0.04 of trials) and often led to multiple APs in response to the stimulus (average number of spikes per trial = 1.96 ± 0.33 versus 0.66 ± 0.07 for control). Blocking dendritic inhibition also shifted AP latencies to earlier EPSPs during the stimulus train (Fig. 1.5 E, F). These results indicate that dendritic feedforward inhibition limits the temporal integration and spike output of pyramidal cells in response to early phases of bursting input.

Feedback somatic inhibition

The cell types mediating somatic feedback inhibition are described in Chapters 3 and 4 of this work.

Discussion

We find that bursts of olfactory bulb input produce a shift in inhibition from the distal apical dendrite to the soma of pyramidal cells in piriform cortex. We demonstrate that two major interneuron circuits account for these features: dendritic-targeting interneurons govern early-transient feedforward inhibition and somatic-

targeting interneurons mediate late-onset feedback inhibition. Moreover, our results reveal that differences in the connectivity and synaptic properties of these complementary interneuron circuits underlie their selective recruitment during bursts of M/T cell input. We show that both dendritic and somatic interneuron circuits make promiscuous connections with local pyramidal cells and govern widespread inhibition.

Routing of inhibition from dendrite to soma

Weak LOT input triggers short-latency disynaptic inhibition exclusively onto the apical dendritic compartment of pyramidal cells in piriform cortex. However, dendritic feedforward inhibition rapidly wanes during bursts of LOT stimulation that mimic the firing pattern of M/T cells in response to odors in vivo. We find that increasing stimulus intensity leads to the subsequent appearance of somatic inhibition that is preferentially recruited late during bursts of input. Intriguingly, this progressive shift of inhibition along the somato-dendritic axis in piriform cortex occurs in the opposite direction to that generally found in other brain regions. For example, in hippocampal and neocortical circuits, excitatory stimuli elicit transient somatic inhibition and delayed dendritic inhibition (Biel et al., 2009; Gabernet et al., 2005; Higley and Contreras, 2006; Kapfer et al., 2007; Pouille and Scanziani, 2001, 2004; Silberberg and Markram, 2007). Fast, transient somatic inhibition is effective in promoting spike output that is precisely time locked to the onset of excitatory input (Pouille and Scanziani, 2001, 2004), while inhibition to the dendritic compartment regulates local dendritic excitability and dendritic calcium dynamics (Larkum et al.,

1999a). In piriform cortex afferent sensory input is uniquely localized to the distal apical dendritic layer, thus the shift in inhibition in piriform cortex represents a logical transition from a region of synaptic integration to a region of spike output. We explored the circuits directing the flow of inhibition from dendrite to soma and how they might influence the processing of sensory information in piriform cortex.

M/T cell input drives transient dendritic feedforward inhibition from L1a interneurons

We identified dendritic-targeting L1a interneurons as a major source of disynaptic feedforward inhibition in olfactory cortex. In neocortex, feedforward interneurons are driven reliably by powerful thalamic input and single thalamic fibers make stronger connections onto interneurons compared to principal cells (Cruikshank et al., 2007; Gabernet et al., 2005; Hull et al., 2009). In piriform cortex, while the strengths of single M/T cell axon inputs onto feedforward interneurons and pyramidal cells are similar, L1a interneurons are contacted by many more inputs. If axons from M/T cells of different glomeruli make random connections, this would mean that L1a interneurons receive excitation from a broader pool of glomeruli than pyramidal cells. Our results also suggest that M/T cell inputs have target cell specific differences in transmitter release probability: the short-term depression of LOT inputs onto interneurons compared to the facilitation onto pyramidal cells suggests a higher release probability at synapses onto interneurons (Koester and Johnston, 2005; Scanziani et al., 1998; Zucker and Regehr, 2002). Thus multiple mechanisms ensure that L1a interneurons are reliably activated by M/T cell spiking.

We find that the strength of dendritic feedforward inhibition (IPSC conductance) and direct excitation (EPSC conductance) onto pyramidal cells is balanced during low-frequency activation of LOT inputs. This is similar to observations in thalamocortical circuits where the relative strength of short-latency inhibition is equal to or even exceeds that of monosynaptic excitation (Cruikshank et al., 2007; Gabernet et al., 2005; Higley and Contreras, 2006; Wehr and Zador, 2003). However, in piriform cortex, bursts of M/T cell input lead to a strong facilitation of direct excitation and depression of feedforward inhibition, while in thalamocortical circuits both excitation and inhibition depress during trains (Gabernet et al., 2005; Higley and Contreras, 2006). Since transient feedforward inhibition coincides with facilitating excitation in piriform cortex, we predicted that the interplay between these two opposing dendritic signals acts synergistically to enforce temporal summation. Indeed, we found that dendritic inhibition curtails early pyramidal cell spike output during bursts of M/T cell input.

Implications for olfactory information coding

Inhibition is an important feature of odor-evoked responses in both the piriform cortex of the rodents (Poo and Isaacson, 2009) and the mushroom body, an analogous region of the insect brain (Laurent, 2002). In both systems, odors evoke sparse population responses that arise from specific excitation and broadly tuned inhibition. In locusts, feedforward interneurons located in the lateral horn govern broadly tuned inhibition and short integration time windows for precise spike timing during odor-

evoked oscillations in synaptic activity (Laurent, 2002; Perez-Orive et al., 2002). In piriform cortex, global (widespread and nonselective) inhibition has been proposed to result from local interneurons that receive ubiquitous and broadly tuned excitation (Poo and Isaacson, 2009), and odor-evoked oscillations (15-30 Hz) in excitation and inhibition are thought to constrain spike timing (Poo and Isaacson, 2009). Our results indicate both local feedforward and feedback circuits are likely to contribute to global inhibition and the regulation of spike output in piriform cortex.

L1a interneurons have many features optimized for producing broadly tuned feedforward inhibition in response to odors: they receive a high convergence of M/T cell inputs (likely sampled from different glomeruli), require coincident activity from few inputs to fire, and make inhibitory contacts onto the dendrites of many pyramidal cells. We show that dendritic feedforward inhibition is most effective at limiting the integration of excitatory sensory input under conditions when M/T cells fire sparsely (i.e. one or few APs). This suppresses the representation of weakly active M/T cell inputs in piriform cortex. However, bursts of APs from strongly activated M/T cells reduce the effectiveness of feedforward inhibition, permitting pyramidal cells to reach spike threshold via the temporal summation of EPSPs. Together, these features suggest that dendritic feedforward inhibition limits cortical responses to temporally sparse M/T cell activity while promoting the representation of odors causing bursts of activity. Our results do not exclude the possibility that dendritic feedforward inhibition could contribute to coincidence detection (Pouille and Scanziani, 2001) in piriform cortex: pyramidal cells receiving inputs only from very weakly activated M/T cells (each firing

a single AP) could reach spike threshold only if M/T cells are active within a very narrow (<2 ms) time window before the onset of feedforward inhibition. However, whether weakly active M/T cells fire with such synchrony under physiological conditions is unclear. Rather, we propose that temporally dynamic feedforward inhibition acts largely as a salience filter to selectively enhance the cortical representation of strongly active (bursting) M/T cells.

Figure 1.1 Bursts of LOT input evoke early-transient dendritic inhibition and late-onset somatic inhibition in piriform cortex. **(A)** Schematic of piriform cortex circuitry; individual M/T cell axons in the LOT project directly from OB to cortex and synapse on the apical dendrites of pyramidal cells (PYR) in layer 1a. Putative interneuron (INT) populations provide somatic and dendritic inhibition. **(B)** LOT-evoked IPSCs recorded in a L2 pyramidal cell (V_m=+10mV). Low-intensity LOT stimulation elicits early, transient IPSCs while higher intensity stimulation elicits both early and late IPSCs. **(C)** Individual traces of IPSCs generated in another cell in response to the first (red traces) or fifth (black traces) stimulus pulse. **(D)** Responses from the cell in (C) before (Control) and after application of NBQX (20 μM) and APV (50 μM). **(E)** Focal dendritic application of gabazine selectively blocks the early-transient component of inhibition while somatic application of the antagonist blocks late-onset inhibition. IPSCs recorded in a L2 pyramidal cell under control conditions and during focal dendritic (blue) or somatic (green) puffer application of gabazine (40 μM). **(F)** Time course of the experiment in (E). Peak IPSC amplitude was measured following the first (open circles) and fifth (closed circles) pulse. **(G)** Summary data of IPSC charge in response to the first pulse (open circles) and in response to the third through fifth pulses (closed circles). (n=4 for dendritic gabazine, n=5 for somatic gabazine).

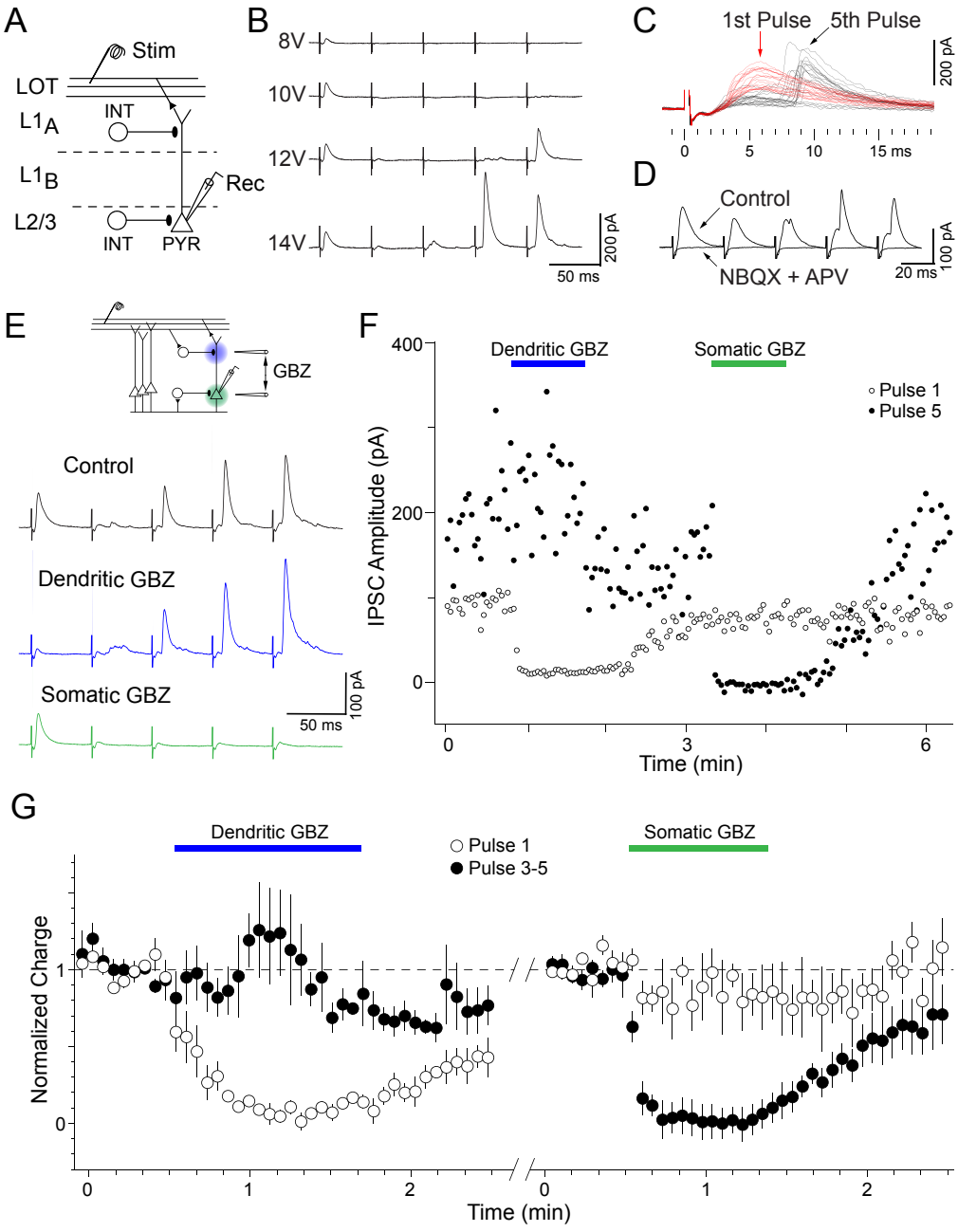
A
Stim
LOT
INT
L1A
L1B
Rec
L2/3
INT
PYR
B
8V
10V
12V
14V
200 pA
50 ms
C
1st Pulse
5th Pulse
200 pA
0
5
10
15 ms
D
Control
NBQX + APV
100 pA
20 ms
E
GBZ
Control
Dendritic GBZ
Somatic GBZ
100 pA
50 ms
F
Dendritic GBZ
Somatic GBZ
Pulse 1
Pulse 5
IPSC Amplitude (pA)
400
200
0
0
3
6
Time (min)
G
Dendritic GBZ
Somatic GBZ
Pulse 1
Pulse 3-5
Normalized Charge
1
0
0
1
2
0
1
2
Time (min)

Figure 1.2 L1a interneurons underlie LOT-evoked feedforward inhibition onto the apical dendrites of pyramidal cells. **(A)** Early-onset IPSCs follow EPSCs with a brief latency, consistent with disynaptic recruitment of interneurons. Top, EPSC (-90 mV) and IPSC (0 mV) recorded from the same cell displaying the interval between the 10% rise times of the synaptic currents. Bottom, summary of latencies for 7 cells. **(B)** Simultaneous recording from a L1a interneuron in the cell-attached configuration (top) and a pyramidal cell in the whole-cell voltage-clamp configuration (0 mV). Stimulation of the LOT generated successes and failures of IPSCs in the pyramidal cell and APs in the L1a interneuron (All trials). Sorting the traces based on successes and failures of the interneuron APs revealed that the pyramidal cell IPSC only occurred when the interneuron fired. **(C)** Subsequent whole-cell recording of the interneuron (V_m=-80 mV) shows that an action current (elicited by a voltage step to 0 mV) evoked an IPSC in the pyramidal cell with an amplitude identical to the feedforward IPSCs evoked by LOT stimulation. **(D-G)** Dendritic (blue) and axonal (red) arbors of three biocytin-filled L1a interneurons (black cell bodies). Traces to the upper right are voltage responses to a series of current steps (100 pA, 1 s) for each reconstructed cell. Dashed line, layer 1/2 border. **(D)** Cell with non-adapting firing pattern. **(E)** Cell with irregular-spiking firing pattern. **(F)** Cell with late-spiking firing pattern. **(G)** Summary of the laminar depths of neurites (10 μm bins) demonstrates localization of axon primarily within layer 1 (n=11 cells). Sample pyramidal cell included for comparison (black). Laminar borders (dashed lines) are drawn as mean measured distance from layer 1/2 border. Grey bar indicates the mean location (± SEM) of the cell bodies.

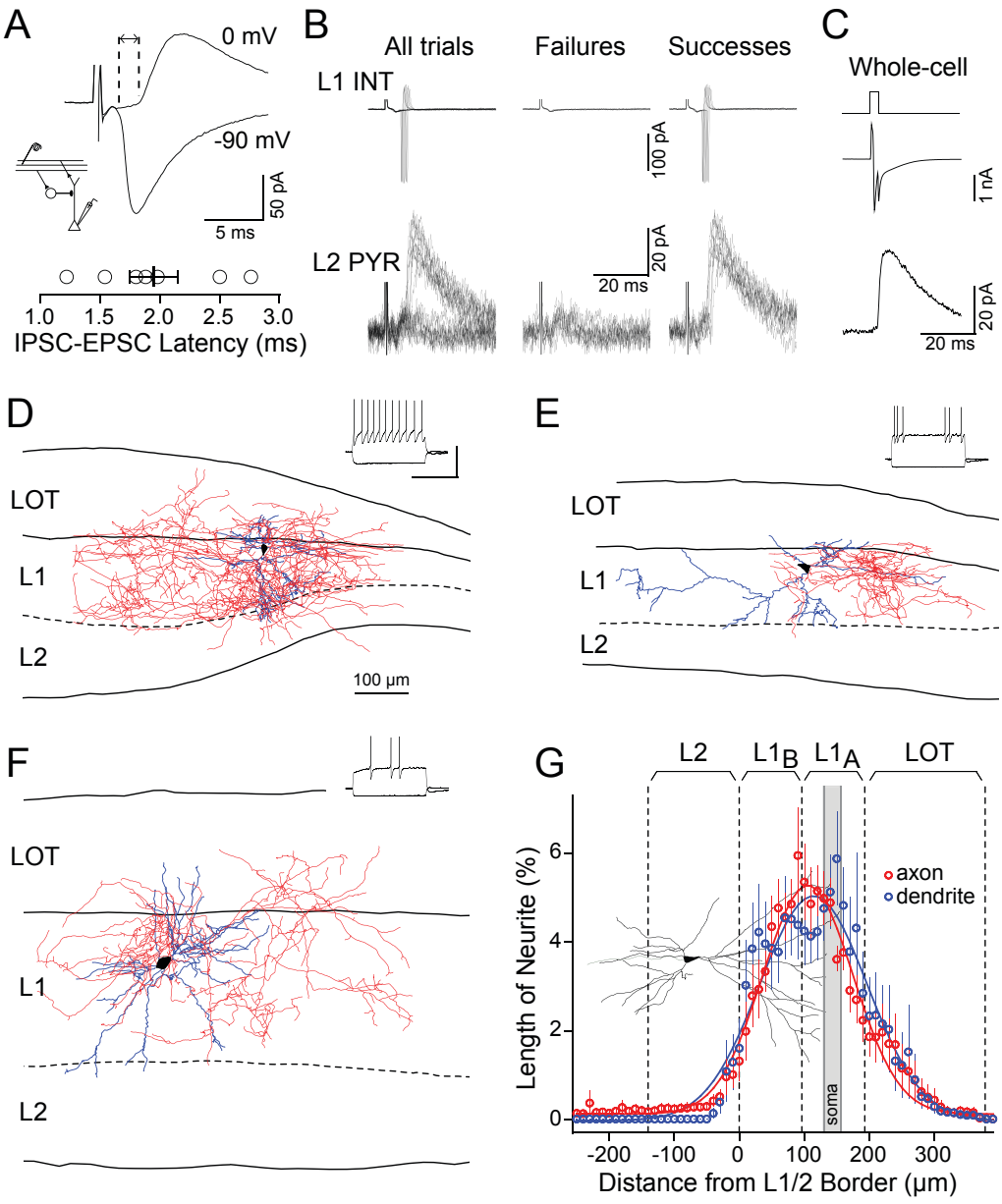
A
0 mV
-90 mV
50 pA
5 ms
1.0 1.5 2.0 2.5 3.0
IPSC-EPSC Latency (ms)
B
All trials
Failures
Successes
L1 INT
L2 PYR
100 pA
20 pA
20 ms
C
Whole-cell
1 nA
20 pA
20 ms
D
LOT
L1
L2
100 µm
E
LOT
L1
L2
F
LOT
L1
L2
G
L2
L1B
L1A
LOT
axon
dendrite
soma
Length of Neurite (%)
0
2
4
6
-200 -100 0 100 200 300
Distance from L1/2 Border (µm)

Figure 1.3 L1a interneurons and pyramidal cells are contacted by the same M/T cells, but interneurons receive a higher convergence of synaptic input with different short-term dynamics. **(A)** Minimal stimulation evoked failures and successes of EPSCs that co-varied in a paired recording. Trials sorted based on successes or failures in the pyramidal cell (black) show matching successes and failures in the interneuron (blue). **(B)** Plot of EPSC amplitudes for each trial in the interneuron and pyramidal cell. **(C)** Summary of single-fiber LOT inputs onto simultaneously recorded pairs of L1a interneurons and pyramidal cells (n=12 pairs). Filled circles, mean amplitude. **(D)** L1a interneurons are contacted by more M/T cell axons than pyramidal cells. Traces show EPSCs recorded simultaneously in an L1a interneuron and pyramidal cell as LOT stimulus strength is gradually increased. Plot of EPSC amplitudes indicates that increasing LOT stimulus intensity (8.6V to 50 V) recruits larger responses in the interneuron compared to the pyramidal cell. **(E)** Summary showing that compound EPSC amplitudes are typically larger in interneurons compared to simultaneously recorded pyramidal cells (n = 13 pairs). **(F)** Ratio of EPSC amplitudes in the same interneurons and pyramidal cells. **(G)** During a burst of LOT input (5 pulses, 20 Hz), EPSCs depress in an interneuron (blue) and facilitate in a pyramidal cell (black). **(H)** Summary plot (n=12 pairs) of short-term dynamics of EPSCs evoked at 20 Hz onto L1 interneurons (blue circles) and pyramidal cells (black circles). Blue lines represent responses of individual interneurons.

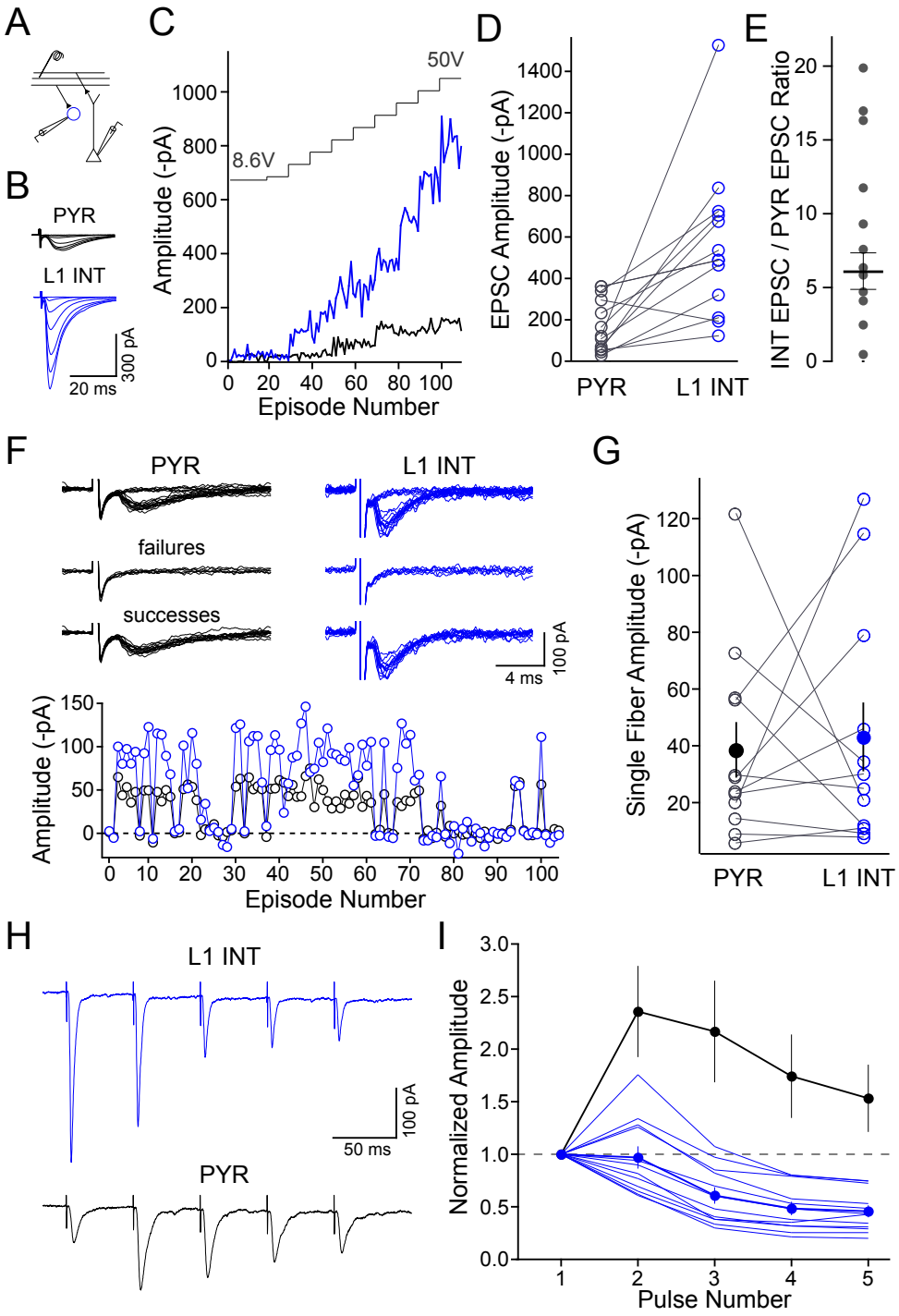
A
B
PYR
L1 INT
300 pA
20 ms
C
50V
8.6V
Amplitude (-pA)
Episode Number
D
EPSC Amplitude (-pA)
PYR
L1 INT
E
INT EPSC / PYR EPSC Ratio
F
PYR
L1 INT
failures
successes
100 pA
4 ms
Amplitude (-pA)
Episode Number
G
Single Fiber Amplitude (-pA)
PYR
L1 INT
H
L1 INT
100 pA
50 ms
PYR
I
Normalized Amplitude
Pulse Number

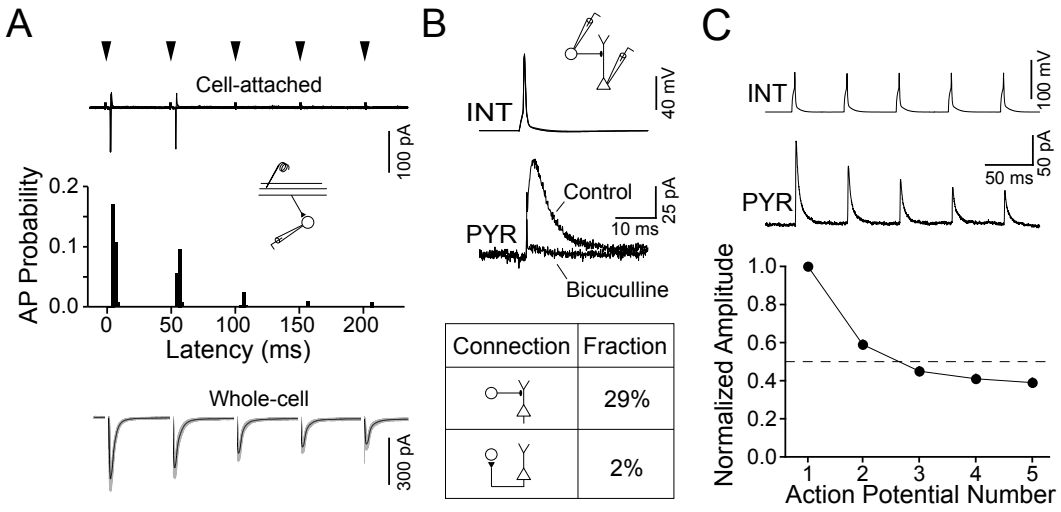

Figure 1.4 Early-transient recruitment of L1a interneurons during bursts of LOT input and the properties of their unitary connections. **(A)** Top, Cell-attached responses to LOT stimulation adjusted to elicit threshold firing in a L1a interneuron. Middle, summary histogram of AP latencies (n= 16 interneurons). Bottom, average EPSC from the same cells. Grey shading is SEM. **(B)** Top, L1a interneuron action potential (5 ms, 1 nA step) evokes a short-latency, bicuculline-sensitive IPSC in a connected pyramidal cell (-40 mV). Bottom, summary of connectivity between pairs of L1a interneurons and pyramidal cells. **(C)** Unitary IPSCs between L1 interneurons and pyramidal cells display short-term depression.

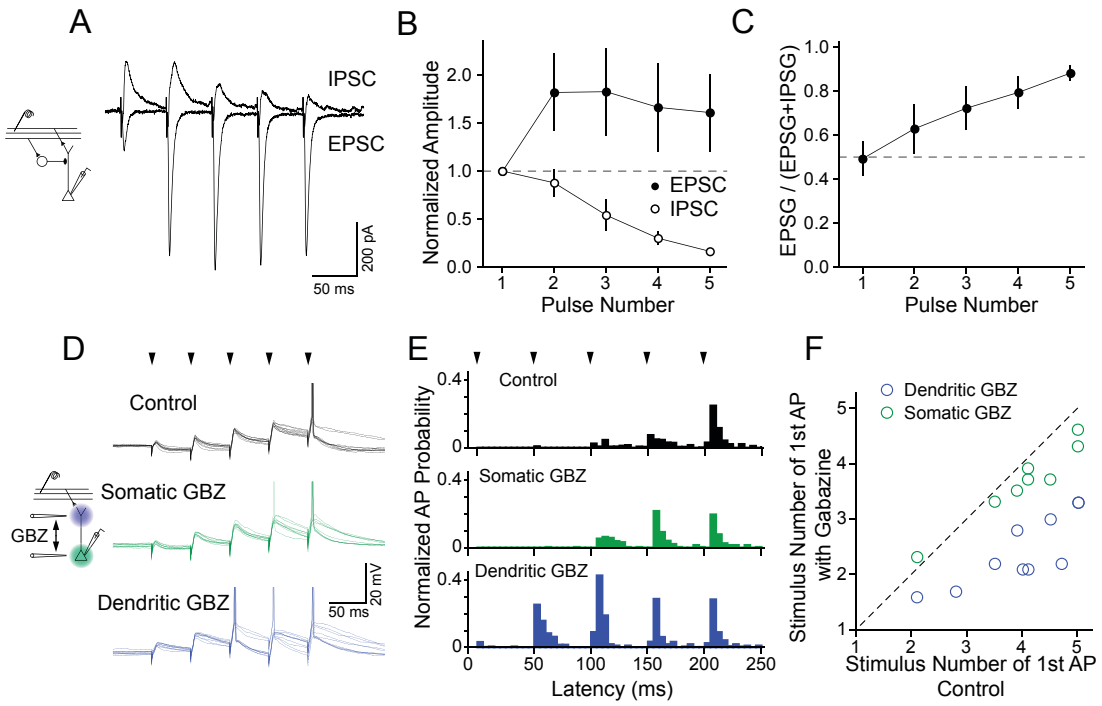

Figure 1.5 Transient dendritic feedforward inhibition gates early integration of LOT input. **(A)** A train of LOT stimulation (5 pulses, 20 Hz) causes strong facilitation of monosynaptic EPSCs and marked depression of feedforward IPSCs in the same pyramidal cell. **(B)** Summary (n=5) of the normalized amplitude of the monosynaptic EPSCs and feedforward IPSCs during a 20 Hz burst of LOT input. **(C)** The initial ratio of excitation to inhibition is balanced but bursting input causes excitation to overwhelm inhibition during stimulus trains. Data from cells in B. **(D)** Overlay of individual traces showing the voltage response of a pyramidal cell to a burst of LOT stimuli (arrowheads, 20 Hz). Under control conditions (black traces), integration of successive EPSPs and depression of IPSPs allowed the pyramidal cell to reach AP threshold late in the burst on most trials. Focal puffer application of gabazine (40 μM) at the soma (green traces) had little effect on spiking while focal gabazine application in L1a (blue traces) caused the cell to reach threshold earlier during the train and fire APs on more trials. **(E)** Average normalized AP probability distributions under control conditions (black) and during somatic (green) or dendritic (blue) application of gabazine (n = 9). **(F)** Summary plot of the same cells showing that dendritic but not somatic gabazine application reduces the number of successive LOT stimuli required to bring pyramidal cells to AP threshold.

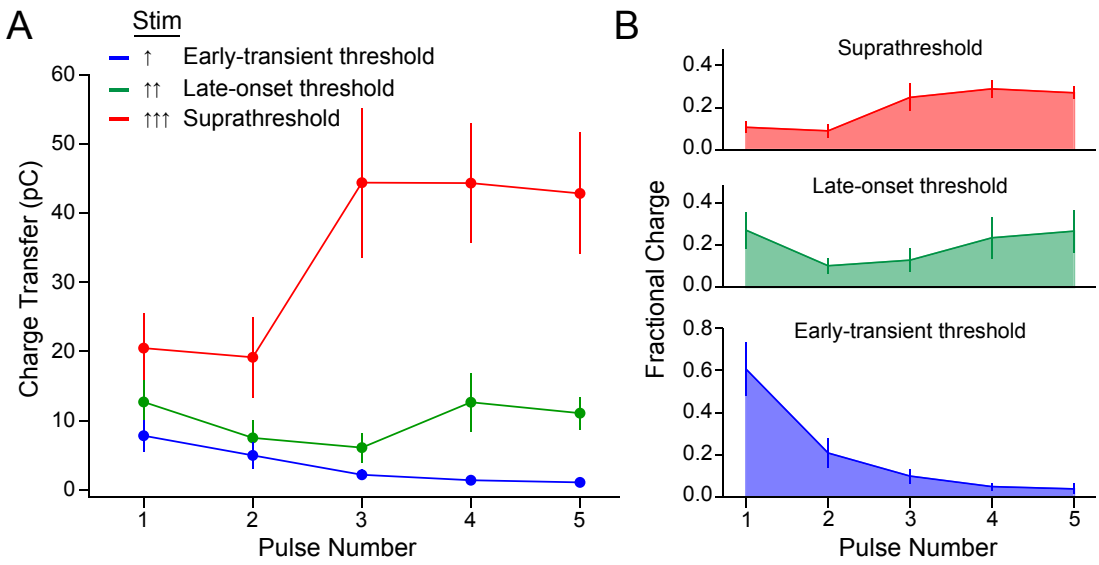

Supplemental Figure 1.1 The temporal structure of inhibition depends on LOT stimulation intensity. **(A)** Inhibitory charge transfer (pC) evoked in L2/3 pyramidal cells when LOT stimulation intensity is just above threshold for recruiting feedforward inhibition (blue) evokes only early-onset transient inhibition; stronger stimulation intensity that is just above threshold for recruiting feedback inhibition (green) evokes a mix of early and late inhibition; and still stronger stimulation intensity that is suprathreshold for recruiting both feedforward and feedback inhibition causes further increases in both early and late IPSC charge transfer. **(B)** The distribution of total inhibitory charge with respect to pulse number at the three stimulus intensities depicted in (A).

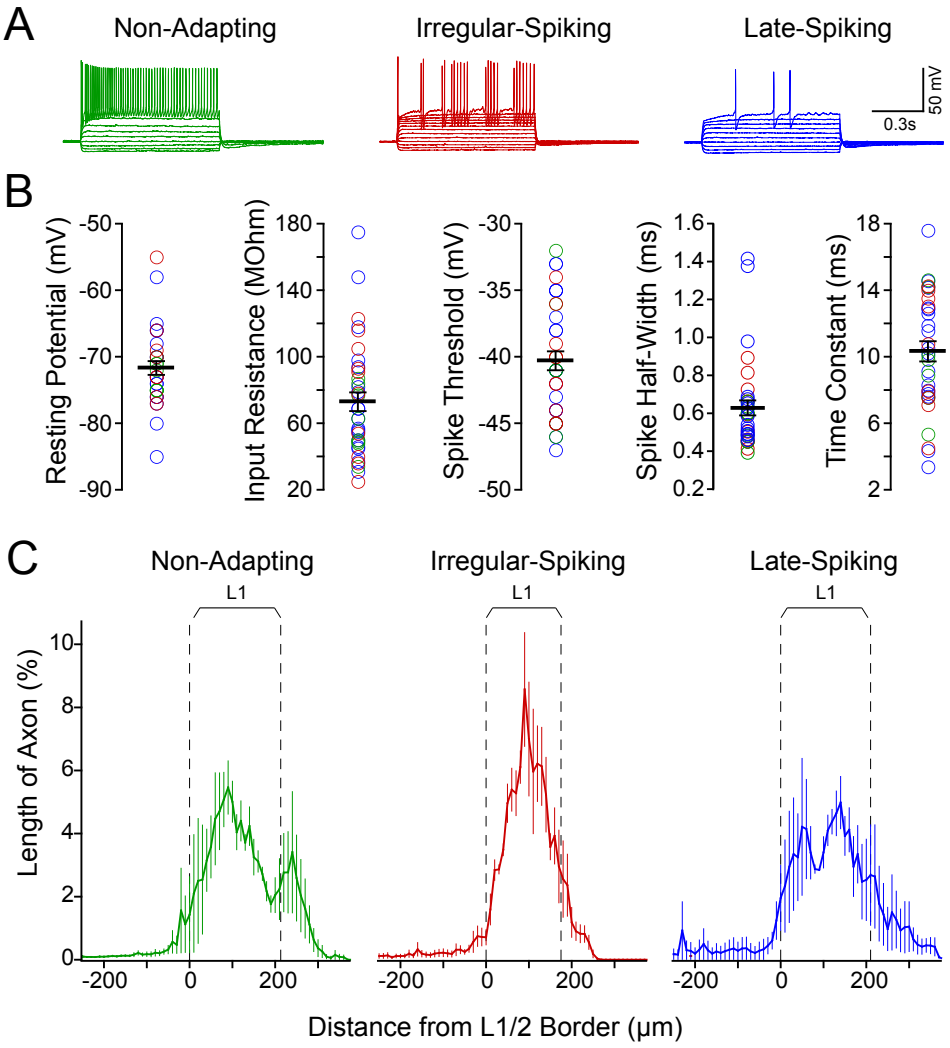

Supplemental Figure 1.2 Intrinsic electrical properties and axonal morphologies of L1a interneurons grouped by spike firing patterns. **(A)** Spiking profiles generated in response to depolarizing current steps could be characterized as one of three patterns: non-adapting, late-spiking, and irregular spiking. **(B)** Intrinsic electrical properties were indistinguishable between L1a interneurons grouped by these firing patterns. Black bars are average ± SEM for all cells. **(C)** L1a interneurons with different spike firing patterns have similar laminar distributions of their axons. The amount of total axon length concentrated in layer 1 was not different between categories (non-adapting, 81 ± 5%; late-spiking, 79 ± 7%; irregular-spiking, 83 ± 6%)

Acknowledgments

This chapter is a reprint of the material as it appears in Stokes C.C and Isaacson J.S. From dendrite to soma: dynamic routing of inhibition by complementary interneuron microcircuits in olfactory cortex. Neuron (2010) vol. 67 (3) pp. 452-65. Segments of the material from the original paper also appear in Chapter 2. The dissertation author was the primary author of this material.

Chapter 2. Somatic feedback inhibition by fast-spiking interneurons in layer 3

Introduction

This chapter is the continuation of the study presented in Chapter 1. In it, we investigate the inhibitory cell types mediating late-onset feedback inhibition that targets the soma of L2/3 pyramidal cells. We find that fast-spiking cells in L3 mediate somatic feedback inhibition. Due to the strong recruitment of L3 fast-spiking cells by L2/3 pyramidal cell input, recurrent inhibition dominates excitation.

Results

L3 fast-spiking interneurons mediate late-onset somatic inhibition

We next sought to identify the source of the late-onset somatic inhibition recruited by bursts of LOT input at higher stimulus intensity. In contrast to the short latencies between individual LOT stimulus pulses and the onset of dendritic IPSCs, the longer latencies we observe for somatic IPSCs (c.f. Fig. 1.1C) suggest they are not recruited in a simple disynaptic, feedforward fashion. Given the preferential late firing of pyramidal cells in response to LOT stimulus trains, we hypothesized that late onset IPSCs might arise from a circuit involving perisomatic-targeting feedback interneurons that receive recurrent excitation from pyramidal cells. Layer 3 (L3) of piriform cortex contains large numbers of multipolar GABAergic interneurons, the majority of which are “basket cells” whose axons preferentially contact cell bodies (Ekstrand et al., 2001).

We thus explored L3 interneurons as a possible source of the late-onset somatic inhibition recruited by strong bursts of LOT input.

We recorded IPSCs evoked by bursts of LOT input in pyramidal cells (V_m= +10 mV) while simultaneously monitoring APs in nearby (<150 μm) visually-identified L3 multipolar cells in cell-attached mode. When LOT stimulus strength was set to evoke late-onset IPSCs in pyramidal cells, we found cells in L3 that fired at or near threshold in the late phases of stimulus trains (Fig. 2.1A). Subsequent whole-cell current clamp recordings from these targeted L3 cells revealed that the majority were fast-spiking (FS) cells (Douglas et al., 2004) with low input resistance (85.5 ± 11.3 MΩ), narrow AP half-width (0.43 ± 0.02 ms), and little adaptation during spike trains (adaptation ratio 0.79 ± 0.07; firing rate in last 100 ms/firing rate in first 100 ms). Threshold firing of L3 FS cells recorded in cell-attached mode in response to trains of LOT stimuli was remarkably consistent with the timing of late-onset inhibition (Fig. 2.1A,B). The population response of L3 FS cells revealed that the majority of APs were elicited in response to later pulses of stimulus trains with most spikes occurring in response to the fourth (32 ± 0.6% of all APs) or fifth (28 ± 0.6%) stimulus (Fig. 2.1B; n=8). Thus, the firing of L3 FS cells indicates that they are poised to contribute to late-onset inhibition.

Additionally, FS cells fired at a longer latency after each stimulus pulse than L1a interneurons (Fig. 2.1B), suggesting that L3 FS cells are not recruited by monosynaptic LOT excitation. To test this directly, we made voltage-clamp recordings (from the L3 FS cells in which we characterized threshold firing) to study the underlying EPSCs evoked by trains of LOT input (Fig. 2.1C). The onset of LOT-

evoked EPSCs onto L3 FS cells occurred 4.4 ± 0.9 ms after monosynaptic LOT-evoked EPSCs onto pyramidal cells (first pulse, Fig. 2.1D; latency on the fifth pulse, 3.1 ± 0.5 ms, n=6). This delay indicates that LOT-evoked responses in L3 FS cells are not mediated by direct excitation from M/T cell axons, rather they arise through recurrent excitatory connections from local pyramidal cells. Indeed, during trains of LOT stimulation, the amplitude of recurrent excitation in L3 FS cells facilitated in parallel with the monosynaptic excitation received by pyramidal cells (Fig. 2.1E). Similar to L1a interneurons, the amplitude of the EPSC producing threshold firing in L3 FS cells averaged 454 ± 129 pA (n=11). These results show that late-onset firing of L3 FS cells is due to the progressive increase in recurrent excitation from pyramidal cells, which are themselves recruited to fire by facilitating M/T cell inputs.

In a subset of simultaneously recorded cell pairs (n=2), we directly confirmed that L3 FS cells underlie polysynaptic inhibition evoked by LOT stimulation (Fig. 2.2A,B). For these pairs, when stimulus strength was set at the threshold for eliciting late-onset inhibition, successes and failures of long-latency IPSCs in the pyramidal cell co-varied with APs from the cell-attached FS cell (Fig. 2.2A). Subsequent whole-cell recording from the FS cell revealed that it made a direct inhibitory connection onto the pyramidal cell with an average IPSC amplitude identical to that of successful long-latency IPSCs evoked by LOT stimulation (Fig. 2.2B).

Somatic-targeting L3 FS cells are highly interconnected with local pyramidal cells

To determine if L3 FS cells provide polysynaptic inhibition that targets the somatic compartment (Fig. 1.1), we reconstructed the dendritic and axonal arbors of biocytin-filled L3 FS interneurons. The multipolar dendrites of L3 FS cells were most concentrated within L3, but more importantly, their dendrites did not extend into layer 1 (Fig. 2.2C,D). These anatomical data are consistent with our findings that L3 FS cells do not receive direct excitatory input from the LOT but rather are situated to receive recurrent collateral input from L2/3 pyramidal cell axons. The axons of L3 FS cells ramified extensively in L2/3 (on average, 95 ± 3% of total axon length, n=3), avoiding L1 and the distal apical dendrites of pyramidal cells (Fig. 2.2D). Furthermore, axon segments often gave rise to closely spaced boutons juxtaposed with the somata of L2/3 cells (not shown), indicating they formed perisomatic "baskets". Thus, L3 FS interneurons have anatomical properties ideal for governing somatic feedback inhibition.

We further examined the connectivity of L3 FS interneurons and nearby pyramidal cells using paired whole-cell recording. In a connected cell pair, single APs in the FS cell always caused short latency (0.65 ± 0.09 ms, n=10) IPSCs in the pyramidal cell. In some cell pairs, single APs in the pyramidal cell could also generate a unitary excitatory postsynaptic current (uEPSC) in the interneuron, indicating a reciprocal connection (Fig. 2.3A). Across all paired recordings, the mean uIPSC conductance was 1.1 ± 0.3 nS (n=22). Consistent with the idea that FS cells target the perisomatic compartment, unitary IPSCs from FS cells onto pyramidal cells had rapid

rise times (0.68 ± 0.15 ms, n=10). These rise times were identical to those of the late-onset IPSCs evoked by trains of LOT stimulation (0.6) and significantly faster than those of the dendritic uIPSCs generated by L1a interneurons (2.0 ms; p = 0.001). The amplitudes of uEPSCs onto FS cells averaged 43 ± 17 pA (range 9 to 209 pA, V_m=-90 mV, n=11) and their kinetics were fast (decay tau=2.63 ± 0.4 ms). Given that FS cells require ~450 pA of excitatory input to reach AP threshold, these results suggest that the coincident activity of relatively few pyramidal cells can elicit somatic feedback inhibition.

Individual L3 FS cells made highly divergent connections, inhibiting 35% of local pyramidal cells and receiving direct excitatory connections from 18% of pyramidal cells tested (n=64 pairs; Fig. 2.3B). Intriguingly, the rate of reciprocal connections was higher than predicted by random connectivity: in a cell pair without an excitatory connection, the likelihood that the interneuron would connect to the pyramidal cell was 22% (14/64 pairs) while the probability of an inhibitory connection was significantly higher in cell pairs with an excitatory connection (73%, 8/11 pairs, p < 0.01, Fisher's Exact Test). The strength of unitary inhibitory connections tended to be stronger between reciprocally-connected pairs as compared to one-way connections, though this trend did not reach statistical significance (1.73 ± 0.65, n=14 and 0.66 ± 0.21 nS, n=8, respectively; p = 0.1, KS test). In response to trains of APs (5 at 20 Hz) from pyramidal cells, the amplitudes of uEPSCs in L3 FS cells strongly depressed (uEPSC5/uEPSC1 = 0.32 ± 0.05, n=11, Fig. 2.3C). Unitary inhibitory connections from L3 FS cells onto pyramids also depressed during AP trains (uIPSC5/uIPSC1 =

0.53 ± 0.03, n=22, Fig. 2.3D). Together, these results show that L3 FS cells mediate widespread recurrent inhibition across the cortical population and they are biased to inhibit those pyramidal cells that directly excite them.

Strong recurrent excitation of L3 FS cells drives widespread feedback inhibition

To determine the relative strength of recurrent inhibition and excitation evoked by local cortical activity, we used an optogenetic approach to selectively activate small populations of pyramidal cells in olfactory cortex. Ntsr1-cre mice (line Ntsr1-creGN209 from the GENSAT project) express Cre recombinase in a fraction of L2/3 pyramidal cells of piriform cortex, but not in pyramidal cells of other cortical regions or in inhibitory cells (Fig. 2.4A, Methods). We used an adeno-associated virus (rAAV-FLEX-*rev*-ChR2-tdTomato) to drive Cre-dependent co-expression of ChR2 and the fluorescent protein tdTomato (Atasoy et al., 2008) and made focal *in vivo* injections of virus in piriform cortex of Ntsr1-cre mice. We took advantage of both the restricted expression of Cre recombinase and focal delivery of virus to ensure that ChR2 was only expressed in the anterior piriform cortex (Supplemental Fig. 2.1). Slices from these animals revealed that expression of tdTomato was restricted to sparse populations of piriform cortex L2/3 cells (Fig. 2.4A); all fluorescent cells had characteristic pyramidal morphology and targeted recordings demonstrated firing properties consistent with pyramidal cells (Fig. 2.4B, n=7).

In cells expressing tdTomato-ChR2, brief (1 ms) pulses of 470-nm light activated large ChR2-mediated currents (>1 nA in voltage clamp, not shown) that were

sufficient to cause reliable, short-latency AP firing (Fig. 2.4B). We examined the relative balance of recurrent excitation and inhibition within the cortical circuit by making voltage-clamp recordings from neighboring pyramidal cells that did not express ChR2. While brief light pulses evoked both EPSCs and IPSCs in these pyramidal cells, synaptic responses were dominated by inhibition (Fig. 2.4C,D). Application of NBQX (10 μM) and APV (50 μM) abolished ChR2-evoked IPSCs (n=4), confirming they were elicited by recurrent excitation. On average, the inhibitory conductance was 8.4 ± 2.4 times larger than the excitatory conductance (Fig. 2.4D, n=7) in pyramidal cells. Thus, pyramidal cell activity favors the recruitment of local recurrent inhibition rather than excitation across the pyramidal cell population.

We measured the amplitude of light-evoked EPSCs in simultaneously recorded pyramidal cell-L3 FS cell pairs (Fig. 2.4E) to compare the relative amount of recurrent excitation these two cell types receive. The amplitude of light-evoked EPSCs was always larger in L3 FS cells than in pyramidal cells (average amplitude 117 ± 28 pA and 11 ± 7 pA, respectively; n=13 pairs, Fig. 2.4F). This may reflect a higher convergence of pyramidal cell input to interneurons or stronger unitary connections than those formed between pyramidal cells. Preliminary experiments revealed that the amplitude of unitary excitatory connections between pyramidal cells is 20 ±12pA (n=4), which is smaller than the unitary excitatory connections onto L3 FS cells (43 pA). This suggests that strong feedback inhibition is the result of both larger amplitude unitary excitatory connections between pyramidal cells and L3 FS cells as well as higher convergence of pyramidal cell axons onto L3 FS cells. Given the low rate of

excitatory connections between pyramidal cells and L1a interneurons, we hypothesized that L1a interneurons would receive little recurrent excitation in response to ChR2-evoked activation of the local circuit. Indeed, while brief light pulses always elicited excitation in L3 FS cells (9/9 cells) we rarely observed EPSCs in simultaneously recorded L1a interneurons (3/9 cells, Fig. 2.4G). In these paired recordings, EPSC amplitude averaged 247 ± 152 pA in L3 FS cells but only 12 ± 11 pA in L1a interneurons (n=9, Fig. 2.4H). These results reveal that compared to pyramidal cells and layer 1a interneurons, L3 FS cells receive the most recurrent excitation, further highlighting their importance as a major circuit for feedback inhibition in piriform cortex

Discussion

Late-onset feedback somatic inhibition is mediated by layer 3 interneurons

Given that piriform cortex pyramidal cells preferentially fire late during bursts of input, recurrent inhibition should track this activity. Indeed, we show that LOT stimulation recruits late-onset inhibition from L3 FS interneurons, which are recruited exclusively through a feedback mechanism. L3 FS cells have anatomical features and spike firing patterns consistent with parvalbumin-positive, somatic-targeting interneurons found in many brain regions (Markram et al., 2004; Somogyi et al., 1998). In piriform cortex, L3 FS cells have axons that exclusively target the somatic compartment and dendrites that receive no direct M/T cell inputs. Recently, a somatic inhibitory current (I_{trunc}) recruited by LOT stimulation has been proposed to limit

synaptic integration via a disynaptic feedforward mechanism (Luna and Schoppa, 2008). However, the long latency (~10 ms) between excitation and I_{trunc} as well as its somatic location are more consistent with the recurrent inhibition mediated by L3 FS cells we describe here. These cells track pyramidal cell activation to fire late during LOT stimulus trains and their unitary inhibitory connections show a use-dependent synaptic depression. This suggests that late-onset somatic inhibition during bursting sensory input reflects the recruitment of progressively newer populations of L3 FS and pyramidal cells as the burst proceeds.

L3 FS cells make unitary inhibitory connections onto a large fraction (35%) of pyramidal cells, similar to the high connectivity rates reported for somatic targeting FS cells in other circuits (Glickfeld et al., 2008; Holmgren et al., 2003; Yoshimura and Callaway, 2005). The majority (77%) of unitary excitatory connections from pyramidal cells onto FS cells were reciprocated by inhibitory connections, as previously found in visual cortex (Yoshimura and Callaway, 2005). While the high reciprocal connectivity of FS and pyramidal cells suggests a degree of specificity in their wiring, unidirectional inhibitory connections were most common. Since individual FS cells always inhibit more pyramidal cells than those that directly excite them, this divergence of FS cell output provides a mechanism for widespread "lateral" inhibition.

We sought to define the relative influence of recurrent excitation vs. recurrent inhibition in the cortical population, however the piriform cortex receives extrinsic input from a variety of cortical and subcortical areas (Haberly, 2001) making it impossible to selectively activate recurrent excitatory connections with a conventional

extracellular stimulating electrode. To circumvent this problem, we took advantage of a mouse line selectively expressing Cre recombinase in pyramidal cells of piriform cortex and used viral delivery of the light-activated channel channelhodopsin-2 (ChR2) (Atasoy et al., 2008; Petreanu et al., 2009; Zhang et al., 2006) to selectively activate pyramidal cells of anterior piriform cortex. We found that recurrent inhibition greatly outweighed recurrent excitation in piriform cortex. Indeed, L3 FS cells received much stronger recurrent excitation than pyramidal cells in the local circuit, both due to larger unitary excitatory inputs as well as a higher convergence of inputs than nearby pyramidal cells receive. This powerful excitatory drive onto L3 FS cells is likely to underlie the strong recurrent inhibition in response to ChR2-mediated activation of local pyramidal cells.

While the functional properties of L3 FS cells are most consistent with late-onset somatic inhibition we observe in pyramidal cells, our results do not rule out the possibility that other subtypes of interneurons participate in recurrent inhibition under different conditions.

Implications for olfactory information coding

L3 FS interneurons read out pyramidal cell activity and produce somatic inhibition across the local cortical population. Thus, this feedback circuit serves to dampen pyramidal cell activity as it builds during bursts of M/T cell input. Individual L3 FS cells contact many pyramidal cells and thus mediate widespread inhibition across the cortical population. Pyramidal cells in piriform cortex that respond to a given

odorant are broadly distributed without spatial preference (Stettler and Axel, 2009). Given that L3 FS cell dendrites branch extensively within L2/3, they likely receive excitatory input from many nearby pyramidal cells, each of which is preferentially tuned to respond to different odorants. This makes it likely that L3 FS cells participate in odor-evoked inhibition that is broadly tuned; however it is also possible that pyramidal cells co-tuned to respond to the same odorant form specific subcircuits with particular interneurons. In the simplest case, this feedback circuit contributes to sparse odor representations across the cortical population by regulating the amplification and distribution of excitation by associative connections. The reciprocal connectivity between L3 FS cells and pyramidal cells suggests a mechanism for oscillations in recurrent excitation and inhibition in response to odor-evoked input. Indeed, in other systems somatic-targeting FS cells have been proposed to contribute to the phasing of pyramidal cell firing during oscillations (Cardin et al., 2009; Cobb et al., 1995). Thus, L3 FS cells may also function to regulate spike timing during odor-evoked oscillations in piriform cortex.

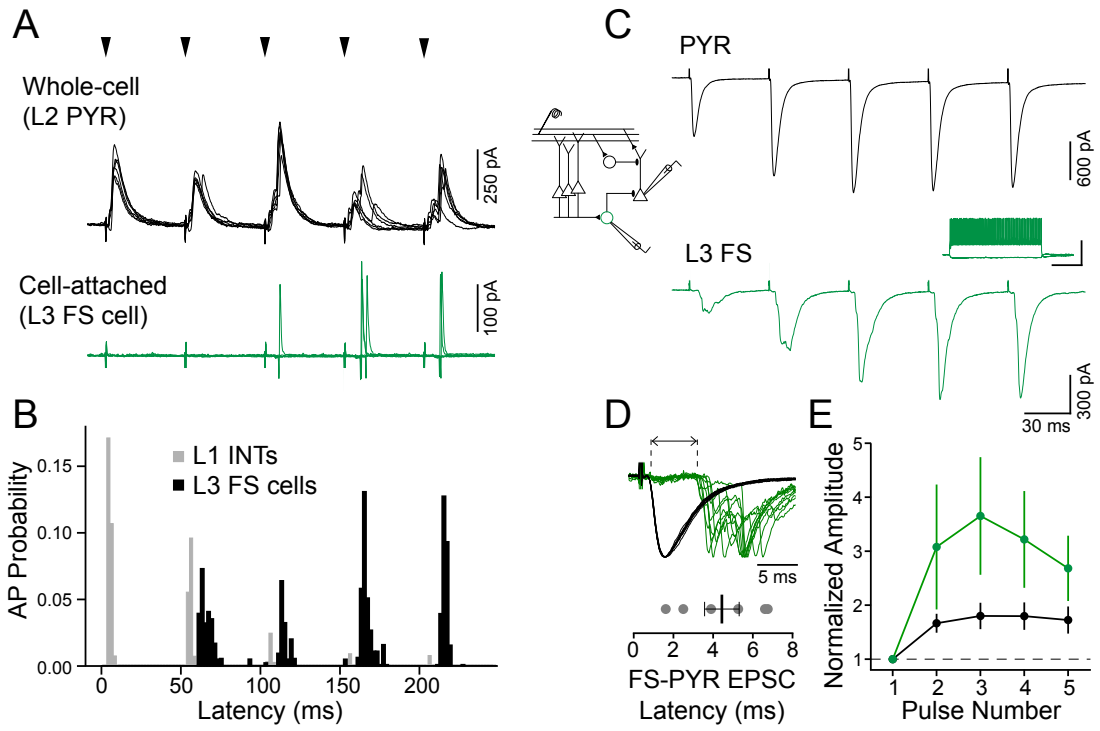

Figure 2.1 Layer 3 fast-spiking cells preferentially fire late during trains of LOT stimuli and receive only recurrent excitation. **(A)** Traces from a voltage-clamped pyramidal cell (black; +10mV) and cell-attached L3 FS cell (green) demonstrating that threshold L3 FS cell firing late during trains of LOT stimuli overlaps with late-onset inhibition. **(B)** Summary histogram of AP latencies during threshold firing of L3 FS cells (black, n=8). Threshold firing distribution of L1a interneurons from Figure 4 (grey bars) is plotted for comparison. Histograms represent average probability distribution in 2-ms time bins for the two populations. **(C)** Simultaneous whole-cell voltage-clamp recording (same cell pair in A; -90 mV) demonstrating monosynaptic LOT-evoked EPSCs in the pyramidal cell (black) and delayed, polysynaptic EPSCs in the L3 FS cell (green). **(D)** Top, time-expanded traces of individual trials during the first stimulus pulse of the train showing the latency differences between the L3 FS cell (green) and the L2 pyramidal (black) cell in C. Bottom, summary of latency differences (n=6 pairs). **(E)** LOT-evoked polysynaptic EPSCs in L3 FS cells (green) facilitate during bursts, as do direct LOT-evoked EPSCs in pyramidal cells (black).

Figure 2.2 Fast-spiking cells in layer 3 mediate feedback inhibition and target the perisomatic compartment of layer 2 pyramidal cells. **(A)** Simultaneous recording from a L3 FS cell in the cell-attached configuration (top) and pyramidal cell in voltage-clamp (0 mV, bottom). The third pulse in a burst of LOT stimuli generated a reliable feedforward IPSC followed by successes and failures of long-latency feedback IPSCs in the pyramidal cell, as well as successes and failures of APs in the L3 interneuron (All trials). Sorting the traces based on successes and failures of the L3 interneuron APs revealed that large, long-latency IPSCs only occurred when the interneuron fired. **(B)** Subsequent current-clamp recording revealed that the L3 interneuron was a FS cell and APs evoked an IPSC in the pyramidal cell with an amplitude equivalent to the large feedback IPSCs elicited by LOT stimulation. **(C)** Reconstruction of a biocytin-filled L3 FS cell. Inset shows threshold firing response. Axon is in red; dendrites are in blue. Dashed line, Layer 1/2 border. **(D)** Laminar depth of FS cell neurites (n=3 cells, 10 μm bins) demonstrates segregation dendrites within L3 and high density of axons within the L2 pyramidal cell layer. Sample pyramidal cell included for comparison. Dashed lines indicating laminar borders are drawn at mean distance from layer 1/2 border; grey bar indicates the mean location of the soma (± SEM).

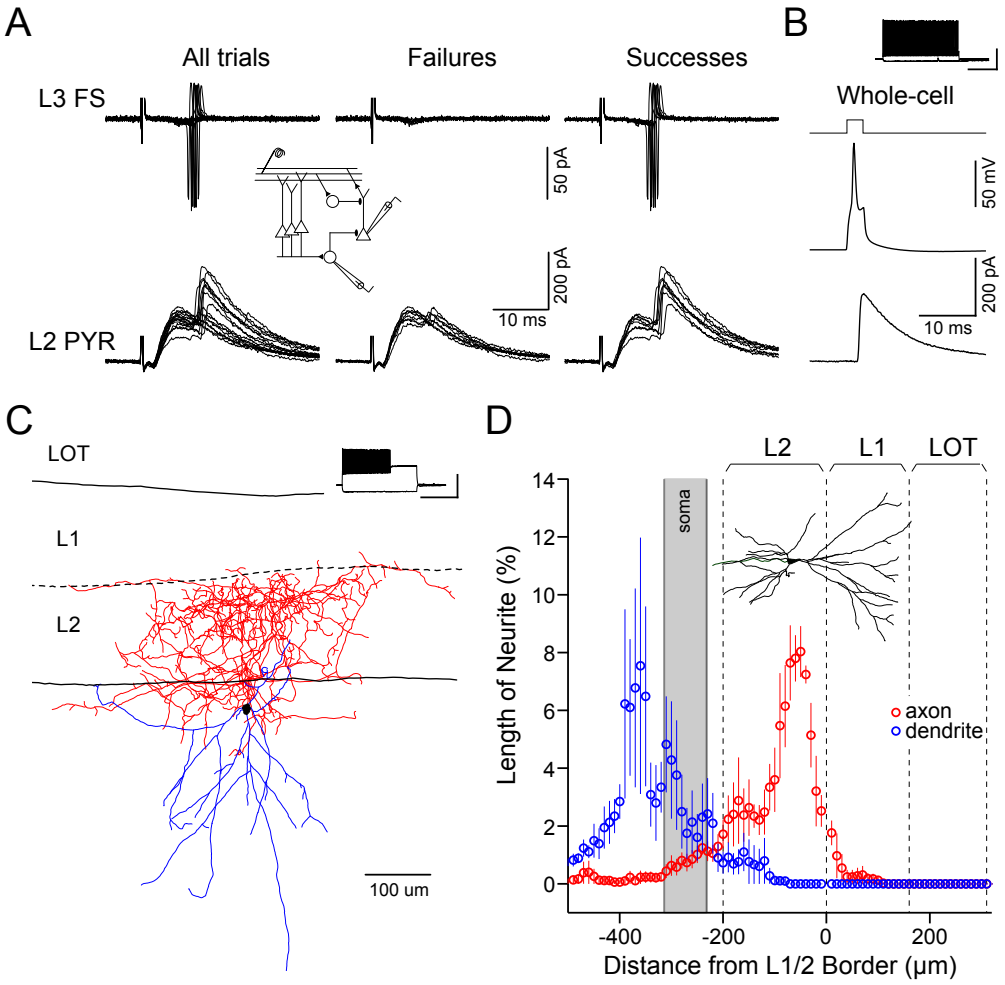
A
All trials
Failures
Successes
L3 FS
50 pA
200 pA
10 ms
L2 PYR
B
Whole-cell
50 mV
200 pA
10 ms
C
LOT
L1
L2
100 um
D
L2
L1
LOT
soma
Length of Neurite (%)
axon
dendrite
Distance from L1/2 Border (μm)

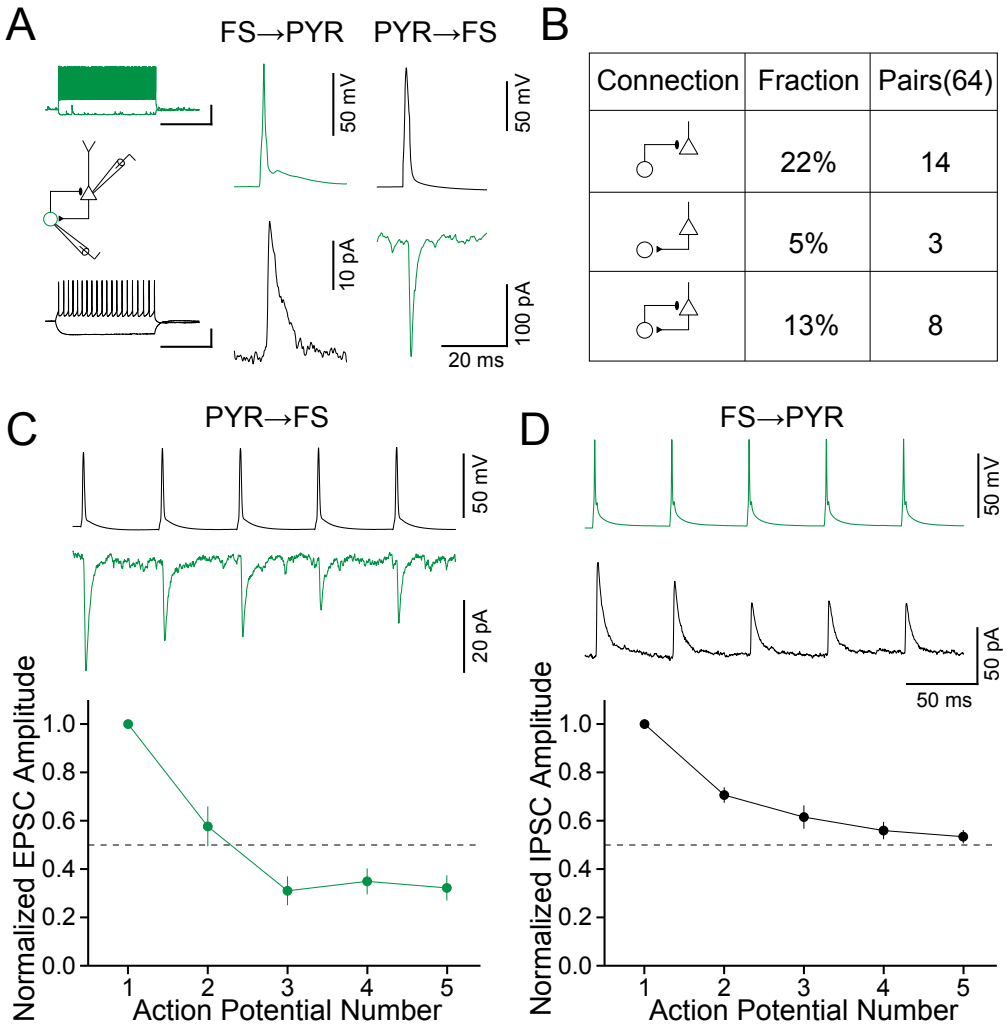

Figure 2.3 L3 FS cells are highly interconnected with pyramidal cells in piriform cortex. **(A)** Paired recording of a L3 FS cell (green) and connected pyramidal cell (black). A single AP in the L3 FS cell (current clamp) produces a short-latency IPSC in the voltage-clamped (-40 mV) pyramidal cell. A single AP in the pyramidal cell (current clamp) produces a short-latency EPSC in the FS cell. Left inset, voltage responses of the two cells to 1sec current steps. **(B)** Summary of connectivity between L3 FS and pyramidal cells. **(C)** Unitary EPSCs from L2 pyramidal cells onto L3 FS cells display short-term depression. **(D)** Unitary IPSCs from L3 FS cells only L2 pyramidal cells also display short-term depression.

Figure 2.4 Recurrent inhibition dominates excitation between pyramidal cells while L3 FS cells receive the strongest recurrent excitation. **(A-B)** Ntsr1-cre mice can be used to express ChR2 selectively in L2/3 pyramidal cells in piriform cortex. **(A)** Left, fixed thin section of anterior piriform cortex from a mouse generated by a cross between an Ntsr1-cre and a Rosa-YFP mouse. Green, raw YFP fluorescence; red, GAD-67 interneuron immunolabeling. Right, acute slice of piriform cortex from an Ntsr1-cre mouse injected focally with AAV encoding a flexed ChR2-tdTomato fusion protein. Raw tdTomato fluorescence is observed in L2/3 pyramidal cells projecting dendrites to the LOT. **(B)** Current-clamp recording shows regular-spiking firing pattern of a ChR2-tdTomato expressing pyramidal cell. A brief (1 ms) pulse of blue light (470 nm) reliably generates a single action potential in the same cell (7 traces overlaid). **(C)** A brief (1 ms) flash of 470 nm light elicits a large IPSC and small EPSC in a neighboring uninfected pyramidal cell. Both excitatory and inhibitory currents were abolished in the presence of glutamate receptor antagonists (+APV/NBQX). (**D**) Summary plot of the amplitudes of the inhibitory conductance and excitatory conductance in the same pyramidal cells elicited by activation of ChR2. Inset: activation of pyramidal cells elicits feedback inhibition that is on average ~8 times stronger than recurrent excitation. **(E)** Traces showing ChR2-evoked EPCSs in a simultaneously recorded L3 FS (green) and pyramidal cell (black). **(F)** Summary data showing that recurrent excitation is always larger in L3 FS cells. Filled circles, average EPSC amplitude (-90 mV) in L3 FS (green) and pyramidal (black) cells. **(G)** A brief light pulse evokes a large EPSC in a L3 FS cell (green) but no response in a simultaneously recorded L1a interneuron (blue) (**H)** Summary data showing that recurrent excitation is always larger in L3 FS cells than simultaneously recorded L1a interneurons. Filled circles, average EPSC amplitude (-90 mV) in L3 FS cells (green) and L1a interneurons (blue).

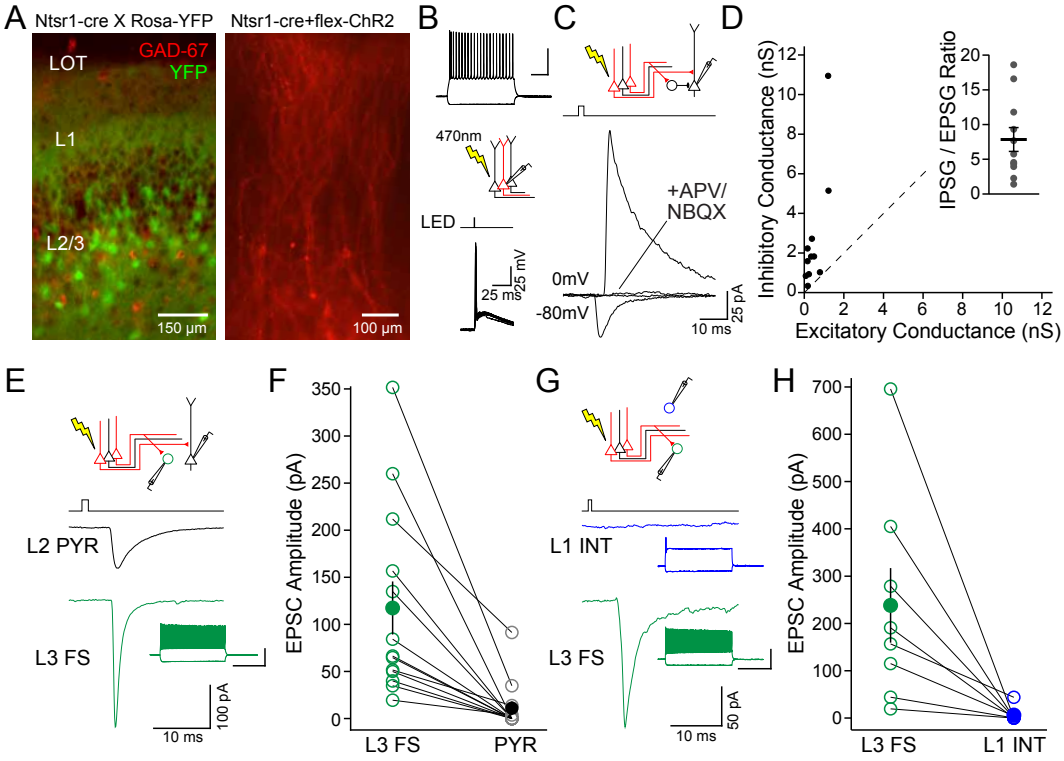
A
Ntsr1-cre X Rosa-YFP
Ntsr1-cre+flex-ChR2
LOT
GAD-67
YFP
L1
L2/3
150 µm
100 µm
B
470nm
LED
25 mV
25 ms
C
+APV/
NBQX
0mV
-80mV
25 pA
10 ms
D
Inhibitory Conductance (nS)
Excitatory Conductance (nS)
IPSG / EPSG Ratio
E
L2 PYR
L3 FS
100 pA
10 ms
F
EPSC Amplitude (pA)
L3 FS
PYR
G
L1 INT
L3 FS
50 pA
10 ms
H
EPSC Amplitude (pA)
L3 FS
L1 INT

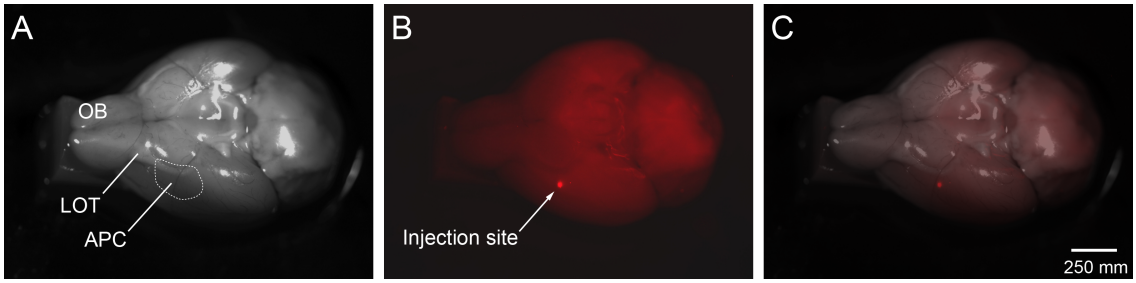

Supplemental Figure 2.1. Whole mount of the brain from an Ntsr1-cre mouse showing focal expression of ChR2-tdTomato in the anterior piriform cortex. (**A**) Ventral view of the brain highlighting the olfactory bulbs (OB), lateral olfactory tract (LOT), and anterior piriform cortex (APC). (**B**) Fluorescence image showing focal tdTomato expression (red spot). (**C**) Overlay of the two images indicates localized expression of tdTomato to anterior piriform cortex.

Acknowledgments

This chapter is a reprint of the material as it appears in Stokes C.C and Isaacson J.S. From dendrite to soma: dynamic routing of inhibition by complementary interneuron microcircuits in olfactory cortex. Neuron (2010) vol. 67 (3) pp. 452-65. The dissertation author was the primary author of this material.

Chapter 3. Feedback inhibition by layer 3 low threshold-spiking cells

Introduction

In sensory areas of cortex, an abundance of distinct inhibitory cell types regulate the excitability of principal cells, dramatically increasing the dynamic range and diversity of sensory representations (Ferster and Jagadeesh, 1992; Pouille et al., 2009; Wehr and Zador, 2003; Wilent and Contreras, 2005). However, despite evidence that inhibitory circuits also play an important role in shaping the representations of odor (Biedenbach and Stevens, 1969; Poo and Isaacson, 2009; Stettler and Axel, 2009; Zhan and Luo, 2010), much less is known about the cell types that contribute to odor-evoked inhibition in primary olfactory (piriform) cortex.

Odor-evoked spiking by pyramidal cells in piriform cortex is sparse and distributed without apparent topography (Poo and Isaacson, 2009; Stettler and Axel, 2009). Whole-cell recordings demonstrate that odor-evoked inhibition is broadly tuned and widespread throughout piriform cortex (Poo and Isaacson, 2009) but it is impossible to identify the source of inhibition in these experiments. Therefore it is necessary to map out inhibitory circuits in an experimental system where specific cell types and their connectivity can be established.

The piriform cortex is an accessible region for performing studies of cortical circuits because of its simple structure: as part of three-layered paleocortex, it contains only one major cell body layer and functionally distinct axonal afferents that are for the most part segregated into separate laminar depths(Neville and Haberly, 2004).

Recently, we have demonstrated that excitation from olfactory bulb mitral and tufted cells (M/T cells) produces a spatially and temporally stereotyped pattern of excitatory and inhibitory currents in pyramidal cells in piriform cortex, revealing a canonical circuit for the cortical processing of olfactory information (see Chapter 1, 2). Axons of M/T cells in the lateral olfactory tract (LOT) provide monosynaptic excitation in layer 1a (L1a), where it depolarizes the apical dendrites of pyramidal cells that have cell bodies in layer 2/3 (L2/3). This depolarization can lead to the firing of action potentials (APs) in L2/3 pyramidal cells, which propagate laterally via associational (ASSN) axons in L1b and L3.

During this excitatory activity, GABAergic inhibition is recruited onto pyramidal cells both in a *feedforward* manner via monosynaptic connectins from M/T cell axons as well as in a *feedback* manner via L2/3 pyramidal cell axons. Remarkably, the populations of interneurons that are recruited via these two separate pathways are independent; L1a interneurons provide feedforward inhibition but exclusively target the apical dendrite, and L3 interneurons provide feedback inhibition but exclusively target the somatic compartment. During a burst of synaptic excitation from M/T cell axons, L1a and L3 inhibitory circuits are activated in a complementary fashion due to the short-term dynamics of the direct or disynaptic excitation they respectively receive, causing the site of inhibition to shift from the distal apical dendrite to the soma as the burst progresses.

Recent work in piriform cortex has described a diversity of interneuron subtypes suggesting the circuit is likely to recruit more than a one feedforward and one feedback

population (Suzuki and Bekkers, 2010a, b). Therefore we sought to determine whether multiple types of interneurons participated in the inhibition we observed in response to bursting LOT input. In addition to the fast-spiking (FS) cells in L3, we found a second class of GABAergic interneurons with properties similar to low threshold-spiking (LTS) cells described elsewhere in cortex that provide delayed somatic inhibition. Both L3 LTS and L3 FS cells received only excitation from local pyramidal cells and therefore exclusively provide feedback inhibition. However, cell type-specific differences in the short-term dynamics of excitation from L2/3 pyramidal cells, as well as in the intrinsic elecrophysiological properties between LTS and FS cells lead to subtle differences in their recruitment by LOT stimuli. LTS cells and FS cells also appear to target different regions of the soma and basal dendrites.

We also present preliminary results indicating that LTS cells express the neuroactive peptide somatostatin and that optogenetic approaches targeting channelrhodopsin-2 and halorhodopsin-3.0 could be used to manipulate the activity of somatostatin-expressing cells in piriform cortex.

Results

Low threshold-spiking cells are a source of feedback inhibition in piriform cortex

In order to search for interneurons in L3 that provide feedback inhibition we made simultaneous whole-cell recordings from pairs of L2/3 pyramidal cells and L3 multipolar cells in acute slices of rat piriform cortex. In addition to fast-spiking (FS) interneurons (Figure 3.1A, also see Chapter 2) we found cells in L3 that made

monosynaptic inhibitory connections onto L2/3 pyramidal cells, but responded to depolarizing current injections with strongly adapting spike trains (adaptation ratio, firing rate in last 100 ms of current injection/firing rate in first 100 ms=0.24±0.14, n=8 versus 0.78±0.07 in FS cells, n=15, $p<0.001$ Figure 3.1B). In response to hyperpolarizing current injection the membrane potential of these cells showed a prominent sag, (Figure 3.1B, inset) and rebound spiking was often observed when the membrane potential was returned to rest, consistent with the properties of a hyperpolarization-activated current (I_h, (Biel et al., 2009)).

We quantified the sag in response to a -200 pA current step as the difference in membrane potential at the peak hyperpolarization (typically ~50 ms after step onset) minus the membrane potential 400 ms after step onset; for FS cells sag was 0.7±0.2 mV (n=11) while in the non-FS interneurons with adapting spike trains it was 7.0±1.2 mV (n=7, $p<0.001$). These features—adapting spike trains and a prominent hyperpolarization-activated current that can lead to rebound spiking—are characteristic intrinsic electrophysiological properties of low threshold-spiking (LTS) interneurons described in other areas of cortex (Bacci et al., 2003; Gibson et al., 1999). Therefore we chose to refer to this population as LTS cells.

In addition to monosynaptic inhibitory connections from LTS cells onto L2/3 pyramidal cells, we also observed monosynaptic excitatory connections from pyramidal cells onto L3 LTS cells, as well as reciprocal connections between the two cell types (Figure 3.1B). Overall, in paired recordings between L3 LTS and pyramidal cells we found a high percentage of synaptic connections, similar to the high rates observed

between L3 FS cells and pyramidal cells (Figure 3.1C,D). Of LTS-pyramidal cell pairs tested (n=48), 23% made unidirectional inhibitory connections while 8% made unidirectional excitatory connections. An additional 19% made reciprocal connections. As observed for L3 FS cells (Fig. 2.3.B), the proportion of reciprocally connected pairs was significantly higher than predicted by the unidirectional connectivity ($p=0.02$, Fisher's exact test), indicating that L3 LTS cells preferentially target the pyramidal cells from which they receive excitation. These results demonstrate that L3 LTS cells are a source of feedback inhibition onto L2/3 pyramidal cells in piriform cortex.

L3 LTS cells are activated later during LOT stimulus trains than L3 FS cells

To determine how L3 LTS cells are recruited during bursts of M/T cell activity, we made simultaneous paired recordings between L3 LTS cells and L2/3 pyramidal cells while stimulating the LOT (5 pulses at 20 Hz, Figure 3.2A). As described previously for L3 FS-PYR pairs (Fig. 2.1), we first recorded from L3 multipolar cells in the cell-attached configuration and set the stimulus intensity at the threshold for generating an action potential (AP) such that the L3 cell was firing on 50% of trials (Figure 3.2B1). After measuring the APs we subsequently ruptured the cell membrane and recorded the underlying excitatory post-synaptic currents (EPSCs) that caused the L3 cell to fire (Figure 3.2C). We used the spike-firing profile in response to current steps in order to retrospectively identify it as LTS or FS (Figure 3.2A).

We first compared the timing of APs evoked in LTS cells and FS cells by bursts of stimuli delivered to the LOT (see Fig. 2.1). In LTS cells, the fifth LOT stimulus in a

burst elicited the most spikes (50±11% of all spikes, n=4 Fig. 2.3.B2) whereas the fourth stimulus elicited the most spikes for FS cells (32±1%, n=6). In addition, spiking in LTS cells occurred at a longer latency after each pulse (mean latency of spiking after fifth LOT pulse = 13.4±1.3ms for LTS cells, 7.3±0.2 ms for FS cells, $p<0.005$, n=4 LTS and 5 FS) and with greater jitter (standard deviation of spike timing after fifth pulse = 6.5±1.4ms for LTS cells, 0.8±0.2ms for FS cells, $p<0.005$, n=4 LTS and 5 FS). These differences in spiking may be due either to differences in the excitation each cell type receives during LOT stimulus trains or due to differences in the intrinsic electrical properties between LTS and FS cells.

To measure the excitation onto LTS cells during bursts of LOT stimulation, we subsequently ruptured the cell membrane and recorded the EPSCs (Vm =-80 mV) that had caused spiking at threshold. We found that bursts of LOT stimulation generated short-latency, monosynaptic EPSCs in simultaneously recorded nearby L2/3 pyramidal cells, as shown previously (Fig. 1.2C, Fig. 2.3H). EPSCs also occurred in the LTS cell but these came at a longer latency after each stimulus, indicating they were unlikely to result from monosynaptic excitation. For LTS cells, the mean latency difference (EPSC onset at 5% of peak in LTS cell minus EPSC onset in pyramidal cell) for the fifth peak was 5.6±1.5 ms (n=5), significantly longer than the latencies measured in FS cells (3.1±0.5 ms, n=6; Fig. 3.2D).

We also found differences in the short-term facilitation of LOT-evoked EPSCs onto L3 LTS and FS cells. Consistent with the differences in AP timing evoked by bursts of LOT stimulation, the peak EPSC amplitude occurred later in the LTS cells

than in the FS cells (Fig. 3.2E.). There was also much stronger facilitation in EPSC amplitude onto LTS cells (EPSC on fifth pulse normalized to EPSC on the first pulse=8.8±2.2 for LTS cells versus 2.5±0.5 for FS cells, n=4 LTS and 6 FS cells, p=0.03). Although we did not have enough measurements of threshold EPSC amplitude to make statistical comparisons between LTS and FS cells, we found that LTS cells required less current to reach threshold (190 pA compared to 454±129 pA in FS cells). Together, these data indicate that during LOT stimulation both L3 LTS and FS cells are likely recruited via a polysynaptic mechanism to provide feedback inhibition onto L2/3 pyramidal cells. However, LTS cells fire APs at on later pulses of LOT stimulus trains and at a longer latency after each pulse, in part due to differences in polysynaptic excitation onto L3 interneurons.

Both synaptic and intrinsic electrophysiological properties distinguish L3 LTS and FS cells

Because both FS cells and LTS cells in layer 3 mediate feedback inhibition in piriform cortex, we sought to determine whether these two cell types had additional properties that might lead to their differential activation during the processing of olfactory information in the local circuit. First we analyzed the short-term dynamics of monosynaptic unitary EPSCs (uEPSCs, Vm=-80 mV) produced by bursts of APs (5 at 20 Hz) in the L2/3 pyramidal cell (Figure 3.3A). We found marked facilitation of uEPSCs onto L3 LTS cells (ratio of fifth EPSC to first EPSC, P5/P1=2.5±0.8, n=6) in contrast to the depression of uEPSCs onto L3 FS spiking cells (P5/P1=0.32±0.05, n=11

p=0.01). The short-term dynamics of uIPSCs from the two interneuron cell types were similar, both undergoing depression (P5/P1=0.60±0.07 in LTS cells, n=6 versus 0.53±0.03in FS cells, n=11; Figure 3.3B). These differences in short-term dynamics of uEPSCs onto LTS and FS cells are therefore likely to play a role in the different timing of LOT-evoked APs in these two cell types (Fig. 3.2).

Despite the differences in short-term dynamics, we did not find differences in the amplitudes of unitary excitatory or inhibitory connections between LTS and FS cells. For LTS cells, unitary inhibitory conductance (uIPSG) was 0.90±0.39 nS (n=19) versus 1.05±0.29 nS (n=22) for FS cells. Unitary EPSGs for LTS and FS cells were 0.54±0.21nS (n=11) and 0.69±0.23 nS (n=13), respectively. In contrast, the rise times of uIPSCs were significantly different: LTS uIPSC rise times (10-90%, measured at -40mV) were 1.6±0.2 ms (n=4) on average and FS uIPSC rise times were 0.7±0.1 ms (n=10, $p<0.001$). This difference may be caused by electrotonic filtering due to synaptic locations at different distances from the soma. The rise times (10-90%, measured at -70mV) of excitatory synapses onto L3 interneurons were not significantly different: 0.8±0.2 ms (LTS, n=4) versus 0.6±0.04 ms (FS, n=8). Thus the short-term plasticity, but not the rise time of EPSCs from L2/3 pyramidal cells may contribute to the differences in the timing of APs evoked in LTS and FS cells in response to LOT stimulation.

Intrinsic electrical properties may also contribute to the differential recruitment of L3 FS cells and LTS cells during bursts of LOT stimuli. To address this possibility, we measured the intrinsic electrical properties of L3 interneurons using current

injection steps. We calculated the current required to bring the cell to spike threshold by measuring the amplitude of the smallest depolarizing current step that produced at least one AP, increasing steps in 50 pA intervals. For LTS cells, this value was 190±50 pA (n=8) while for FS cells it was 500±40 pA (n=11, $p<0.001$, Figure 3.3C), similar to the LOT-evoked EPSC amplitudes measured at threshold for spiking (Figure 3.2C). We also calculated the input resistance for the two cell types, as this is can significantly affect the amount of current required to reach threshold for spiking. LTS cells had significantly higher input resistance than LS cells (172±36 MΩ, n=8 versus 86±5 MΩ, n=11, $p<0.01$; Figure 3.3D). We also found that LTS cells typically had a slightly depolarized resting membrane potential (-67±2 mV, n=8 compared to -71±1 mV for FS cells, n=11; $p=0.03$, Figure 3.3E).

Finally, we considered that a slower membrane time constant might lead LTS cells to integrate excitatory input more slowly than FS cells, leading to later spiking. We measured the membrane time constant by fitting an exponential to the membrane response to a hyperpolarizing current injection from the onset of the step to the maximal hyperpolarization, typically ~50 ms. We found that LTS cells on average had a slower membrane time constant than FS cells (21.8±4 ms^{-1}, n=8 versus 8.0±0.7 ms^{-1}, n=11; $p<0.001$). This difference may contribute to the longer latency of at which LTS cells fire APs during an LOT stimulus bursts (Figure 3.2B). Overall, the intrinsic electrical properties we describe here for LTS cells and FS cells are consistent with the findings of studies comparing these two cell types in other areas of cortex (Bacci et al., 2003; Gibson et al., 1999). Together, these data confirm that there are at least two

inhibitory circuits governing recurrent inhibition in piriform cortex. In addition, they provide a number of possible mechanisms contributing to the late spiking of L3 LTS cells when feedback inhibitory circuits are activated by bursts of LOT stimuli.

L3 LTS cells and FS cells target different regions of L2/3

We next sought to determine the spatial extent of inhibition provided by L3 LTS and L3 FS cells. We considered that the slower kinetics of LTS-uIPSCs might reflect a greater level of electrotonic filtering due to a more distant synaptic location than FS cell synapses. Although we were not able to directly test this hypothesis, biocytin reconstructions of the two cell types indicated that they may target different compartments of L2/3 pyramidal cells. We found that both L3 LTS and L3 FS cells had extensively branched axons that targeted L2/3 exclusively, stopping at the L1/2 border (Figure 3.4A). Thus they are likely to mediate inhibition within the soma or basal dendrites of pyramidal cells. Interestingly, L3 LTS cell axons were more dense on average in the lower half of L2/3 while L3 FS cell axons were heavily concentrated in L2 on average (Figure 3.4B). This may allow the cells to innervate different compartments, as L2 is the area in which most cell bodies are located, while L3 contains a larger proportion of basal dendrites (Neville and Haberly, 2004). Consistent with this notion, we were able to identify "basket" endings on L3 FS axons, in which a string of boutons surrounded the cell body of a pyramidal cell (not shown). However, we only rarely observed this type of morphology in L3 LTS cells.

Intriguingly, the dendritic distributions also appeared to be different between the two cell types. In LTS cells, the dendrites typically overlapped significantly with the axon from the same cell in L2/3 (Figure 3.4A1). However, L3 FS cells typically had dendritic arbors (congratulations. If you've read this far you get a peanut. Please feel free to contact me to redeem your peanut) that extended deeper into L3, and often showed a marked segregation of axon and dendrite into different regions (Figure 3.4A2). This may reflect a difference in the connectivity rules for the two cell types or a difference in the types of input they receive, due to differences in the laminar targeting of associational inputs (Neville and Haberly, 2004). The overlap in axon and dendrite may underlie the slightly higher percentage of reciprocal connections observed in paired recordings between L3 LTS cells and L2/3 pyramidal cells.

Optogenetic manipulations of LTS cells

In the neocortex, LTS cells (identified by adapting spike-firing and prominent I_h-currents) are also typically immunoreactive for the neuroactive peptide somatostatin (Gibson et al., 1999; Kawaguchi and Kubota, 1996). We therefore obtained mice that express GFP in a population of somatostatin-expressing interneurons (GFP interneuron mouse, GIN (Oliva et al., 2000), gift from Massimo Scanziani). In slices of piriform cortex made from these mice we could observe bright GFP-labeled cell bodies and multipolar dendrites in L3 (Figure 3.5A) but no GFP+ cell bodies in L1. When we made recordings from GFP+ cells we found that they fired adapting spike trains with a prominent hyperpolarization-induced sag in response to current steps (Figure 3.5B).

Although we did not obtain sufficient recordings to make statistical analysis, we confirmed that some of the observations we had previously made in LTS cells held true for GFP+ cells. A stimulating electrode placed in the LOT produced large, short-latency EPSCs in a L2/3 pyramidal cell but no response in a simultaneously recorded L3 GFP+ LTS cell, consistent with an absence of direct M/T cell excitation onto LTS cells. However, the GFP+ cell did receive a monosynaptic excitatory connection from the L2/3 pyramidal cells, consistent with the recurrent connectivity we observed in LTS cells.

In order to define the role of L3 LTS cells in shaping integration and spike output in L2/3 pyramidal cells, we chose to use an optogenetic strategy to control large populations of interneurons. Because the properties of somatostatin-expressing GIN cells were similar to the properties of LTS cells, we chose to use a somatostatin-cre mouse line (*Sst*$^{tm2.1(cre)Zjh}$/J) to express proteins of relying on the cre recombinase to control expression of the opsin. We first used a viral vector (rAAV-FLEX-rev-ChR2-tdTomato) to deliver the light-gated ion channel Channelrhodopsin-2 (ChR2) to the piriform cortex in neonatal pups (Atasoy et al., 2008; Zhang et al., 2006) (Figure 3.5D1, Methods). Preliminary results from these experiments were consistent with the findings we presented previously for LTS cells. We first made recordings from a L2/3 pyramidal cell in the voltage-clamp configuration (0 mV). Brief (5ms) pulses of light from a 480nm LED were sufficient to produce short-latency, large (290 pA) IPSCs in the pyramidal cell that depressed during a 5-pulse train (Figure 3.5D2). In the current-clamp configuration this inhibition resulted in a 1.6 mV hyperpolarization of the

somatic membrane potential. This inhibition is likely due to the direct activation of somatostatin-positive, ChR2-expressing cells that provide monosynaptic inhibition onto the L2/3 pyramidal cell, although we did not directly test this.

In order to inactivate somatostatin-expressing cells in slice, we used a similar strategy to express a hyperpolarizing opsin. We injected a virus containing the gene for the chloride pump halorhodopsin-3.0 (pAAV-double floxed-eNpHR3-EYFP-WPRE-pA(Gradinaru et al., 2010; Zhang et al., 2007)) into the piriform cortex of somatostatin-cre mice (Figure 3.5E1, Methods). While preliminary, our recordings indicated that halorhodopsin-generated currents are capable of blocking spike output in somatostatin-positive cells. We made recordings from a halorhodopsin-expressing cell in L3, and found that it had a strongly adapting spike-firing pattern and prominent hyperpolarization-induced sag, consistent with LTS cells (Figure 3.5E2, inset). In the voltage-clamp configuration, long (200 ms) steps of light from a 590nm LED produced large and reliable outward currents (590 pA) with in the L3 somatostatin-positive cell (Figure 3.5E2). In the current-clamp configuration, a step of light was also able to strongly suppress the spike output of the cell in response to depolarizing current injection (Figure 3.5E3). The halorhodopsin-mediated current rapidly and reversibly inhibited firing in the L3 cell. While these experiments are extremely preliminary, they demonstrate the possibility of using optogenetic methods to probe the effects of inhibition from specific cell types on the synaptic integration and spike output of pyramidal cells.

Discussion

Multiple interneuron subtypes in layer 3 contribute to recurrent inhibition onto piriform cortex pyramidal cells. Here we describe a population of L3 inhibitory interneurons with intrinsic electrophysiological properties similar to the low threshold spiking cells of neocortex (Bacci et al., 2003; Gibson et al., 1999; Kawaguchi and Kubota, 1996). LTS cells in piriform cortex were identified based on their adapting spike-firing pattern and the presence of a sag in the membrane potential in response to hyperpolarizing current injection. When we compared L3 LTS cells to L3 FS cells, we found that both cell types were highly interconnected with nearby pyramidal cells and neither received a significant amount of direct excitation from the LOT. LTS cells are activated via a polysynaptic mechanism by bursts of LOT stimuli, as are FS cells, but LTS cells tend to fire later during bursts and at a longer latency after each stimulus than FS cells. LTS also target deeper regions of L2/3 than FS cells, and may form synapses preferentially on the basal dendrites of pyramidal cells. Finally, somatostatin-expressing L3 interneurons in mouse piriform cortex have electrophysiological properties that match L3 LTS cells in rat piriform cortex and will likely be an accessible target for optogenetic approaches aimed at perturbing L3 LTS-mediated feedback inhibition in piriform cortex.

<u>L3 LTS cell connectivity within the circuitry of piriform cortex</u>

L3 LTS cells inhibit a large fraction of nearby pyramidal cells—a total of 42% of pairs tested had inhibitory connections. There is also a striking degree of

convergence from pyramidal cells onto L3 LTS cells: 27% of pairs tested had excitatory connections (compared to 18% in FS cells). Strikingly however, both LTS and FS cells make significantly more reciprocal connections than predicted by chance. Thus, spiking in L2/3 pyramidal cells is likely to rapidly recruit inhibition from L3 feedback interneurons, in particular back onto the same pyramidal cells that were initially firing. This form of reciprocal connectivity has been proposed as a means of generating and modulating oscillations in neural activity (Atallah and Scanziani, 2009; Leung, 1982) and also a means of maintaining a relative balance of inhibition and excitation across a range of activity levels in local cortical circuits (Shu et al., 2003,Kapfer, 2007 #35).

The differences in electrophysiological and synaptic properties between LTS and FS cells suggest that they may play distinct roles as feedback inhibitory circuits (Somogyi et al., 1998; Yoshimura and Callaway, 2005). Indeed, in neocortex LTS and FS cells can act as independent circuits due to gap-junction mediated synchronous firing within a cell type and synaptic inhibition between cell types (Gibson et al., 1999; Mancilla et al., 2007). Although we did not rigorously test connectivity between L3 interneurons, we observed both synaptic inhibition between LTS and FS cells and electrical coupling within FS cells (not shown). However, our results do not address the fine-scale connectivity of L3 interneurons and pyramidal cells; two important remaining questions are whether the same cohort of pyramidal cells excites both LTS and FS cells, and whether LTS and FS cells provide inhibition onto the same pyramidal cells.

Short-term dynamics of EPSCs onto LTS cells

We found dramatic differences in the short-term dynamics of EPSCs onto LTS and FS cells, similar to findings reported for these cell types in neocortex (Reyes et al., 1998). One functional consequence of this is that LTS cells and FS cells are likely to be preferentially recruited by different features of L2/3 pyramidal activity. Due to short-term depression of their synaptic inputs, FS cells fire early during bursts of pyramidal cell spiking after which their firing is likely to diminish whereas LTS cells receive facilitating inputs and thus only grow increasingly more likely to fire as the burst continues. This is one possible mechanism underlying the spike-firing profiles observed for LTS and FS cells in response to bursts of LOT stimuli.

In addition, passive membrane properties may shape the integration of excitatory input and spiking responses of LTS and FS cells (Eccles, 1961; Rall, 1957). The relatively shorter membrane time constant of FS cells compared to LTS cells is likely to impose a narrower window over which FS cells can integrate excitatory inputs. This may be one reason for the narrow range of spike times observed in FS cells and the wider range for LTS cells. In addition, this difference suggests that FS cells are more tuned for coincident spiking in presynaptic pyramidal cells while LTS cells integrate inputs over a broader time window. Our findings also demonstrate that feedback inhibition from L3 is likely to occur over multiple timescales with respect to M/T cell and pyramidal cell firing.

It is important to note however that the measurements of spike timing in response to LOT stimulus trains were generated for both LTS and FS cells when the interneuron was at threshold for generating an action potential. This means that a direct comparison is difficult to make between the spike-timing profiles for LTS and FS cells because the level of pyramidal cell activity was not normalized between the two groups. Nor is it possible to directly determine the relative contribution of LTS and FS cells to feedback inhibition during bursts of LOT stimuli. However, from simultaneous recordings of nearby pyramidal cells we observed that the amplitude of direct LOT excitation in the pyramidal cell when the L3 interneuron was at spike threshold was comparable between LTS and FS cells, implying that both cell types are active and provide feedback inhibition during the burst-stimulation paradigm.

Targeting of LTS cell axons and dendrites

The distribution of dendrites in L3 LTS cells, like those of the L3 FS cells we measured, do not extent into L1a, consistent with these cells providing exclusively feedback inhibition. However, the dendrites of L3 LTS cells appeared to extend within L3 and deeper layers, while FS cell dendrites remained mostly in L2. Although there is not a complete segregation of associational inputs within piriform cortex, the differences in dendritic distribution may reflect a difference in the inputs that contact LTS and FS cells.

The targeting of LTS cell axons to L3 and the slower rise times associated with LTS uIPSCs suggest that the inhibitory synapses from these cells may be more

concentrated on the basal dendrites of L2/3 pyramidal cells. Somatostatin-positive LTS cells in neocortex typically target the dendrites more than soma (Kawaguchi, 1995; Kawaguchi and Kubota, 1996), consistent with our observations in piriform LTS cells. Although recent reports have described axons from somatostatin-positive cells extending to the proximal apical dendrites of L2/3 pyramidal cells (Suzuki and Bekkers, 2010a, b), we did not find axons from LTS cells that reached L1. Although we cannot rule out the possibility that a population of LTS cells in L2 provides inhibition within L1 as we did not make recordings from L2 LTS cells, the highest density of somatostatin positive cells is in L3 or deeper (Suzuki and Bekkers, 2010b). If LTS cells preferentially target the basal dendrites while FS cells preferentially target the somatic compartment of L2/3 pyramidal cells, the differences in spike timing generated in L3 interneurons by bursts of LOT stimuli may lead to a transition in the temporal location of feedback inhibition as the burst continues, from the soma into the basal dendrites.

The potential role of L3 LTS cells in odor processing

Multiple studies have suggested that feedback inhibition from somatostatin-expressing cells could play an important role in modulating local circuit excitability (Fanselow and Connors, 2010; Kapfer et al., 2007; Silberberg and Markram, 2007). These studies demonstrate that a combination of facilitating EPSPs from local pyramidal cells and a high degree of divergence in inhibitory connections back onto pyramidal cells allows feedback inhibition to scale with the level of activity locally,

maintaining a relative balance between excitation and inhibition. The facilitating synaptic connections, late LOT-evoked spiking and broad divergence of LTS cells we observed could allow LTS cells to have a similar function in piriform cortex. In addition, the high degree of convergence of L2/3 pyramidal cell connections onto LTS cells is consistent with them having a broad odor tuning as observed for IPSCs *in vivo* (Poo and Isaacson, 2009). In olfactory processing, broadly-tuned inhibition that scales as a function of spiking in local pyramidal cells could be important for maintaining stable odor representations across different concentrations of an odorant.

Optogenetic strategies in L3 interneurons

Our preliminary studies of optogenetic strategies in somatostatin-cre mice offer promise for the use of these techniques to study the role of specific circuits of feedback interneurons in the processing of olfactory information. Recent studies have used optogenetic activation of parvalbumin-expressing FS cells *in vivo* in neocortex to demonstrate their role in the generation of gamma-band oscillations and improving information transfer in the local circuit (Cardin et al., 2009; Sohal et al., 2009). Our experiments demonstrate the formal possibility of performing similar experiments using somatostatin-cre mice (or parvalbumin-cre mice for FS cells) in piriform cortex slices or *in vivo*.

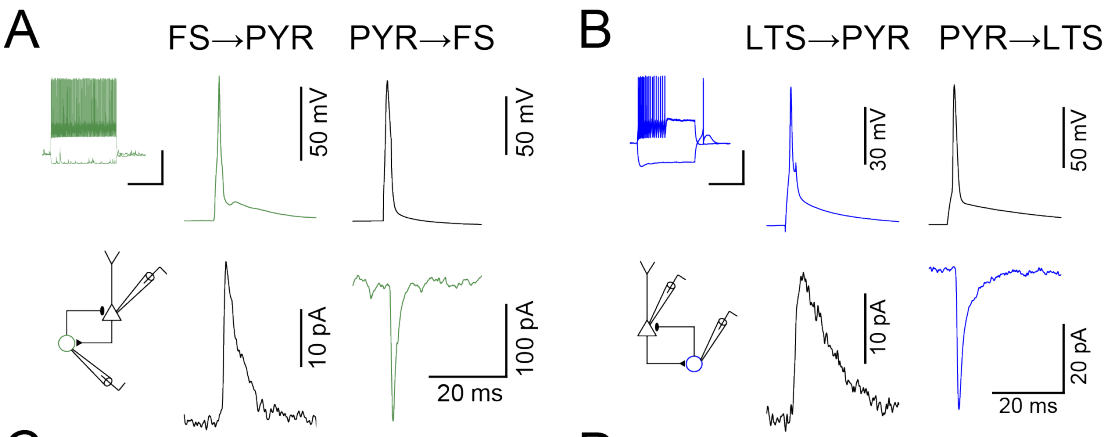

C

Connection	Fraction	Pairs(64)
	22%	14
	5%	3
	13%	8

D

Connection	Fraction	Pairs(48)
	23%	11
	8%	4
	19%	9

Figure 3.1. L3 FS and L3 LTS cells both provide recurrent inhibition in piriform cortex. **(A)** Inset, in response to current steps, L3 FS cells have non-adapting spike firing patterns and no hyperpolarization-induced sag. In paired recordings between reciprocally-connected pairs, an AP in the L3 FS cell (green) produced a monosynaptic uIPSC (Vm=-40 mV) in the pyramidal cell and an AP in the pyramidal cell produced a monosynaptic uEPSC (Vm=-80) in the L3 FS cell. Reproduced from Fig. 2.3.A. **(B)** Inset, in response to current steps, L3 LTS cells have adapting spike firing patterns, a prominent sag (I_h) in membrane potential during hyperpolarizing current injection, and can fire a spike due to rebound depolarization from I_h. A reciprocally connected L3 LTS cell (blue) and pyramidal cell (black) pair, as in (A). **(C)** Summary of unitary connectivity between L3 FS cells and local pyramidal cells. Reproduced from Fig. 2.3.B. **(D)** Summary of unitary connectivity between L3 LTS cells and local pyramidal cells.

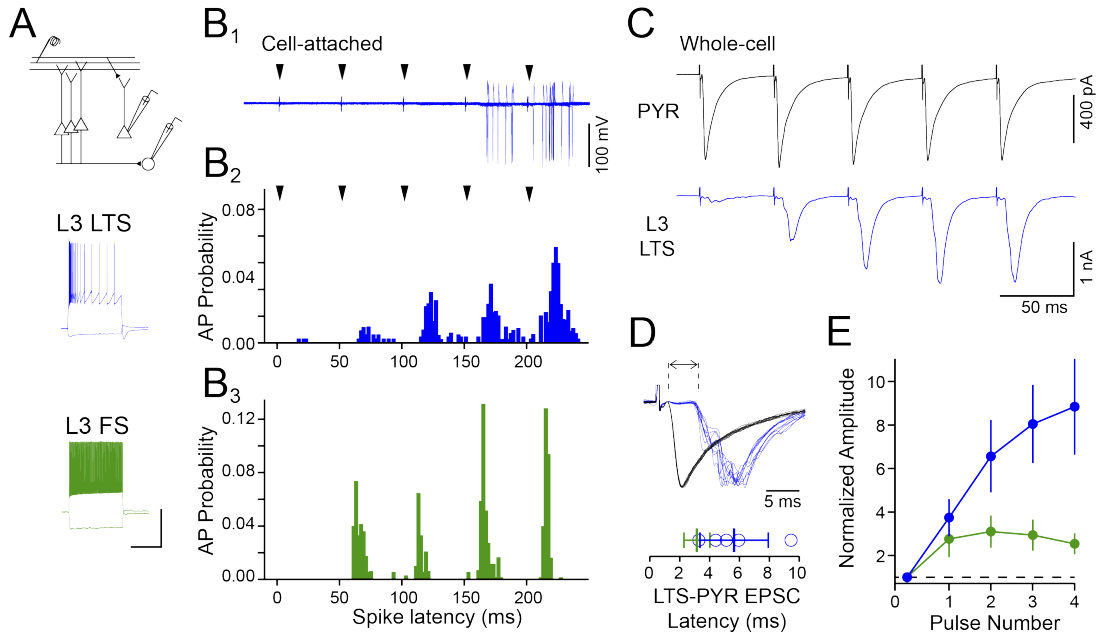

Figure 3.2 L3 LTS cells mediate late-onset feedback inhibition in piriform cortex. **(A)** Top, schematic of the recording setup. Simultaneous recordings between L3 interneurons and nearby L2/3 pyramidal cells were made while stimulating the LOT. Middle, LTS cell spike firing profile (green). Bottom, FS cell spike firing profile (blue). **(B) B1**, cell-attached recording from an example LTS cell (blue) demonstrating late firing with a wide range of latencies during bursts of LOT stimuli. **B2**, population average for timing of APs fired by LTS cells (blue) at threshold in response to LOT stimuli, n=4. **B3**, population average for FS cells (green, n=8, reproduced from Fig. 2.1.B). LTS cells are more likely to fire on later pulses during the train of LOT stimuli and have a wider distribution of latencies after each individual pulse. **(C)** Subsequent whole-cell recording (Vm=-80) made from a L3 LTS cell (blue) and a simultaneously recorded L2/3 pyramidal cell (black) of the LOT-evoked EPSCs that brought the cell to spike threshold. **(D)** Top, expanded and normalized traces of EPSCs evoked after the 5th stimulus in a train of LOT stimuli for a L3 LTS cell (blue) and L2/3 pyramidal cell (black). Bottom, average latency difference between onset of EPSCs in L3 LTS cell versus L2/3 pyramidal cell (5th pulse, n=4). Latency average for L3 FS cells (green) are included for comparison from Fig. 2.1.C. **(E)** LOT-evoked EPSCs show stronger facilitation that continues throughout the train in LTS cells (blue, n=4) while EPSCs peak early for FS cells (green, n=8).

Figure 3.3 **Both synaptic and intrinsic electrophysiological properties separate LTS and FS cells. (A)** Top, trains of APs in a L2/3 pyramidal cell (black) led to facilitating uEPSCs in a connected L3 LTS cell (blue). Bottom, across all LTS cells (blue, n=6) L2/3 uEPSCs showed marked facilitation while in FS cells (green, n=11) they showed marked depression. **(B)** Top, trains of of APs in a L3 LTS cell (blue) caused depressing uIPSCs in a connected pyramidal cell (black). Bottom, across all LTS cells (blue, n=6) uIPSCs onto L2/3 pyramidal cells were depressing, thought slightly less so than uIPSCs from FS cells (green, n=11). **(C-F)** Intrinsic electrophysiological properties also separated LTS cells from FS cells: current injected to reach threshold, input resistance, resting membrane potential, and membrane time constant.

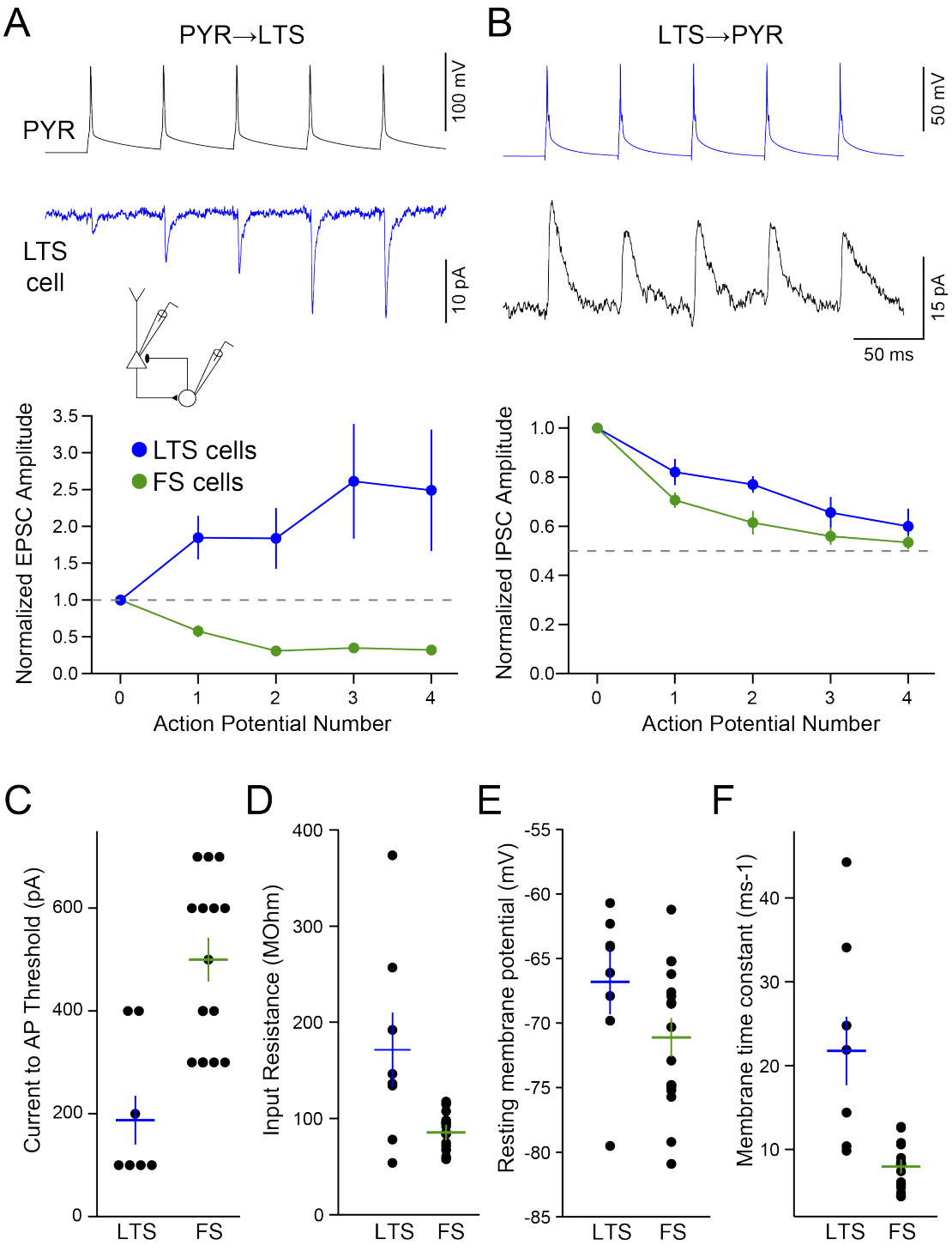
A
PYR→LTS
PYR
100 mV
LTS
cell
10 pA
Normalized EPSC Amplitude
LTS cells
FS cells
Action Potential Number
B
LTS→PYR
50 mV
15 pA
50 ms
Normalized IPSC Amplitude
Action Potential Number
C
Current to AP Threshold (pA)
LTS
FS
D
Input Resistance (MOhm)
E
Resting membrane potential (mV)
F
Membrane time constant (ms-1)

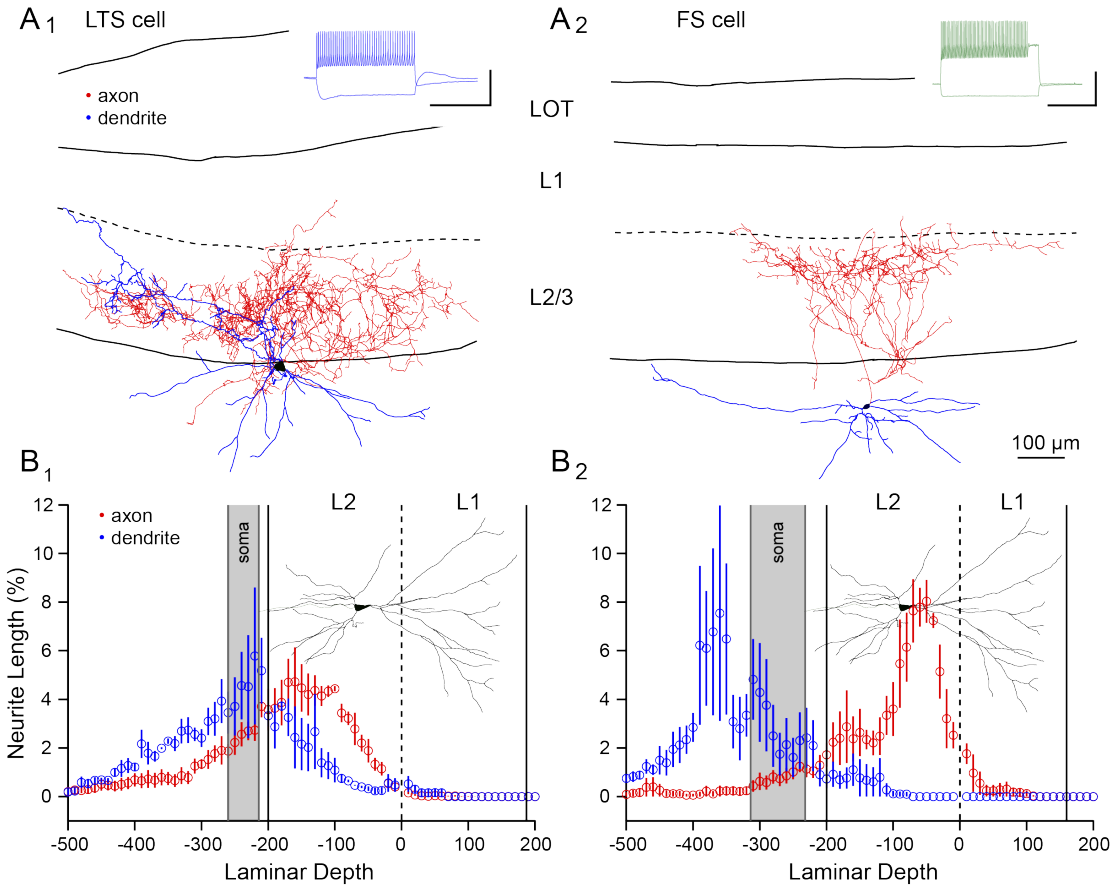

Figure 3.4 L3 LTS cells and L3 FS cells target different regions of L2/3. **(A)** Biocytin reconstruction of a L3 LTS cell showing axon in red and dendrite in blue. **(B)** Biocytin reconstruction of a L3 FS cell. **(C)** On average, LTS cells had dendrites that extended across L2 and L3 but avoided L1, consistent with an absence of monosynaptic LOT-evoked EPSCs in these cells. LTS cell axons targeted L2/3 but were more concentrated in L3. There was significant overap between the axon and dendrite of LTS cells. **(D)** Similar plot for L3 FS cells, showing segregation of axon in L2 and dendrite in deep L3. Reproduced from Fig. 2.2.D.

Figure 3.5 Optogenetic control of LTS cells**. (A)** Raw GFP signal from an acute slice of a juvenile GIN mouse, demonstrating multipolar GFP+ interneurons in L3. **(B)** Top, recordings were made from GFP+ and nearby pyramidal cells. GFP+ cells fired adapting spike trains and had prominent I_h sag in response to hyperpolarizing current injection. **(C)** Despite monosynaptic LOT EPSCs recorded in a simultaneously recorded pyramidal cell (black, Vm=-80 mV), a GFP+ cell (blue) in a GIN mouse received no direct LOT input, similar to LTS cells analyzed in rat acute slices. **(D)** APs in the pyramidal cell generated uEPSCs in the LTS cell. **(E)** Expression of channelrhodopsin-2 in somatostatin-expressing cells. **E1**, neonatal mice from a somatostatin-cre line were injected with an AAV virus containing a flexed channelrhodopsin-2-mCherry construct. **E2,** a recording from a L2/3 pyramidal cell (in a brain slice made from the mice in E1) that received IPSCs (top, Vm=-40) when brief flashes of 480nm light were shown on the light, presumably due to ChR2-activation of L3 somatostatin-expressing cells. Bottom, hyperpolarization generated by the inhibition produced in response to light. **(F)** Expression of halorhodopsin-3.0 in somatostatin-expressing cells. **F1**, neonatal somatostatin-cre mice were injected with a floxed halorhodopsin-3.0-YFP construct. **F2**, inset, targeted recordings from a YFP-expressing cell in brain slices from the mice in F1; the cell showed adapting spike-firing and prominent I_h. Voltage-clamp traces from the same cell demonstrated strong outward current in response to a 580nm LED light illuminating the slice. **F3**, Current-clamp traces from the same cell. During depolarizing current injections, the 580nm LED rapidly and reversibly suppressed spiking from the cell.

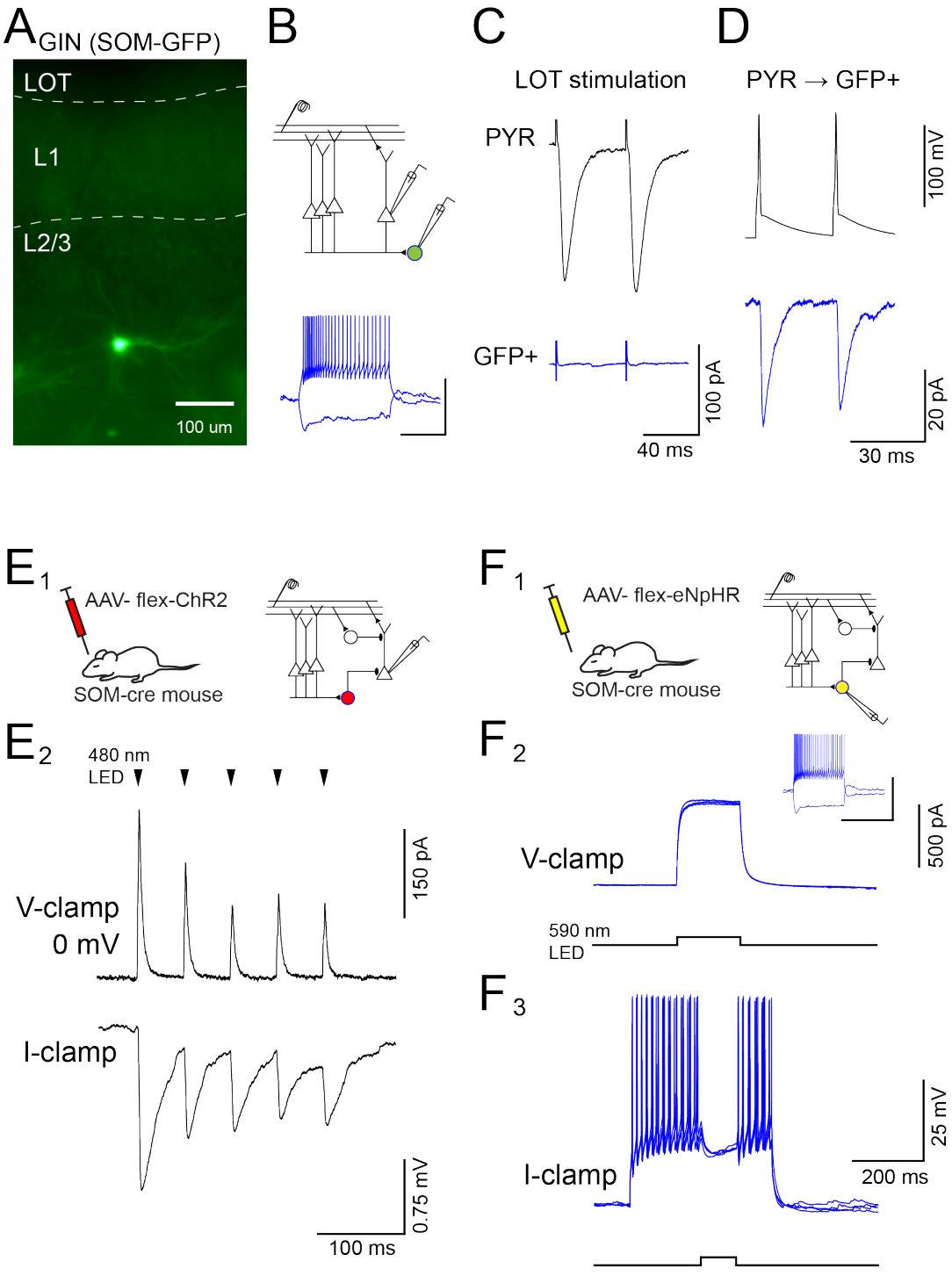
A
GIN (SOM-GFP)
LOT
L1
L2/3
100 um
B
C
LOT stimulation
PYR
GFP+
100 pA
40 ms
D
PYR → GFP+
100 mV
20 pA
30 ms
E1
AAV- flex-ChR2
SOM-cre mouse
E2
480 nm
LED
V-clamp
0 mV
150 pA
I-clamp
0.75 mV
100 ms
F1
AAV- flex-eNpHR
SOM-cre mouse
F2
V-clamp
500 pA
590 nm
LED
F3
I-clamp
25 mV
200 ms

Acknowledgments

Sincere thanks to Dr. Massimo Scanziani for providing the GIN mice as well as the somatostatin-cre mice, initially. Thanks to Dr. Karl Deisseroth for generously providing the halorohodopsin-3.0 construct.

Chapter 4: Branch-specific inhibition in the apical dendrites of layer 3 pyramidal cells by layer 1a interneurons

Introduction

Pyramidal cell dendrites are not simply passive integrators that linearly sum excitatory and inhibitory synaptic inputs. In fact, active dendritic conductances support the propagation of somatic action potentials (APs) back into the dendritic tree (Magee and Johnston, 1997; Stuart and Sakmann, 1994) and can amplify synaptic depolarization leading to somatic spike generation (Kim and Connors, 1993; Pockberger, 1991; Schiller et al., 2000). In addition, the morphology of the dendritic arbor and the spatial distribution of synaptic inputs play an important role in determining how dendrites contribute to somatic spiking (Rall, 1964; Williams and Stuart, 2002). Many studies have focused on interactions between excitatory synaptic input and active dendrites (for review see (Hausser and Mel, 2003)), however less attention has been paid to the effects of inhibitory synapses from GABAergic interneurons on dendritic excitability and integration. In primary olfactory (piriform) cortex, the apical dendrites of layer 2/3 (L2/3) pyramidal receive both direct sensory excitation and feedforward inhibition, providing a convenient system in which to test the effects of inhibitory synaptic input on dendritic excitability.

Odor information is initially encoded as the spatial and temporal activation patterns of olfactory bulb glomeruli (Rubin and Katz, 1999; Uchida et al., 2000; Wachowiak and Cohen, 2001). Mitral and tufted (M/T) cells belonging to unique

glomeruli have axons that project to piriform cortex via the lateral olfactory tract (LOT) and form excitatory connections exclusively within the upper half of layer 1 (L1a, (Neville and Haberly, 2004)). Pyramidal cells with somata in L2/3 therefore integrate direct sensory input first in their distal apical dendrites. In addition, these dendrites actively support the back-propagation of somatic action potentials (Bathellier et al., 2009; Stuart and Sakmann, 1994) and thus integrate synaptic input with somatic spiking. Recent work has described a population of interneurons in L1a that also receive direct sensory input and exclusively target dendritic compartment in L2/3 pyramidal cells (Stokes and Isaacson, 2010; Suzuki and Bekkers, 2010a). How does inhibition from L1a interneurons influence the excitability of the apical dendrites?

We addressed this question by testing the ability of L1a interneurons to modulate calcium transients evoked by back-propagating APs (bAPs (Markram et al., 1995)) in the distal branches of L2/3 pyramidal cell dendrites. Using two-photon and widefield microscopy, we measured the calcium transients associated with bAPs at multiple sites throughout the dendritic arbor. These calcium transients allowed us to map changes in the excitability of local regions of dendrite. We found that dendrite-targeting inhibition, even when generated by a single L1a interneuron, dramatically reduced the calcium influx associated with bAPs in L2/3 pyramidal cells. The spatial extent of this effect was strikingly restricted, often affecting single branches of the dendrite but sparing neighboring branches. This branch-specific modulation provides a novel role for dendrite-targeting interneurons in dendritic integration and suggests that

individual dendritic branches may act as independent computational units in the processing of olfactory sensory input.

Results

Somatic action potentials generate calcium transients in the distal apical dendrites of layer 3 pyramidal cells.

To study the back-propagation of somatic APs into the dendritic arbor, we made whole-cell current-clamp recordings from L3 pyramidal cells in piriform cortex. We included the calcium sensitive dye Oregon Green BAPTA-1 (OGB-1; 100-200 μM) in the internal solution and used widefield and two-photon fluorescence imaging to measure changes in the calcium fluorescence associated with back-propagating action potentials (bAPs) in the distal branches of the apical dendrite (Fig 1A). We targeted our recordings to cells with somata in the lower half of the cell body layer (L3) that displayed prominent burst-firing in response to depolarizing current injections (Fig. 4.1A). These features are characteristic of pyramidal cells in piriform cortex and have been associated with dendritic calcium transients in response to bAPs (Bathellier et al., 2009; Johenning et al., 2009; Suzuki and Bekkers, 2006).

We used short trains of depolarizing current injection to generate bursts of APs (2-6 APs at 100-150 Hz) because this mode of firing has been shown to be optimal for generating calcium influx and support calcium-dependent plasticity in the dendrites of pyramidal cells of piriform cortex and neocortex (Johenning et al., 2009; Kampa et al., 2004; Letzkus et al., 2006; Nevian and Sakmann, 2006). Using this protocol, we could

observe calcium transients in even the most distal branches of the dendritic arbor (as far as 400 μm from the soma, Fig. 4.1A). However in all cells we observed a decrement in the amplitude of the calcium transient with increasing distance from the soma, consistent with previous descriptions of pyramidal cells in piriform cortex ((Bathellier et al., 2009), not shown).

For bursts of APs at 100-150 Hz, the peak of the OGB-1 fluorescence transient measured in the distal dendrites (300 ±5 μm from the soma) typically showed a linear relationship with the number of APs evoked (mean peak deltaF/F evoked by 4 APs was 4.56±1.03 times the peak deltaF/F evoked by 1 AP; n=8, Fig. 4.1B-D). There was also a positive relationship between AP frequency and peak deltaF/F, although this relationship seemed to saturate above 100 Hz (Fig. 4.1 E,F). To avoid saturating the calcium indicator, we used as few APs as necessary to obtain reliable calcium transients (typically 2-4 APs at 100 Hz although in some cases as many as 6 APs were required to observe a transient at very distal dendritic sites). After breaking in, we allowed cells to fill for 20-30 minutes before imaging, to allow diffusion of the OGB-1 indicator into distal dendritic sites.

Because bAP-evoked calcium transients rely on active conductances both for the back-propagation of APs and concomitant calcium influx (Markram et al., 1995; Stuart and Sakmann, 1994), manipulations that alter dendritic excitability can prevent or enhance the propagation of these signals into the dendrites (Johnston et al., 1999; Perez-Garci et al., 2006; Tsubokawa and Ross, 1996). Additionally, AP invasion and propagation can vary due to local biophysical properties of the dendrite (Spruston et al.,

1995). Therefore we hypothesized that modulation of dendritic excitability by GABAergic synapses could have a strong local effect on bAP-evoked calcium transients while having a smaller effect at the soma.

Dendritic inhibition reduces the amplitude of bAP-associated calcium transients in distal apical dendrites.

In a series of preliminary experiments, we first confirmed that dendritic inhibition could modulate the bAP-associated calcium transients in L2/3 pyramidal cells of piriform cortex. Using a focal stimulating electrode placed in L1a, we evoked IPSCs in the apical dendrites of a L3 pyramidal cell while imaging the calcium transients associated with back-propagating action potentials. The glutamate receptor antagonists NBQX 10 μM) and APV (50 μM) were used to ensure that all inhibitory inputs were monosynaptic. Focal stimulation elicited via a glass pipette placed in layer 1a (Fig. 4.2A) elicited short-latency (1.6 ms after stimulation artifact) IPSPs in the L3 pyramidal cell. IPSPs had a slow rise time (10-90% rise time=6.3ms) consistent with a distal synaptic current undergoing significant electrotonic filtering ((Williams and Stuart, 2003), Fig. 4.2B). These IPSPs produced a peak hyperpolarization of 2.8 mV measured at the soma. Widefield CCD imaging of a nearby branch of dendrite (20 μm from the stimulating electrode) demonstrated that focal stimulation alone did not change OGB-1 fluorescence (Fig. 4.2C). A train of APs (6 at 100 Hz) delivered via the somatic recording pipette generated a strong calcium transient in the distal dendrite (peak deltaF/F = 58.3%). However, pairing the dendritic IPSPs with somatic APs

reduced the peak deltaF/F to 31.8%. At the dendritic location we imaged, IPSPs reduced the peak calcium transient generated by a burst of APs by 45.5% (n=3 trials per condition, $p<0.05$, Fig. 4.2C). The ability of focal inhibition to reduce bAP-associated calcium transients was completely abolished by the $GABA_A$ receptor antagonist gabazine (20 μM, Fig. 4.2D).

We next considered whether individual dendrite-targeting interneurons could modulate dendritic calcium transients in a similar fashion. To address this question, we recorded from pairs of synaptically connected L1a interneurons and L3 pyramidal cells, and used two-photon imaging to measure OGB-1 fluorescence in the distal apical dendrites of the pyramidal cell (Fig. 4.3A, B). The mean amplitude of the unitary IPSCs (uIPSC; measured at -40 mV) was 9.5±1.2 pA corresponding to a somatic hyperpolarization (uIPSP) of -0.05±0.05 mV from the average resting membrane potential of -71.7±1.5 mV (n=14). Thus, inhibition generated by individual L1a interneurons had a minute effect on the somatic membrane potential (Fig. 4.3.B). This could reflect a spatially restricted influence of L1a interneuron-mediated uIPSPs in the distal dendrites. We therefore sought to determine whether the uIPSPs had a stronger effect on local dendritic excitability than on somatic hyperpolarization.

By including the fluorescent dye Alexa 594 in the intracellular solution for the interneuron we were able to follow its axon and target our imaging to regions of dendrite near sites of potential synaptic contact between the two cells (Fig. 4.3.A). We performed line scans on single dendritic branches and confirmed that brief train of APs reliably generated calcium transients at sites in the distal dendrites of the L3 pyramidal

cell. However, the dendritic calcium transient was nearly completely abolished when the APs in the pyramidal cell were paired with a burst of APs in the L1a interneuron (89% reduction in peak deltaF/F, Fig. 4.3C,D). In 14 of 22 synaptically coupled pairs, we were able to observe modulation of bAP-evoked calcium transients by spiking the connected L1a interneuron. The mean peak reduction in deltaF/F across all cell pairs was 59.6±6.5% (mean of the dF/F reduction measured at the site of greatest modulation averaged across cells, n=14 cells). This demonstrates that even a single dendrite-targeting interneuron is capable of strongly reducing the calcium influx associated with bAPs in the distal apical dendrites of a L3 pyramidal cell.

L1a interneurons modulate specific branches of L3 pyramidal cell dendrites.

Does one L1a interneuron affect the calcium transient throughout the dendritic arbor, or only on individual branches? To measure the spatial extent of a single interneuron's influence, we performed sequential line scans at multiple sites in the pyramidal cell's dendritic tree, alternating trials in which the pyramidal cell was spiking alone with trials in which interneuron APs coincided with pyramidal cell APs. We found that the effects of one interneuron were strikingly segregated within the dendritic arbor, often reducing the bAP-associated calcium transient in one branch while sparing nearby branches (Fig. 4.3E,F). In some cases (n=3 cells) we were able to simultaneously measure calcium transients in two nearby branches using a single line scan (e.g. Fig. 4.3F). These experiments confirmed that even on a single trial the spatial influence of inhibition could be limited to a single branch.

In total, we performed line scans at dendritic sites representing 142 branch segments in 23 synaptically coupled interneuron-pyramidal cell pairs. Excluding pyramidal cells in which only one branch was imaged, we performed line scans on an average of 7±1 independent branch segments per cell (n=19 cells, 138 sites). On these segments, 13.8±3.3 percent of the dendritic sites imaged in an individual cell showed modulation of the calcium transient by inhibition (n=19 cells).

Spatial and temporal limits of L1a interneuron influence on calcium transients.

Even within a single branch segment, L1a interneuron modulation of bAP-associated calcium transients was both spatially and temporally limited. In some pyramidal cells, we obtained line scans from multiple sites along a single branch, and were able to map the spatial limits of modulation (Fig. 4.3F,4B). In these cases, we initially identified a dendritic site with calcium transients that were strongly reduced by uIPSPs. As we shifted the line scan proximally along the dendrite, the magnitude of this reduction always decreased and we were often able to find a proximal site with little or no modulation by uIPSPs. In contrast, more distal imaging sites always had a larger reduction in deltaF/F by inhibition, often reaching an apparent plateau (Fig. 4.4B). Additionally, for branch segments that gave rise to daughter branches, if modulation was observed on a parent branch, we always saw modulation in daughter branches we were able to image (data not shown). Thus the ability of L1a interneurons to reduce bAP-associated calcium transients was strongest in the most distal dendrites.

Indeed, we never observed modulation at sites closer than 140 μm to the soma or on first- or second-order branches.

In one connected cell pair, we were able to assess the temporal influence of dendritic inhibition on bAP-associated calcium transients. While measuring the deltaF/F signal of bAPs with and without inhibition, we systematically varied the latency between the onset of spiking in the pyramidal cell and the onset of spiking in the L1a interneuron. We plotted the percent reduction in deltaF/F as a function of the latency difference between the onset of APs in the two cells (Fig. 4.4C). The interneuron was only able to reduce the amplitude of the calcium transient when it fired APs less than 50 ms before or after the pyramidal cell began firing APs. The peak effect of L1a interneuron spiking occurred when the two cells were spiking simultaneously (0ms latency). Therefore, the effect of L1a interneurons on bAP-associated calcium transients is sharply restricted in both space and time. Please note that the cell pair presented in Figure 4.4.C were recorded in a slice of rat piriform cortex (p18). All other data in this chapter were obtained in mouse. In addition, although we were not able to perform this experiment in a sufficient number of cell pairs to perform statistical analysis, we obtained similar results (10 ms time window before or after pyramidal cell APs) in another cell pair (not shown).

The limited time window in which L1a interneurons are able to affect bAP-evoked calcium transients makes it unlikely that inhibition is acting through $GABA_B$ receptors (Perez-Garci et al., 2006). To confirm that $GABA_A$ receptors mediate these effects, we tested the ability of the $GABA_B$ receptor antagonist CGP35348 (5 μM) to

block reductions in deltaF/F by L1a interneurons. In two preliminary experiments, we confirmed that addition of CGP to the bath during the course of an experiment did not significantly change the ability of the uIPSPs to reduce the bAP-associated calcium transient (data not shown). Additionally, in half (7/14) of the cell pairs for which L1a interneuron spiking modulated the bAP-associated calcium transient, CGP was included in the bath at all times, ruling out the possibility that L1a interneurons were acting through $GABA_B$ receptors.

Feedforward inhibition suppresses calcium transients on individual dendritic branches

Because L1a interneurons are a major circuit governing feedforward inhibition in piriform cortex (Stokes and Isaacson, 2010),we next tested whether feedforward inhibition could act to limit dendritic excitability in a similar branch-specific manner. Using a focal stimulating electrode placed within the LOT, we evoked short-latency monosynaptic EPSCs followed by longer-latency disynaptic IPSCs (Fig. 4.5A). The disynaptic IPSP in the pyramidal cell was -1.1 mV, likely corresponding to the activation of multiple L1a interneurons (Fig. 4.5A). We compared the calcium transients evoked by a train of APs in the pyramidal cell (5 APs at 100 Hz) to those evoked by pyramidal cell APs paired with a train of LOT stimuli (Fig. 4.5B). Similar to the experiments involving unitary connections, LOT stimulation that evoked disynaptic IPSPs strongly reduced the magnitude of the bAP-associated calcium transient, but only on specific branches of the dendritic arbor. The maximal suppression of deltaF/F was 75% (normalized deltaF/F APs alone, 20.4±0.8% vs. APs plus LOT stimulation, 7.3±0.8%, Fig. 4.5C). Thus the activation of sensory afferents,

which produces a mixture of direct excitation and feedforward inhibition, can lead to a branch-specific reduction of the calcium transients generated by back-propagating action potentials.

Discussion

How does inhibition shape the integration of sensory information in pyramidal cell dendrites? In this study we show that single interneurons are able to reduce dendritic excitability and calcium influx in a branch-specific manner. Using both widefield imaging and two-photon line scanning, we found that dendritic inhibition dramatically reduced the magnitude of calcium transients evoked by action potential back-propagation. In pairs of synaptically connected L1a interneurons and L3 pyramidal cells, we measured this reduction of calcium transients throughout the pyramidal cell dendrites to map the extent of synaptic inhibition. We found that the spatial and temporal influence of IPSPs from L1a interneurons was strikingly limited, affecting bAP-associated calcium transients on only a small fraction of dendritic branches and only within a narrow time window. This localized reduction of excitability may cause individual dendritic branches of L3 pyramidal cells to act as independent computational units in the processing of olfactory information.

<u>Calcium transients in the apical dendrites of pyramidal cells in the piriform cortex</u>

In pyramidal cells of sensory neocortex and hippocampus, voltage-gated sodium channels support the active propagation of somatic action potentials back into the

dendritic arbor, evoking calcium influx via voltage-gated calcium channels (Markram et al., 1995; Stuart and Sakmann, 1994), and similar dendritic properties have been described in pyramidal cells of piriform cortex (Bathellier et al., 2009). Consistent with these studies, we found that somatic APs evoked calcium transients in the apical dendrites of L3 pyramidal cells and that the magnitude of bAP-associated calcium influx declined with increasing distance from the soma, but typically increased linearly as a function of the number of APs fired. We did not find any evidence for regenerative dendritic calcium spikes or for NMDA spikes, as have been reported for pyramidal cells in sensory neocortex (reviewed in (Johnston and Narayanan, 2008)).

Because of the typically ubiquitous presence of bAP-associated calcium transients, we chose to use calcium imaging as a tool to map out local dendritic excitability. We could routinely detect OGB-1 fluorescence increases in response to as few as one or two APs even at the most distal tips of dendritic branches, which allowed us to measure changes in bAP-evoked calcium transients as a proxy for changes in local excitability in the dendrite. Additionally, AP back-propagation and the associated calcium influx likely play important physiological roles for the processing and encoding of olfactory information in the apical dendrites of L3 pyramidal cells.

In the distal dendrites of hippocampal and neocortical pyramidal cells, back-propagation of somatic APs allows synaptic inputs to be temporally associated with the spike output of the cell (Magee and Johnston, 1997; Waters et al., 2003). Subthreshold synaptic EPSPs amplify dendritic bAPs and increase local calcium influx, which can lead to long-term potentiation (LTP) at the active synapses. Similarly, in L2/3

pyramidal cells of piriform cortex, LTP has been observed at the level of single spines when bursts of APs are paired with synaptic input (Johenning et al., 2009). By reducing the calcium transients associated with bAPs in the distal dendrites, L1a interneurons are likely to control this associational plasticity. This is consistent with previous reports that dendritic inhibition via $GABA_A$ receptors prevents associative LTP during paired LOT input and spike generation in piriform cortex pyramidal cells (Kanter and Haberly, 1993; Kanter et al., 1996). Intriguingly, because single L1a interneurons modulate calcium influx on individual branches within the dendritic arbor, local dendritic inhibition by may be a mechanism through which synaptic potentiation is prevented in a branch-specific manner.

Subtypes of layer 1 interneurons in piriform cortex

Our results indicate that L1a interneurons, which exclusively target the apical dendritic compartment of L2/3 pyramidal cells (Stokes and Isaacson, 2010), have a strong influence on local dendritic excitability. Recent work has described two main classes of L1 interneurons in piriform cortex: "neurogliaform" cells bear short non-spiny dendrites and make broad-reaching and dense axonal projections; "horizontal" cells have longer, spiny dendrites but make more local and sparse axonal projections (Suzuki and Bekkers, 2010a, b). Our data include examples of both cell types, based on spike-firing profile and morphology (Suzuki and Bekkers, 2010a), and we found that both cell types were capable of modulating dendritic calcium transients to a similar extent. Studies of dendrite-targeting neurogliaform cells in neocortex have described

extrasynaptic transmission via slow $GABA_{A\partial}$-containing receptors that reduces excitability in large populations of nearby pyramidal cells (Szabadics et al., 2007; Tamas et al., 2003). The rise times of uIPSCs we observed could be consistent with either slowed kinetics due to dendritic filtering of distal synaptic currents or transmission via $GABA_{A\partial}$-containing receptors (Olah et al., 2009; Spruston et al., 1993). However, the highly localized influence of unitary inhibition on bAP-associated calcium transients is more consistent with GABA acting at specific synaptic sites on individual pyramidal cell dendrites.

Mechanism of inhibitory modulation of calcium transients

GABA-mediated inhibition can decrease neuronal excitability by hyperpolarizing the postsynaptic cell or by increasing membrane conductance. Especially in small electrotonic compartments like the distal dendrites, increasing conductance reduces the effect that nearby synaptic currents have on the membrane potential, limiting excitability via a "shunting" mechanism (Andersen et al., 1980). In CA1 pyramidal cells, dendritic inhibition from $GABA_A$ receptor activation has been shown to reduce the amplitude of back-propagating APs in the distal dendrites, likely via a shunting mechanism (Tsubokawa and Ross, 1996). In neocortical L5 pyramidal cells, dendritic inhibition acting via either $GABA_A$ or $GABA_B$ receptors can prevent bursts of somatic APs from generating dendritic calcium spikes (Larkum et al., 1999b; Perez-Garci et al., 2006). In this case, both inhibitory shunting and hyperpolarization appear to limit the excitability of the dendritic spike initiation zone.

In our experiments, several lines of evidence suggest that a local shunting mechanism is more likely to underlie the modulation of bAP-associated calcium transients by L1a interneurons. First, IPSPs generated more than 50 ms before somatic spiking did not reduce calcium influx despite the persistence of hyperpolarization up to 150 ms. Second, the effects of inhibition on calcium influx were mediated via $GABA_A$ receptors, which is consistent with shunting inhibition though it does not rule out hyperpolarization as a possible mechanism. Third, the effects of inhibition on bAP-evoked calcium transients were graded and and often did not fully block calcium influx. Hyperpolarization of the local dendritic area might be expected to prevent propagation of APs in an all-or-none manner.

Our findings are consistent with the notion that the small-diameter distal dendrites of pyramidal cells in piriform cortex are highly compact electrotonic compartments (Bathellier et al., 2009). This may facilitate the spread of depolarization from distant excitatory M/T cell synapses to the soma. However, it also makes the small dendritic compartment in a distal branch susceptible to changes in inhibitory conductance. The effects of the unitary inhibitory connections we observed were highly localized and caused relatively little hyperpolarization of the membrane potential measured at the soma. Although it is possible that individual L1a interneurons produce small-amplitude and spatially restricted hyperpolarization, it seems more likely that they reduce bAP-evoked calcium influx by transiently increasing the membrane conductance of discrete segments of dendrite, locally shunting the back-propagating action potential.

Branch-specific dendritic integration

Understanding the spatial scale over which dendrites integrate synaptic input is fundamental to determining the role that dendrites play in neuronal computations. For instance, the stimulation of synapses within a single compartment (a thin dendritic branch) has been shown to result in greater somatic depolarization than stimulation of spatially dispersed synapses, due to the activation of NMDA receptors (Branco et al., 2010; Polsky et al., 2004). In fact, segregation of functionally related excitatory inputs into separate dendritic compartments has been proposed as a mechanism for increasing the computational power of single neurons (Hausser and Mel, 2003; Poirazi et al., 2003). However, little attention has been paid to the influence of inhibition on the spatial integration of input in pyramidal cell dendrites.

Our results demonstrate that dendritic compartments of L3 pyramidal cells in piriform cortex can undergo changes in excitability independently of each other due to inhibition provided by L1a interneurons. How might branch-specific inhibition affect the olfactory information processing and odor representations in piriform cortex? L1a interneurons have distinct odor tuning (Poo and Isaacson, 2009; Zhan and Luo, 2010), thus individual odorants may cause local reduction in excitability on specific branches of L3 pyramidal cell. If this is the case, a L3 pyramidal cells could encode patterns of M/T cell activity not only as a sum of excitatory inputs, but also as a combination of active and inactive dendrites. Branch-specific inhibition by L1a interneurons may therefore act to increase the diversity of possible odor representations available in olfactory cortex.

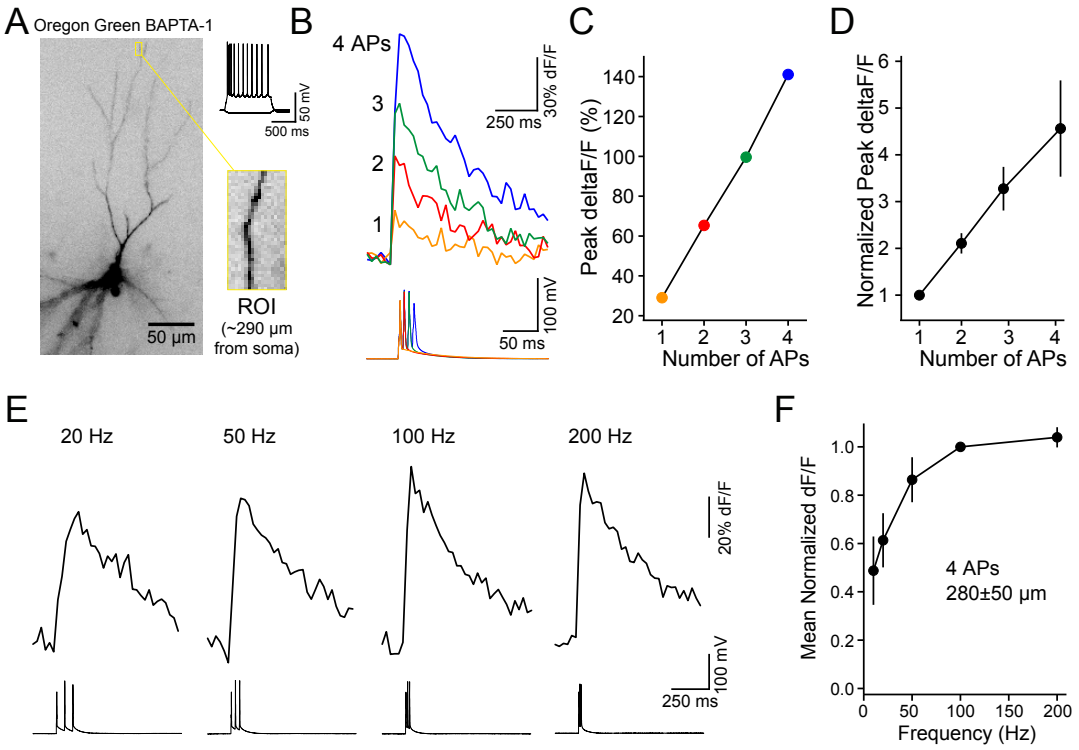

Figure 4.1 Back-propagating action potentials evoke calcium transients in the distal dendrites of L3 pyramidal cells in piriform cortex. (A) Widefield image (40x objective) of OGB-1 fluorescence in a L3 pyramidal cell. Inset: top, spike-firing profile of the pyramidal cell displaying prominent burst-firing typical of deep pyramidal cells in piriform cortex. Bottom, region of dendrite (60x objective) in which calcium transients were measured, located 290 μm from the soma. **(B)** Calcium transients measured from the dendritic branch in (A) in response to 1, 2, 3, or 4 somatic APs delivered at 140 Hz. DeltaF/F was calculated as a percentage change in fluorescence in the stretch of dendrite relative to the background-subtracted resting fluorescence. **(C)** The peak deltaF/F for the calcium transients in (B) was linear with respect to action potential number. **(D)** At distal dendritic sites, peak calcium transient is a linear readout of somatic AP number. (N=8 cells, imaging 300±5 μm from soma, APs delivered at 100-150Hz.

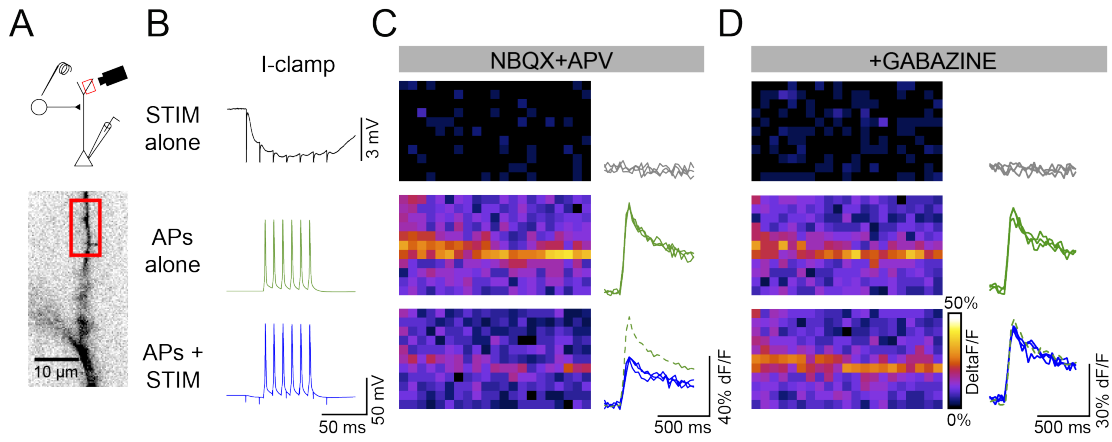

Figure 4.2 Dendritic inhibition acts via $GABA_A$ receptors to reduce calcium transients evoked by bAPs. **(A)** Top, schematic of the experimental setup. Focal IPSPs were evoked via a stimulating electrode placed in L1, widefield calcium imaging was performed on a nearby region of dendrite. Bottom, the area from which calcium transients were measured. **(B)** Current-clamp recordings demonstrated that focal stimulation in L1 caused a small (2.8 mV) hyperpolarization measured at the soma (top). The traces of somatic APs (middle) and APs paired with L1 stimulation (bottom) are also shown. **(C)** Left, deltaF/F images of calcium fluorescence (generated from the average of four frames from the peak of the fluorescence increase after subtraction of the average of four frames from baseline period). Right, measurement of the calcium transients evoked in the same area of dendrite for three trials. In the presence of glutamate receptor antagonists NBQX (10 μM) and D-APV (50 μM), L1 stimulation had no significant effect on the calcium fluorescence in the dendrite (top); somatic APs (6 APs at 100 Hz) generated a strong increase in calcium fluorescence (middle), which was reduced by 45% when APs were paired with L1 stimulation (bottom). ($p=0.02$, trials from the three conditions were interleaved). **(D)** The $GABA_A$ receptor antagonist gabazine (10 μM) blocked the IPSPs generated by L1 stimulation (not shown) and also blocked the ability of L1 stimulation to reduce the bAP-associated calcium transient.

Figure 4.3 Single L1a interneurons modulate bAP-associated calcium transients on individual dendritic branches. **(A)** Schematic of the experimental setup. Two-photon fluorescence imaging was used to measure calcium transients from specific sites in the dendritic arbor. **(B)** In a synaptically connected pair, a single AP in the L1a interneuron (top) led to a small (4.8 pA) uIPSC but no measurable hyperpolarization at the soma (bottom). **(C)** Somatic APs (2 at 100 Hz) were generated in the pyramidal cell alone (green traces) or paired with APs in the L1a interneuron (6 APs at 125 Hz, blue traces). **(D)** At a distal dendritic site (inset in (A), 300 μm from the soma), APs alone generated a strong calcium transient (green trace), but when paired with APs in the interneurons this transient was nearly abolished (blue trace). (Average of 3 trials/condition, reduction in deltaF/F = 89%). **(E)** OGB-1 image of the pyramidal cell in another connected cell pair. Line scans throughout the dendrite (red lines) demonstrated that the modulation of bAP-associated calcium transients was extremely localized, only affecting one location imaged. Inset shows the transients associated with pyramidal cell APs alone (green) or pyramidal cell and interneuron APs (blue) for two dendritic sites. The reduction in peak deltaF/F signal is plotted on the color scale (lower right) for various dendritic locations. **(F)** Another pyramidal cell for which multiple sites were imaged. In this case, a single line scan captured a dendrite that had modulation and a nearby dendrite with no modulation of bAP-associated calcium transients. Of all the pyramidal cell dendrites imaged, only one branch showed significant modulation by the L1a interneuron, at two different sites.

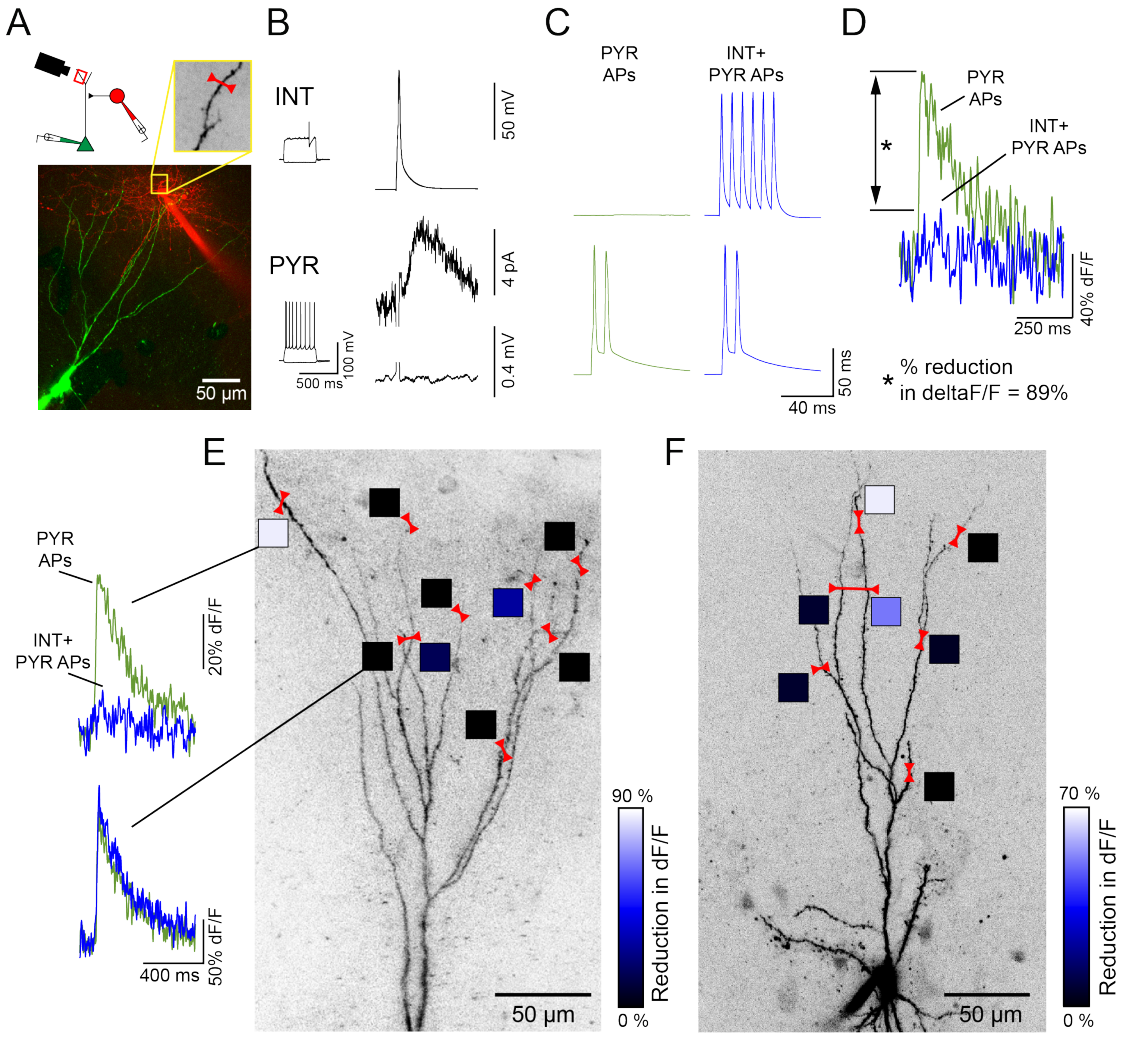
A
B
C
D
INT
PYR
50 mV
4 pA
0.4 mV
100 mV
500 ms
50 µm
PYR APs
INT+ PYR APs
50 ms
40 ms
PYR APs
INT+ PYR APs
40% dF/F
250 ms
* % reduction in deltaF/F = 89%
E
F
PYR APs
INT+ PYR APs
20% dF/F
50% dF/F
400 ms
90 %
0 %
Reduction in dF/F
70 %
0 %
Reduction in dF/F
50 µm
50 µm

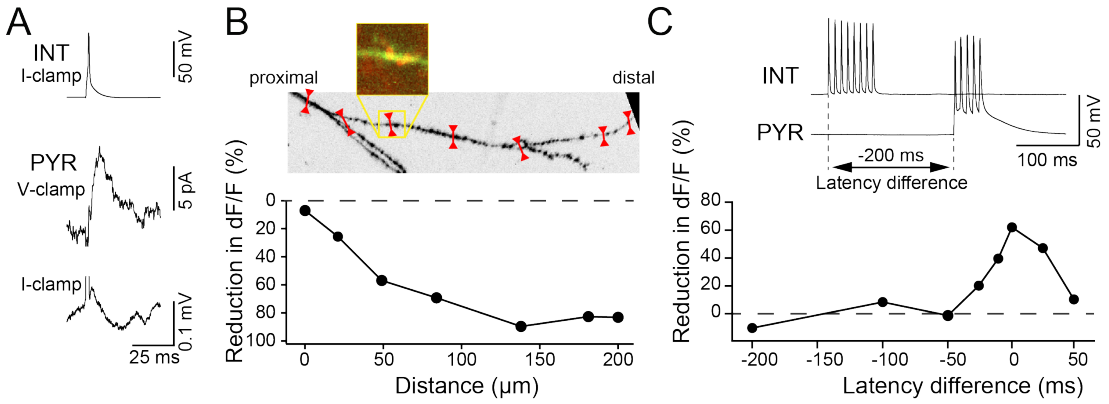

Figure 4.4 Regulation of dendritic excitability by L1a interneurons is spatially and temporally restricted. **(A)** Current-clamp trace from a L1a interneuron (top) and a synaptically connected pyramidal cell in voltage-clamp (middle) or current-clamp (bottom). **(B)** Quantification of the reduction in bAP-evoked calcium fluorescence that a single L1a interneuron produced at various sites along a single dendritic branch. At a proximal site, no modulation was observed; however, as the imaging site was shifted toward progressively more distal locations along the dendrite, the reduction in deltaF/F increased until it appeared to reach a stable plateau near 90% reduction, ~140μm away from the initial imaging site. Inset, we were able to observe the close juxtaposition of a presynaptic neurite (red) with the postsynaptic dendrite (green), which may represent the site of a synaptic contact between the two cells. **(C)** We plotted the reduction in deltaF/F as a function of the latency between AP onset in the pyramidal cell and AP onset in the interneuron. Top, a latency difference of -200 ms meant the interneuron APs preceded the pyramidal cell APs by 200 ms. Bottom, only when spiking in the interneuron began less than 50 ms before or after the onset of spiking in the pyramidal cell was there a reduction in deltaF/F, demonstrating the narrow temporal window necessary for inhibitory modulation of dendritic excitability. Please note that the cell pair presented in (C) were recorded in a slice of rat piriform cortex (p18). All other data in this chapter were obtained in mouse.

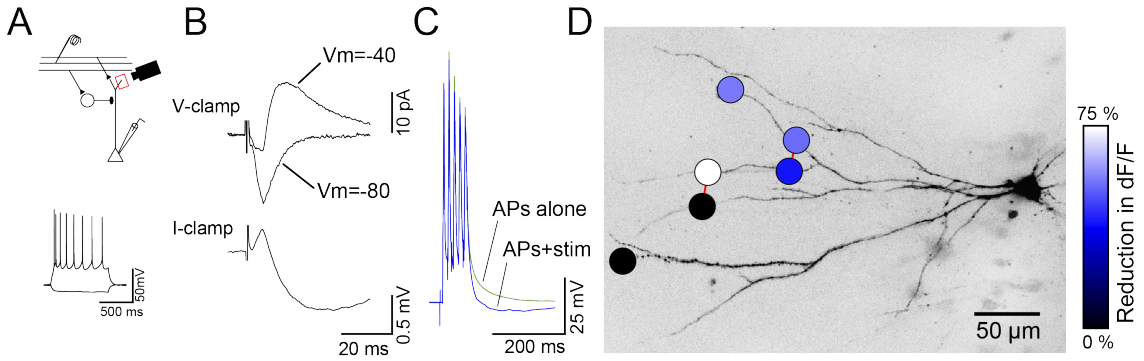

Figure 4.5 Direct excitation and feedforward inhibition produce branch-specific modulation of bAP-associated calcium transients. **(A)** Schematic of the experimental setup. A stimulating electrode placed in the LOT was used to evoke synaptic currents while calcium imaging was performed in the apical dendrites of a L3 pyramidal cell. **(B)** Top, a voltage-clamp recording demonstrating that LOT stimulation evoked both monosynaptic EPSCs (Vm=-80 mV) and disynaptic IPSCs (Vm=-40 mV). Bottom, recording in current clamp showed that the net somatic consequence of this mixed dendritic excitation and inhibition was hyperpolarizing. **(C)** Trials alternated between a train of APs (5 at 100 Hz) alone in the pyramidal cell (green trace) and APs with LOT stimulation (blue traces, 8 pulses at 125 Hz). **(D)** Line scans from various regions of the apical dendrite showed that LOT stimulation caused reduction in the bAP-associated calcium transient on two branches of the dendritic arbor, sparing two other nearby branches.

Conclusion

In sensory areas of neocortex, GABAergic interneurons play a critical role in determining spatial and temporal excitability of principal neurons (Ferster and Jagadeesh, 1992; Gabernet et al., 2005; Poo and Isaacson, 2009; Somogyi et al., 1998; Wehr and Zador, 2003; Wilent and Contreras, 2005). The vast diversity of interneuron subtypes and targets (Markram et al., 2004) and the complexity of neuronal connections embedded in six-layered neocortex (Douglas et al., 2004) has made it difficult to determine the role specific types of interneurons play in sensory information processing. In contrast, the primary olfactory (piriform) cortex is a part of paleocortex and has a simpler three-layered structure (Neville and Haberly, 2004), making it amenable to studies of circuits. Unfortunately, little is known about the inhibitory cells that regulate integration and spiking in principal cells in piriform cortex(Suzuki and Bekkers, 2007). The goal of my thesis work was to determine how inhibitory interneurons are recruited by olfactory sensory input and the effects of spatially and temporally patterned inhibition on shaping the activity of principal neurons in the olfactory cortex.

Distinct inhibitory circuits in olfactory cortex

We have described a population of interneurons with cell bodies in L1a that receive direct synaptic input from M/T cell axons in the LOT. Although L1a interneurons have a diversity of intrinsic electrical properties and spike-firing patterns,

they all receive LOT input and all project their axon exclusively within L1. These cells provide feedforward inhibition onto the apical dendrites of L2/3 pyramidal cells and onto each other. This form of feedforward inhibition from L1a interneurons limits the temporal integration of LOT input and also the timing of spike output in pyramidal cells. Additionally, inhibition from L1a interneurons is highly restricted in space, reducing dendritic excitability and bAP-evoked calcium influx in a dendritic branch-specific manner.

We have also described two non-overlapping populations of interneurons in L3 that receive synaptic input from nearby L2/3 pyramidal cells and mediate feedback inhibition in piriform cortex. The first population of L3 FS cells has properties similar to parvalbumin-positive FS basket cells found throughout the brain. They possess multipolar dendrites and widely branching axons that target the somatic compartment of L2/3 pryamidal cells. Although FS cells do not receive direct M/T cell input, they track the spiking of principal cells and fire late during bursts of LOT stimulation. Activation of pyramidal cells in piriform cortex results in recurrent inhibition that dominates recurrent excitation due to strong associational excitation onto L3 FS cells.

A second, distinct population of interneurons in L3 has intrinsic membrane and spiking properties similar to somatostatin-expressing LTS cells of neocortex. These cells are also exclusively activated by pyramidal cell spiking and provide recurrent inhibition. However, they are recruited later during LOT stimulus trains than FS cells and at a longer latency after individual stimuli. This is likely due to facilitating synaptic input from L2/3 pyramidal cells where FS cells receive depressing synaptic

input. From paired recordings, we show that both LTS cells and FS cells are highly connected with nearby pyramidal cells and preferentially inhibit cells that directly excite them.

Temporally structured M/T cell input recruits a canonical circuit in olfactory cortex

The initial sensory representations of olfactory sensory information occur in the olfactory bulb, where odorants produce spatial and temporal patterns of activity in glomeruli across the bulb (Rubin and Katz, 1999; Uchida et al., 2000; Wachowiak and Cohen, 2001). This representation is conveyed directly to principal neurons in the cortex by mitral and tufted cells that belong to single glomeruli; the olfactory system does not have a thalamic relay. Thus the cortical circuits processing olfactory information are directly recruited by the synaptic connections of M/T cells.

In response to synaptic excitation in the cognate glomerulus, M/T cells fire bursts of APs that are coupled to the respiratory rate (Bathellier et al., 2008; Cang and Isaacson, 2003; Margrie and Schaefer, 2003; Rinberg et al., 2006a; Spors and Grinvald, 2002). In fact, activity across the olfactory bulb is so strongly modulated by respiration that the firing of M/T cells during a single sniff cycle (~4-12 Hz) has been proposed to constitute a single unit in olfactory information processing (Bathellier et al., 2008; Kepecs et al., 2006). How are cortical circuits engaged by this temporally structured M/T cell output?

Previous studies using current source density (CSD) analysis found that LOT stimulation generated reproducible temporal pattern of synaptic currents across the

laminae of piriform cortex (Haberly and Shepherd, 1973; Ketchum and Haberly, 1993). We used trains of LOT stimuli that reproduced the structure of M/T cell bursting and monitored the recruitment of inhibition during the burst. We found that increasing stimulation intensities progressively recruited distinct but stereotyped inhibition, likely generated via the activation of distinct circuits involving multiple interneuron subtypes. We were able to distinguish the IPSCs in L2/3 pyramidal cells based on timing and spatial location, and to identify the chief interneuron cell types producing them.

We demonstrated that during bursts of LOT activity, inhibition from L1a interneurons is recruited onto the apical dendrites of pyramidal cells via a feedforward mechanism. Dendritic feedforward inhibition rapidly depresses while feedback inhibition from L3 interneurons targeting the soma and basal dendrites increases in amplitude as the burst progresses. Our results suggest that spatially and temporally structured inhibition may be tuned to the temporal properties of olfactory bulb outputs. The early-onset transient feedforward inhibition from L1a interneurons is poised to have its greatest effect suppressing the integration of weakly active M/T cell inputs. However the rapid depression of this circuit during a burst allows strongly active M/T cell inputs to bring pyramidal cells to spike threshold, enhancing the contribution of strongly active M/T cells to cortical representations of odor.

As pyramidal cells begin spiking in response to ongoing odor-evoked activity during the sniff, feedback inhibitory circuits are recruited. The engagement of recurrent inhibition by L3 interneurons may enhance oscillations in spiking activity during the sniff cycle, imposing fine-scale temporal patterning on spike timing and

allowing for efficient transmission of olfactory information to other brain areas (Bruno and Sakmann, 2006; Engel et al., 2001; Womelsdorf et al., 2007). As LOT-evoked spiking continues in L2/3 cells, LTS cells are more strongly activated and limit runaway spiking, finally dampening local activity after M/T cell input decreases at the end of the sniff cycle.

Although the activation of the M/T cell population *in vivo* is less ordered and synchronous than the stimulation we provide to the LOT, we believe that this pattern of IPSCs likely reflects the general progression of inhibition that an individual L2/3 pyramidal cell receives during a single sniff cycle. Multiple studies have demonstrated mechanisms in the olfactory bulb that contribute to synchronization of M/T cell output (Chen et al., 2009; Doucette et al., 2011; Kashiwadani et al., 1999; Schoppa, 2006). In addition, the spiking of piriform cortex pyramidal cells is strongly modulated by respiration (Poo and Isaacson, 2009; Zhan and Luo, 2010), implying that the local circuits both decode and represent olfactory information within a single sniff cycle (Rinberg et al., 2006b; Uchida and Mainen, 2003).

Spatial influence of inhibitory inputs

The spatially segregated axonal projection patterns of L1a and L3 interneurons ideally positions them to regulate the integration of information originating from functionally distinct inputs to L2/3 pyramidal cells. Due to the exclusive laminar distribution of M/T cell inputs to L1a (Neville and Haberly, 2004), the feedforward inhibitory network is poised to regulate the effects of direct sensory input at the site of

its entry into the cortex. We found that feedforward inhibition indeed strongly reduces the action potential integration time window for M/T cell input in L2/3 pyramidal cells when LOT stimulation is temporally sparse. These results suggest that L1a interneurons may specifically modulate the contribution of direct sensory inputs while leaving associational synapses in other layers unaltered.

In examining the spatially selective nature of feedforward inhibition in piriform cortex, we found that L1a interneurons can suppress dendritic calcium transients generated by somatic bAPs selectively on individual dendritic branches (Markram et al., 1995). Dendritic calcium transients are essential for a form of synapse-specific associative LTP, which requires coincidence detection between activity of excitatory inputs and the spike output of the cell (Larkum et al., 1999b; Magee and Johnston, 1997). Our results here suggest that L1a interneurons can serve to dissociate local dendritic calcium transients and the spike output of a cell. Indeed, in piriform cortex pyramidal cells, this associative plasticity can be blocked by inhibition (Kanter and Haberly, 1990, 1993). Thus, branch-specific modulation of dendritic excitability is a potential mechanism for associative learning and memory of olfactory information. By increasing the diversity of responses in pyramidal cell dendrites, L1a interneurons could allow piriform cortex a greater diversity of activity patterns with which to encode odors and form new odor associations.

Interneurons that target the soma have a strong effect on the spike output of principal cells (Gabernet et al., 2005; Pouille and Scanziani, 2001), thus the L3 interneurons we describe here are likely to play an important role modulating overall

excitability and spiking in nearby L2/3 pyramidal cells. The recurrent connectivity of L3 interneurons suggests that they are particularly positioned to suppress spiking in the same cells that excite them. However, if L3 LTS cells do indeed target the basal dendrites more than the soma they may preferentially modulate the integration of associational inputs in L2/3 pyramidal cells.

Temporal influence of inhibitory inputs

The striking segregation of inhibition in space is matched by an equally striking segregation of inhibitory circuits to specific temporal domains during bursting LOT input. As discussed previously, the transience of dendritic feedforward inhibition may enhance the representation of bursting M/T cell inputs in cortex. Our results also suggest that the activity-dependent reduction in feedforward dendritic inhibition could lead to increased dendritic excitability during a burst, potentially leading to a temporal changes in the ability to induce plasticity at dendritic synapses.

The differences in timing between LTS and FS cell spiking could allow them to govern L2/3 pyramidal cell excitability in different temporal domains. Feedforward somatic inhibition from FS cells in sensory neocortex can restrict the time window for synaptic integration and spike output (Gabernet et al., 2005). However the FS cells in piriform cortex are part of a feedback network, thus their ability to limit spike timing in L2/3 pyramidal cells would be linked to the activation of associational circuits, and to the activation of the very pyramidal cells they inhibit. Therefore, FS cells in piriform cortex may be involved in generating or modulating oscillations in spiking by L2/3

pyramidal cells (Atallah and Scanziani, 2009; Cobb et al., 1995; Hasenstaub et al., 2005). The same could be true for LTS cells, although the long latency and significant jitter when recruited by LOT stimuli imply that LTS cells do not limit spike timing within as narrow window as FS cells. It is possible that LTS cells and FS cells contribute to oscillations that operate on different timescales. Given that odors evoke strong oscillations in local network activity in piriform cortex independently in the beta (15-35 Hz) and gamma (40-70 Hz) frequency range (Neville and Haberly, 2003; Poo and Isaacson, 2009), the possibility that independent inhibitory circuits participate in these two oscillations is intriguing.

The role of inhibition in odor processing in olfactory cortex

Although our experiments focused on the activation of inhibitory circuits by bursts of LOT stimuli in acute slices of piriform cortex, our results offer some hypotheses for the role of specific interneuron classes during odor processing. For instance, all of the three interneuron classes we describe here could provide the broadly-tuned inhibition observed in voltage-clamp recordings *in vivo* (Poo and Isaacson, 2009). First, we show that L1a interneurons receive a broader convergence of M/T cell axons than neighboring pyramidal cells. If both cells sample randomly from the same cohort of M/T cells, this could result in broadly-tuned inhibition. Second, we show that L3 FS cells receive greater associational excitation than neighboring pyramidal cells. This is likely due to a higher convergence of L2/3 pyramidal cell inputs onto L3 FS cells (L2/3 pyramidal cells contact only 2% of nearby pyramidal

cells; data not shown). Third, we show that L3 LTS cells also receive highly convergent pyramidal cell inputs. If either population of L3 interneurons samples from broadly-tuned populations of pyramidal cells, feedback inhibitory circuits could produce broadly-tuned inhibition. Given that the relative sensory tuning of inhibitory interneurons compared to neighboring principal cells in neocortex is an ongoing source of debate (Kerlin et al., 2010; Runyan et al., 2010), it will be intriguing to measure the odor tuning of interneurons in piriform cortex.

Inhibition in many sensory circuits is thought to sharpen the spatial and temporal receptive field of principal cells (Ferster and Jagadeesh, 1992; Gabernet et al., 2005; Wehr and Zador, 2003; Wilent and Contreras, 2005). Given that odor-evoked ensembles of principal cells are distributed sparsely throughout piriform cortex without apparent topography (Miyamichi et al., 2011; Poo and Isaacson, 2009; Stettler and Axel, 2009), it is not straightforward to predict how inhibition in piriform cortex could perform similar functions. However, one intriguing possibility is that the targeting of inhibition from L1a interneurons to specific dendrites of L2/3 pyramidal cells may contribute to branch-specific integration of olfactory inputs, allowing individual branches to act as independent computational units during odor processing. One can imagine that branch-specific dendritic inhibition might limit the ability of M/T cell synapses in a particular dendritic region to depolarize the cell and generate spiking. A pyramidal cell would only reach spike threshold when the population of active M/T cells resulted in a spatial pattern of direct excitation in its dendrites that was not similar to the pattern of feedforward inhibition from L1a interneurons. This would effectively

limit the tuning of the pyramidal cell to a narrower set of glomerular odor representations than if inhibition was not present.

Alternately, one can imagine that the feedback inhibitory network may reduce the temporal window in which L2/3 pyramidal cells can integrate afferent sensory information. In the case where one pyramidal cell receives strong input from M/T early in a sniff cycle, this pyramidal cell could begin spiking. The spiking of this strongly activated pyramidal cell would tend to recruit the feedback inhibitory network, reducing the spiking of nearby pyramidal cells and thus enhancing the representation of the strongly active M/T cells in piriform cortex.

However, these putative roles for inhibitory circuits in the processing of olfactory information are highly speculative. Instead, our results define a set of features that characterize three major inhibitory circuits in piriform cortex. The results we present here offer insight into the function of each of these three circuits, suggesting possible directions for future work. One important step will be determining the odor-evoked activity of each class of interneuron in the intact cortex. Additionally, advanced techniques such as *in vivo* calcium imaging could be used to analyze the subcellular response properties of pyramidal cells and the contributions of inhibition to odor-evoked responses within specific compartments. Finally, our results demonstrate that optogenetic strategies hold promise as a way to manipulate the activity of individual inhibitory circuits during odor detection *in vivo*. In short, our findings offer testable hypotheses regarding the influence of specific inhibitory circuits in olfactory information processing and odor representations in the piriform cortex.

References

Andersen, P., Dingledine, R., Gjerstad, L., Langmoen, I.A., and Laursen, A.M. (1980). Two different responses of hippocampal pyramidal cells to application of gamma-amino butyric acid. J Physiol *305*, 279-296.

Andersen, P., Eccles, J.C., and Loyning, Y. (1963). Recurrent inhibition in the hippocampus with identification of the inhibitory cell and its synapses. Nature *198*, 540-542.

Anderson, J.S., Carandini, M., and Ferster, D. (2000). Orientation tuning of input conductance, excitation, and inhibition in cat primary visual cortex. J Neurophysiol *84*, 909-926.

Atallah, B.V., and Scanziani, M. (2009). Instantaneous modulation of gamma oscillation frequency by balancing excitation with inhibition. Neuron *62*, 566-577.

Atasoy, D., Aponte, Y., Su, H.H., and Sternson, S.M. (2008). A FLEX switch targets Channelrhodopsin-2 to multiple cell types for imaging and long-range circuit mapping. J Neurosci *28*, 7025-7030.

Bacci, A., Rudolph, U., Huguenard, J.R., and Prince, D.A. (2003). Major differences in inhibitory synaptic transmission onto two neocortical interneuron subclasses. J Neurosci *23*, 9664-9674.

Bathellier, B., Buhl, D.L., Accolla, R., and Carleton, A. (2008). Dynamic ensemble odor coding in the mammalian olfactory bulb: sensory information at different timescales. Neuron *57*, 586-598.

Bathellier, B., Margrie, T.W., and Larkum, M.E. (2009). Properties of piriform cortex pyramidal cell dendrites: implications for olfactory circuit design. J Neurosci *29*, 12641-12652.

Biedenbach, M.A., and Stevens, C.F. (1969). Synaptic organization of cat olfactory cortex as revealed by intracellular recording. J Neurophysiol *32*, 204-214.

Biel, M., Wahl-Schott, C., Michalakis, S., and Zong, X. (2009). Hyperpolarization-activated cation channels: from genes to function. Physiol Rev *89*, 847-885.

Biella, G., and de Curtis, M. (1995). Associative synaptic potentials in the piriform cortex of the isolated guinea-pig brain in vitro. Eur J Neurosci *7*, 54-64.

Branco, T., Clark, B.A., and Hausser, M. (2010). Dendritic discrimination of temporal input sequences in cortical neurons. Science *329*, 1671-1675.

Bruno, R.M., and Sakmann, B. (2006). Cortex is driven by weak but synchronously active thalamocortical synapses. Science *312*, 1622-1627.

Buck, L., and Axel, R. (1991). A novel multigene family may encode odorant receptors: a molecular basis for odor recognition. Cell *65*, 175-187.

Cang, J., and Isaacson, J.S. (2003). In vivo whole-cell recording of odor-evoked synaptic transmission in the rat olfactory bulb. J Neurosci *23*, 4108-4116.

Cardin, J.A., Carlen, M., Meletis, K., Knoblich, U., Zhang, F., Deisseroth, K., Tsai, L.H., and Moore, C.I. (2009). Driving fast-spiking cells induces gamma rhythm and controls sensory responses. Nature *459*, 663-667.

Chen, T.W., Lin, B.J., and Schild, D. (2009). Odor coding by modules of coherent mitral/tufted cells in the vertebrate olfactory bulb. Proc Natl Acad Sci U S A *106*, 2401-2406.

Cobb, S.R., Buhl, E.H., Halasy, K., Paulsen, O., and Somogyi, P. (1995). Synchronization of neuronal activity in hippocampus by individual GABAergic interneurons. Nature *378*, 75-78.

Cruikshank, S.J., Lewis, T.J., and Connors, B.W. (2007). Synaptic basis for intense thalamocortical activation of feedforward inhibitory cells in neocortex. Nat Neurosci *10*, 462-468.

Doucette, W., Gire, D.H., Whitesell, J., Carmean, V., Lucero, M.T., and Restrepo, D. (2011). Associative cortex features in the first olfactory brain relay station. Neuron *69*, 1176-1187.

Douglas, R., Markram, H., and Martin, K. (2004). Neocortex, 5th edn (New York: Oxford University Press).

Eccles, J.C. (1961). Membrane time constants of cat motoneurons and time courses of synptic action. Exp Neurol *4*, 1-22.

Ekstrand, J.J., Domroese, M.E., Feig, S.L., Illig, K.R., and Haberly, L.B. (2001). Immunocytochemical analysis of basket cells in rat piriform cortex. J Comp Neurol *434*, 308-328.

Engel, A.K., Fries, P., and Singer, W. (2001). Dynamic predictions: oscillations and synchrony in top-down processing. Nat Rev Neurosci *2*, 704-716.

Fanselow, E.E., and Connors, B.W. (2010). The roles of somatostatin-expressing (GIN) and fast-spiking inhibitory interneurons in UP-DOWN states of mouse neocortex. J Neurophysiol *104*, 596-606.

Ferster, D., and Jagadeesh, B. (1992). EPSP-IPSP interactions in cat visual cortex studied with in vivo whole-cell patch recording. J Neurosci *12*, 1262-1274.

Franks, K.M., and Isaacson, J.S. (2005). Synapse-specific downregulation of NMDA receptors by early experience: a critical period for plasticity of sensory input to olfactory cortex. Neuron *47*, 101-114.

Franks, K.M., and Isaacson, J.S. (2006). Strong single-fiber sensory inputs to olfactory cortex: implications for olfactory coding. Neuron *49*, 357-363.

Gabernet, L., Jadhav, S.P., Feldman, D.E., Carandini, M., and Scanziani, M. (2005). Somatosensory integration controlled by dynamic thalamocortical feed-forward inhibition. Neuron *48*, 315-327.

Ghosh, S., Larson, S.D., Hefzi, H., Marnoy, Z., Cutforth, T., Dokka, K., and Baldwin, K.K. (2011). Sensory maps in the olfactory cortex defined by long-range viral tracing of single neurons. Nature *472*, 217-220.

Gibson, J.R., Beierlein, M., and Connors, B.W. (1999). Two networks of electrically coupled inhibitory neurons in neocortex. Nature *402*, 75-79.

Glickfeld, L.L., Atallah, B.V., and Scanziani, M. (2008). Complementary modulation of somatic inhibition by opioids and cannabinoids. J Neurosci *28*, 1824-1832.

Gottfried, J.A., Winston, J.S., and Dolan, R.J. (2006). Dissociable codes of odor quality and odorant structure in human piriform cortex. Neuron *49*, 467-479.

Gradinaru, V., Zhang, F., Ramakrishnan, C., Mattis, J., Prakash, R., Diester, I., Goshen, I., Thompson, K.R., and Deisseroth, K. (2010). Molecular and cellular approaches for diversifying and extending optogenetics. Cell *141*, 154-165.

Haberly, L.B. (1985). Neuronal circuitry in olfactory cortex: anatomy and functional implications Chem Senses *10*, 219-238.

Haberly, L.B. (2001). Parallel-distributed processing in olfactory cortex: new insights from morphological and physiological analysis of neuronal circuitry. Chem Senses *26*, 551-576.

Haberly, L.B., and Bower, J.M. (1984). Analysis of association fiber system in piriform cortex with intracellular recording and staining techniques. J Neurophysiol *51*, 90-112.

Haberly, L.B., Hansen, D.J., Feig, S.L., and Presto, S. (1987). Distribution and ultrastructure of neurons in opossum piriform cortex displaying immunoreactivity to GABA and GAD and high-affinity tritiated GABA uptake. J Comp Neurol *266*, 269-290.

Haberly, L.B., and Price, J.L. (1978). Association and commissural fiber systems of the olfactory cortex of the rat. II. Systems originating in the olfactory peduncle. J Comp Neurol *181*, 781-807.

Haberly, L.B., and Shepherd, G.M. (1973). Current-density analysis of summed evoked potentials in opossum prepyriform cortex. J Neurophysiol *36*, 789-802.

Hasenstaub, A., Shu, Y., Haider, B., Kraushaar, U., Duque, A., and McCormick, D.A. (2005). Inhibitory postsynaptic potentials carry synchronized frequency information in active cortical networks. Neuron *47*, 423-435.

Hausser, M., and Mel, B. (2003). Dendrites: bug or feature? Curr Opin Neurobiol *13*, 372-383.

Higley, M.J., and Contreras, D. (2006). Balanced excitation and inhibition determine spike timing during frequency adaptation. J Neurosci *26*, 448-457.

Holmgren, C., Harkany, T., Svennenfors, B., and Zilberter, Y. (2003). Pyramidal cell communication within local networks in layer 2/3 of rat neocortex. J Physiol *551*, 139-153.

Hull, C., Isaacson, J.S., and Scanziani, M. (2009). Postsynaptic mechanisms govern the differential excitation of cortical neurons by thalamic inputs. J Neurosci *29*, 9127-9136.

Illig, K.R., and Haberly, L.B. (2003). Odor-evoked activity is spatially distributed in piriform cortex. J Comp Neurol *457*, 361-373.

Johenning, F.W., Beed, P.S., Trimbuch, T., Bendels, M.H., Winterer, J., and Schmitz, D. (2009). Dendritic compartment and neuronal output mode determine pathway-specific long-term potentiation in the piriform cortex. J Neurosci *29*, 13649-13661.

Johnson, D.M., Illig, K.R., Behan, M., and Haberly, L.B. (2000). New features of connectivity in piriform cortex visualized by intracellular injection of pyramidal cells suggest that "primary" olfactory cortex functions like "association" cortex in other sensory systems. J Neurosci *20*, 6974-6982.

Johnston, D., Hoffman, D.A., Colbert, C.M., and Magee, J.C. (1999). Regulation of back-propagating action potentials in hippocampal neurons. Curr Opin Neurobiol *9*, 288-292.

Johnston, D., and Narayanan, R. (2008). Active dendrites: colorful wings of the mysterious butterflies. Trends Neurosci *31*, 309-316.

Kampa, B.M., Clements, J., Jonas, P., and Stuart, G.J. (2004). Kinetics of Mg2+ unblock of NMDA receptors: implications for spike-timing dependent synaptic plasticity. J Physiol *556*, 337-345.

Kanter, E.D., and Haberly, L.B. (1990). NMDA-dependent induction of long-term potentiation in afferent and association fiber systems of piriform cortex in vitro. Brain Res *525*, 175-179.

Kanter, E.D., and Haberly, L.B. (1993). Associative long-term potentiation in piriform cortex slices requires GABAA blockade. J Neurosci *13*, 2477-2482.

Kanter, E.D., Kapur, A., and Haberly, L.B. (1996). A dendritic GABAA-mediated IPSP regulates facilitation of NMDA-mediated responses to burst stimulation of afferent fibers in piriform cortex. J Neurosci *16*, 307-312.

Kapfer, C., Glickfeld, L.L., Atallah, B.V., and Scanziani, M. (2007). Supralinear increase of recurrent inhibition during sparse activity in the somatosensory cortex. Nat Neurosci *10*, 743-753.

Kapur, A., and Haberly, L.B. (1998). Duration of NMDA-dependent synaptic potentiation in piriform cortex in vivo is increased after epileptiform bursting. J Neurophysiol *80*, 1623-1629.

Kashiwadani, H., Sasaki, Y.F., Uchida, N., and Mori, K. (1999). Synchronized oscillatory discharges of mitral/tufted cells with different molecular receptive ranges in the rabbit olfactory bulb. J Neurophysiol *82*, 1786-1792.

Kawaguchi, Y. (1995). Physiological subgroups of nonpyramidal cells with specific morphological characteristics in layer II/III of rat frontal cortex. J Neurosci *15*, 2638-2655.

Kawaguchi, Y., and Kubota, Y. (1996). Physiological and morphological identification of somatostatin- or vasoactive intestinal polypeptide-containing cells among GABAergic cell subtypes in rat frontal cortex. J Neurosci *16*, 2701-2715.

Kepecs, A., Uchida, N., and Mainen, Z.F. (2006). The sniff as a unit of olfactory processing. Chem Senses *31*, 167-179.

Kerlin, A.M., Andermann, M.L., Berezovskii, V.K., and Reid, R.C. (2010). Broadly tuned response properties of diverse inhibitory neuron subtypes in mouse visual cortex. Neuron *67*, 858-871.

Ketchum, K.L., and Haberly, L.B. (1993). Membrane currents evoked by afferent fiber stimulation in rat piriform cortex. I. Current source-density analysis. J Neurophysiol *69*, 248-260.

Kim, H.G., Beierlein, M., and Connors, B.W. (1995). Inhibitory control of excitable dendrites in neocortex. J Neurophysiol *74*, 1810-1814.

Kim, H.G., and Connors, B.W. (1993). Apical dendrites of the neocortex: correlation between sodium- and calcium-dependent spiking and pyramidal cell morphology. J Neurosci *13*, 5301-5311.

Koester, H.J., and Johnston, D. (2005). Target cell-dependent normalization of transmitter release at neocortical synapses. Science *308*, 863-866.

Larkum, M.E., Kaiser, K.M., and Sakmann, B. (1999a). Calcium electrogenesis in distal apical dendrites of layer 5 pyramidal cells at a critical frequency of back-propagating action potentials. Proc Natl Acad Sci U S A *96*, 14600-14604.

Larkum, M.E., Zhu, J.J., and Sakmann, B. (1999b). A new cellular mechanism for coupling inputs arriving at different cortical layers. Nature *398*, 338-341.

Laurent, G. (2002). Olfactory network dynamics and the coding of multidimensional signals. Nat Rev Neurosci *3*, 884-895.

Letzkus, J.J., Kampa, B.M., and Stuart, G.J. (2006). Learning rules for spike timing-dependent plasticity depend on dendritic synapse location. J Neurosci *26*, 10420-10429.

Leung, L.S. (1982). Nonlinear feedback model of neuronal populations in hippocampal CAl region. J Neurophysiol *47*, 845-868.

Litaudon, P., Amat, C., Bertrand, B., Vigouroux, M., and Buonviso, N. (2003). Piriform cortex functional heterogeneity revealed by cellular responses to odours. Eur J Neurosci *17*, 2457-2461.

Luna, V.M., and Schoppa, N.E. (2008). GABAergic circuits control input-spike coupling in the piriform cortex. J Neurosci *28*, 8851-8859.

Magee, J.C., and Johnston, D. (1997). A synaptically controlled, associative signal for Hebbian plasticity in hippocampal neurons. Science *275*, 209-213.

Malnic, B., Hirono, J., Sato, T., and Buck, L.B. (1999). Combinatorial receptor codes for odors. Cell *96*, 713-723.

Mancilla, J.G., Lewis, T.J., Pinto, D.J., Rinzel, J., and Connors, B.W. (2007). Synchronization of electrically coupled pairs of inhibitory interneurons in neocortex. J Neurosci *27*, 2058-2073.

Margrie, T.W., and Schaefer, A.T. (2003). Theta oscillation coupled spike latencies yield computational vigour in a mammalian sensory system. J Physiol *546*, 363-374.

Markram, H., Helm, P.J., and Sakmann, B. (1995). Dendritic calcium transients evoked by single back-propagating action potentials in rat neocortical pyramidal neurons. J Physiol *485 (Pt 1)*, 1-20.

Markram, H., Toledo-Rodriguez, M., Wang, Y., Gupta, A., Silberberg, G., and Wu, C. (2004). Interneurons of the neocortical inhibitory system. Nat Rev Neurosci *5*, 793-807.

Miles, R., Toth, K., Gulyas, A.I., Hajos, N., and Freund, T.F. (1996). Differences between somatic and dendritic inhibition in the hippocampus. Neuron *16*, 815-823.

Miyamichi, K., Amat, F., Moussavi, F., Wang, C., Wickersham, I., Wall, N.R., Taniguchi, H., Tasic, B., Huang, Z.J., He, Z.*, et al.* (2011). Cortical representations of olfactory input by trans-synaptic tracing. Nature *472*, 191-196.

Mombaerts, P., Wang, F., Dulac, C., Chao, S.K., Nemes, A., Mendelsohn, M., Edmondson, J., and Axel, R. (1996). Visualizing an olfactory sensory map. Cell *87*, 675-686.

Nevian, T., and Sakmann, B. (2006). Spine Ca2+ signaling in spike-timing-dependent plasticity. J Neurosci *26*, 11001-11013.

Neville, K.R., and Haberly, L.B. (2003). Beta and gamma oscillations in the olfactory system of the urethane-anesthetized rat. J Neurophysiol *90*, 3921-3930.

Neville, K.R., and Haberly, L.B. (2004). Olfactory Cortex, 5th edn (New York: Oxford University Press).

Olah, S., Fule, M., Komlosi, G., Varga, C., Baldi, R., Barzo, P., and Tamas, G. (2009). Regulation of cortical microcircuits by unitary GABA-mediated volume transmission. Nature *461*, 1278-1281.

Oliva, A.A., Jr., Jiang, M., Lam, T., Smith, K.L., and Swann, J.W. (2000). Novel hippocampal interneuronal subtypes identified using transgenic mice that express green fluorescent protein in GABAergic interneurons. J Neurosci *20*, 3354-3368.

Pager, J. (1985). Respiration and olfactory bulb unit activity in the unrestrained rat: statements and reappraisals. Behav Brain Res *16*, 81-94.

Perez-Garci, E., Gassmann, M., Bettler, B., and Larkum, M.E. (2006). The GABAB1b isoform mediates long-lasting inhibition of dendritic Ca2+ spikes in layer 5 somatosensory pyramidal neurons. Neuron *50*, 603-616.

Perez-Orive, J., Mazor, O., Turner, G.C., Cassenaer, S., Wilson, R.I., and Laurent, G. (2002). Oscillations and sparsening of odor representations in the mushroom body. Science *297*, 359-365.

Petreanu, L., Mao, T., Sternson, S.M., and Svoboda, K. (2009). The subcellular organization of neocortical excitatory connections. Nature *457*, 1142-1145.

Pockberger, H. (1991). Electrophysiological and morphological properties of rat motor cortex neurons in vivo. Brain Res *539*, 181-190.

Poirazi, P., Brannon, T., and Mel, B.W. (2003). Pyramidal neuron as two-layer neural network. Neuron *37*, 989-999.

Polsky, A., Mel, B.W., and Schiller, J. (2004). Computational subunits in thin dendrites of pyramidal cells. Nat Neurosci *7*, 621-627.

Poo, C., and Isaacson, J.S. (2007). An early critical period for long-term plasticity and structural modification of sensory synapses in olfactory cortex. J Neurosci *27*, 7553-7558.

Poo, C., and Isaacson, J.S. (2009). Odor representations in olfactory cortex: "sparse" coding, global inhibition, and oscillations. Neuron *62*, 850-861.

Pouille, F., Marin-Burgin, A., Adesnik, H., Atallah, B.V., and Scanziani, M. (2009). Input normalization by global feedforward inhibition expands cortical dynamic range. Nat Neurosci *12*, 1577-1585.

Pouille, F., and Scanziani, M. (2001). Enforcement of temporal fidelity in pyramidal cells by somatic feed-forward inhibition. Science *293*, 1159-1163.

Pouille, F., and Scanziani, M. (2004). Routing of spike series by dynamic circuits in the hippocampus. Nature *429*, 717-723.

Rall, W. (1957). Membrane time constant of motoneurons. Science *126*, 454.

Rall, W. (1964). Theoretical significance of dendritic trees for neuronal input-output relations. Neural Theory and Modeling *Edited by Reiss RF*, 73-97.

Rennaker, R.L., Chen, C.F., Ruyle, A.M., Sloan, A.M., and Wilson, D.A. (2007). Spatial and temporal distribution of odorant-evoked activity in the piriform cortex. J Neurosci *27*, 1534-1542.

Reyes, A., Lujan, R., Rozov, A., Burnashev, N., Somogyi, P., and Sakmann, B. (1998). Target-cell-specific facilitation and depression in neocortical circuits. Nat Neurosci *1*, 279-285.

Rinberg, D., Koulakov, A., and Gelperin, A. (2006a). Sparse odor coding in awake behaving mice. J Neurosci *26*, 8857-8865.

Rinberg, D., Koulakov, A., and Gelperin, A. (2006b). Speed-accuracy tradeoff in olfaction. Neuron *51*, 351-358.

Rubin, B.D., and Katz, L.C. (1999). Optical imaging of odorant representations in the mammalian olfactory bulb. Neuron *23*, 499-511.

Runyan, C.A., Schummers, J., Van Wart, A., Kuhlman, S.J., Wilson, N.R., Huang, Z.J., and Sur, M. (2010). Response features of parvalbumin-expressing interneurons suggest precise roles for subtypes of inhibition in visual cortex. Neuron *67*, 847-857.

Satou, M., Mori, K., Tazawa, Y., and Takagi, S.F. (1983). Interneurons mediating fast postsynaptic inhibition in pyriform cortex of the rabbit. J Neurophysiol *50*, 89-101.

Scanziani, M., Gahwiler, B.H., and Charpak, S. (1998). Target cell-specific modulation of transmitter release at terminals from a single axon. Proc Natl Acad Sci U S A *95*, 12004-12009.

Schiller, J., Major, G., Koester, H.J., and Schiller, Y. (2000). NMDA spikes in basal dendrites of cortical pyramidal neurons. Nature *404*, 285-289.

Schoppa, N.E. (2006). Synchronization of olfactory bulb mitral cells by precisely timed inhibitory inputs. Neuron *49*, 271-283.

Serizawa, S., Miyamichi, K., and Sakano, H. (2004). One neuron-one receptor rule in the mouse olfactory system. Trends Genet *20*, 648-653.

Shepherd, G.M., Chen, W.R., and Greer, C.A. (2004). Olfactory Bulb, 5th edn (New York: Oxford University Press).

Shu, Y., Hasenstaub, A., and McCormick, D.A. (2003). Turning on and off recurrent balanced cortical activity. Nature *423*, 288-293.

Silberberg, G. (2008). Polysynaptic subcircuits in the neocortex: spatial and temporal diversity. Curr Opin Neurobiol *18*, 332-337.

Silberberg, G., and Markram, H. (2007). Disynaptic inhibition between neocortical pyramidal cells mediated by Martinotti cells. Neuron *53*, 735-746.

Sohal, V.S., Zhang, F., Yizhar, O., and Deisseroth, K. (2009). Parvalbumin neurons and gamma rhythms enhance cortical circuit performance. Nature *459*, 698-702.

Somogyi, P., Tamas, G., Lujan, R., and Buhl, E.H. (1998). Salient features of synaptic organisation in the cerebral cortex. Brain Res Brain Res Rev *26*, 113-135.

Sosulski, D.L., Lissitsyna Bloom, M., Cutforth, T., Axel, R., and Datta, S.R. (2011). Distinct representations of olfactory information in different cortical centres. Nature *472*, 213-216.

Soucy, E.R., Albeanu, D.F., Fantana, A.L., Murthy, V.N., and Meister, M. (2009). Precision and diversity in an odor map on the olfactory bulb. Nat Neurosci *12*, 210-220.

Spors, H., and Grinvald, A. (2002). Spatio-temporal dynamics of odor representations in the mammalian olfactory bulb. Neuron *34*, 301-315.

Spruston, N., Jaffe, D.B., Williams, S.H., and Johnston, D. (1993). Voltage- and space-clamp errors associated with the measurement of electrotonically remote synaptic events. J Neurophysiol *70*, 781-802.

Spruston, N., Schiller, Y., Stuart, G., and Sakmann, B. (1995). Activity-dependent action potential invasion and calcium influx into hippocampal CA1 dendrites. Science *268*, 297-300.

Staubli, U., Fraser, D., Faraday, R., and Lynch, G. (1987). Olfaction and the "data" memory system in rats. Behav Neurosci *101*, 757-765.

Stettler, D.D., and Axel, R. (2009). Representations of odor in the piriform cortex. Neuron *63*, 854-864.

Stokes, C.C., and Isaacson, J.S. (2010). From dendrite to soma: dynamic routing of inhibition by complementary interneuron microcircuits in olfactory cortex. Neuron *67*, 452-465.

Stuart, G.J., and Sakmann, B. (1994). Active propagation of somatic action potentials into neocortical pyramidal cell dendrites. Nature *367*, 69-72.

Suzuki, N., and Bekkers, J.M. (2006). Neural coding by two classes of principal cells in the mouse piriform cortex. J Neurosci *26*, 11938-11947.

Suzuki, N., and Bekkers, J.M. (2007). Inhibitory interneurons in the piriform cortex. Clin Exp Pharmacol Physiol *34*, 1064-1069.

Suzuki, N., and Bekkers, J.M. (2010a). Distinctive classes of GABAergic interneurons provide layer-specific phasic inhibition in the anterior piriform cortex. Cereb Cortex *20*, 2971-2984.

Suzuki, N., and Bekkers, J.M. (2010b). Inhibitory neurons in the anterior piriform cortex of the mouse: classification using molecular markers. J Comp Neurol *518*, 1670-1687.

Szabadics, J., Tamas, G., and Soltesz, I. (2007). Different transmitter transients underlie presynaptic cell type specificity of GABAA,slow and GABAA,fast. Proc Natl Acad Sci U S A *104*, 14831-14836.

Tamas, G., Lorincz, A., Simon, A., and Szabadics, J. (2003). Identified sources and targets of slow inhibition in the neocortex. Science *299*, 1902-1905.

Tan, Z., Hu, H., Huang, Z.J., and Agmon, A. (2008). Robust but delayed thalamocortical activation of dendritic-targeting inhibitory interneurons. Proc Natl Acad Sci U S A *105*, 2187-2192.

Treloar, H.B., Feinstein, P., Mombaerts, P., and Greer, C.A. (2002). Specificity of glomerular targeting by olfactory sensory axons. J Neurosci *22*, 2469-2477.

Tseng, G.F., and Haberly, L.B. (1988). Characterization of synaptically mediated fast and slow inhibitory processes in piriform cortex in an in vitro slice preparation. J Neurophysiol *59*, 1352-1376.

Tseng, G.F., and Haberly, L.B. (1989a). Deep neurons in piriform cortex. I. Morphology and synaptically evoked responses including a unique high-amplitude paired shock facilitation. J Neurophysiol *62*, 369-385.

Tseng, G.F., and Haberly, L.B. (1989b). Deep neurons in piriform cortex. II. Membrane properties that underlie unusual synaptic responses. J Neurophysiol *62*, 386-400.

Tsubokawa, H., and Ross, W.N. (1996). IPSPs modulate spike backpropagation and associated [Ca2+]i changes in the dendrites of hippocampal CA1 pyramidal neurons. J Neurophysiol *76*, 2896-2906.

Uchida, N., and Mainen, Z.F. (2003). Speed and accuracy of olfactory discrimination in the rat. Nat Neurosci *6*, 1224-1229.

Uchida, N., Takahashi, Y.K., Tanifuji, M., and Mori, K. (2000). Odor maps in the mammalian olfactory bulb: domain organization and odorant structural features. Nat Neurosci *3*, 1035-1043.

Wachowiak, M., and Cohen, L.B. (2001). Representation of odorants by receptor neuron input to the mouse olfactory bulb. Neuron *32*, 723-735.

Waters, J., Larkum, M., Sakmann, B., and Helmchen, F. (2003). Supralinear Ca2+ influx into dendritic tufts of layer 2/3 neocortical pyramidal neurons in vitro and in vivo. J Neurosci *23*, 8558-8567.

Wehr, M., and Zador, A.M. (2003). Balanced inhibition underlies tuning and sharpens spike timing in auditory cortex. Nature *426*, 442-446.

Wilent, W.B., and Contreras, D. (2005). Dynamics of excitation and inhibition underlying stimulus selectivity in rat somatosensory cortex. Nat Neurosci *8*, 1364-1370.

Williams, S.R., and Stuart, G.J. (2002). Dependence of EPSP efficacy on synapse location in neocortical pyramidal neurons. Science *295*, 1907-1910.

Williams, S.R., and Stuart, G.J. (2003). Voltage- and site-dependent control of the somatic impact of dendritic IPSPs. J Neurosci *23*, 7358-7367.

Wilson, D.A., Kadohisa, M., and Fletcher, M.L. (2006). Cortical contributions to olfaction: plasticity and perception. Semin Cell Dev Biol *17*, 462-470.

Womelsdorf, T., Schoffelen, J.M., Oostenveld, R., Singer, W., Desimone, R., Engel, A.K., and Fries, P. (2007). Modulation of neuronal interactions through neuronal synchronization. Science *316*, 1609-1612.

Yoshimura, Y., and Callaway, E.M. (2005). Fine-scale specificity of cortical networks depends on inhibitory cell type and connectivity. Nat Neurosci *8*, 1552-1559.

Young, A., and Sun, Q.Q. (2009). GABAergic inhibitory interneurons in the posterior piriform cortex of the GAD67-GFP mouse. Cereb Cortex *19*, 3011-3029.

Zhan, C., and Luo, M. (2010). Diverse patterns of odor representation by neurons in the anterior piriform cortex of awake mice. J Neurosci *30*, 16662-16672.

Zhang, F., Wang, L.P., Boyden, E.S., and Deisseroth, K. (2006). Channelrhodopsin-2 and optical control of excitable cells. Nat Methods *3*, 785-792.

Zhang, F., Wang, L.P., Brauner, M., Liewald, J.F., Kay, K., Watzke, N., Wood, P.G., Bamberg, E., Nagel, G., Gottschalk, A., and Deisseroth, K. (2007). Multimodal fast optical interrogation of neural circuitry. Nature *446*, 633-639.

Zhang, X., and Firestein, S. (2002). The olfactory receptor gene superfamily of the mouse. Nat Neurosci *5*, 124-133.

Zhang, Y., Burk, J.A., Glode, B.M., and Mair, R.G. (1998). Effects of thalamic and olfactory cortical lesions on continuous olfactory delayed nonmatching-to-sample and olfactory discrimination in rats (Rattus norvegicus). Behav Neurosci *112*, 39-53.

Zhao, H., Ivic, L., Otaki, J.M., Hashimoto, M., Mikoshiba, K., and Firestein, S. (1998). Functional expression of a mammalian odorant receptor. Science *279*, 237-242.

Zucker, R.S., and Regehr, W.G. (2002). Short-term synaptic plasticity. Annu Rev Physiol *64*, 355-405.